

**Deformation and fracture behavior
of simulated particle gels**

Promotor: prof. dr. ir. J. Grasman
hoogleraar in de wiskundige en statistische methoden

Co-promotoren: dr. J.H.J. van Opheusden
universitair docent,
leerstoolgroep wiskundige en statistische methoden

dr. ir. T. van Vliet
universitair hoofddocent,
Wageningen Centre for Food Sciences

Promotiecommissie: prof. dr. M.A. Cohen Stuart
Wageningen Universiteit

prof. dr. B.M. Mulder
AMOLF Amsterdam, Wageningen Universiteit

prof. dr. W. Agterof
Unilever R&D Vlaardingen, Universiteit Twente

prof. dr. C.G. de Kruif
NIZO Ede, Universiteit Utrecht

Anna A. Rzepiela

**Deformation and fracture behavior
of simulated particle gels**

Proefschrift
ter verkrijging van de graad van doctor
op gezag van de rector magnificus
van Wageningen Universiteit,
prof. dr. ir. L. Speelman,
in het openbaar te verdedigen
op dinsdag 15 april 2003
des namiddags te vier uur in de Aula.

ISBN 90-5808-803-0

Abstract

Particle gels are systems of colloidal particles that form weakly bonded percolating networks interpenetrated by a suspending fluid. They are characterized as soft, deformable, elastic solids. Examples in the food domain are yogurt and cheese, in which the particles are casein micelles. In this thesis rheological properties of model particle gels are investigated using Brownian Dynamics (BD) simulations with different approximations.

Aggregation kinetics is discussed for a range of volume fractions. The model is set up to mimic aspects of aggregation of casein micelles in renneted milk. Smoluchowski classical theory is tested by comparing predictions with the BD simulation model. At low volume fractions aggregation rates were found close to the Smoluchowski rates, but they increase sharply at higher concentrations. Only when a large fraction of the particles has already clustered the quasi-stationary solution as used in Smoluchowski theory is attained.

Oscillatory shear tests have been used to study small deformation characteristics of model particle gels. Continuous shear and tensile deformation tests have been used to study large deformation and fracture properties. Two different techniques of shear deformation were employed, namely affine and non-affine deformation, the second being novel in simulation studies of gels. In the affine method strain is applied with a homogenous profile. In the non-affine method strain is applied on the surface of the gel structure and can be transmitted through the network to the bulk. Also two different dynamic descriptions of the model are discussed, one with high energy dissipation, the high damping limit, and one with low energy dissipation, the inertia model.

The small oscillatory shear study showed that the affine technique is insufficient for studying particle gels. The resulting rheology does not depend on details of the network while in real experiments it does. In the non-affine mode, deformation of the network is inhomogeneous depending on network structure and time scale of strain propagation. Moreover a frequency dependent transition can be observed from bulk loading to surface loading. Under continuous shear deformation, regardless of the model used, the particle gels were observed to fracture into lumps that compactified due to local reorganization. Fractal properties of the gels were irreversibly lost at large deformation. Under tensile deformation, within the parameter ranges used, the particle gels were found to be notch insensitive. They exhibit ductile fracture behavior, which was due to global material failure rather than crack propagation.

Contents

1	Introduction	1
1.1	References	6
2	Brownian Dynamics simulation of aggregation kinetics of hard spheres with flexible bonds	9
2.1	Introduction	9
2.2	Brownian Dynamics model	11
2.3	Aggregation kinetics	13
2.4	Results	15
2.5	Discussion	19
2.6	Conclusions	24
2.7	References	24
3	Small non-affine shear deformation of particle gels studied by Brownian Dynamics simulations	27
3.1	Introduction	27
3.2	Simulation details	30
3.2.1	Particle interactions	30
3.2.2	Brownian Dynamics	31
3.2.3	Numeric models	32
3.2.4	Rheology	33
3.3	Results	37
3.3.1	High damping model	40
3.3.2	Inertia model (without particle rotations)	42
3.3.3	Inertia model (with particle rotations)	45
3.4	Discussion	48
3.5	Conclusions	50
3.6	References	51

4	Large shear deformation of particle gels studied by Brownian Dynamics simulations	53
4.1	Introduction	53
4.2	Simulation details	55
4.2.1	Particle interactions	55
4.2.2	Brownian Dynamics algorithm	56
4.2.3	The inertia effects model	56
4.2.4	The high damping model	57
4.2.5	Rheology	58
4.3	Results	59
4.3.1	The high damping model	60
4.3.2	The inertia model	66
4.4	Discussion	70
4.4.1	Yielding	73
4.5	Conclusions	76
4.6	References	76
5	Tensile deformation of particle gels studied by Brownian Dynamics simulations	79
5.1	Introduction	79
5.2	Simulation details	81
5.2.1	Particle interactions	81
5.2.2	Brownian Dynamics	82
5.2.3	Numerical models	83
5.2.4	Rheology	84
5.3	Results	85
5.3.1	High damping model	87
5.3.2	Inertia model	94
5.4	Discussion	97
5.5	Conclusions	99
5.6	References	99
6	Summary and Conclusions	101
	Samenvatting	103
	Acknowledgements	107

Chapter 1

Introduction

There is always much confusion about the definition of a gel. From the viewpoint of phenomenological rheology a gel can be defined as a material which when observed at short times, or high frequencies, behaves as a solid, and at long time scales, or low frequencies as a fluid. Unless this definition is accompanied by a quantification of the terms short, long, high and low, one might conclude that “gel” is just synonymous with “material”. It helps when the “human” time scale is given as reference, but that by definition introduces a large amount of subjectivity. To avoid all such discussion, we use the term gel here to describe a material consisting of a more or less randomly cross-connected network of mechanical elements, with connections that can easily be formed or destroyed, usually in a suspending fluid. Thus we take a more structural viewpoint, assuming that we have knowledge about the microscopic and/or mesoscopic structure and mechanics of the material. In practice of course it will often be the objective of the observations on a material to determine just that structure, but as we are considering theoretical model materials here, we have this luxury. The purpose of such model studies is exactly to investigate how the macroscopic material properties, as observed in phenomenology, depend on that underlying structure. Computer simulations, large scale numerical model calculations, can provide the insight that is needed to make the connection between structure and material properties.

Essentially there are two main types of gels. Polymer gels consist of long chain molecules, with physical or weak chemical interactions responsible for the cross connections between the chains. Particle gels consist of a network of globular objects, called particles, also linked to each other by physical or weak chemical interactions. Essential in both cases is that the individual links can be relatively easily severed, while new links are easily established. We will focus on models for particle gels, especially particles consisting of protein material. Examples of proteins or protein particles capable of forming particle gels are casein micelles, β -lactoglobulin [1,2] and soy glycinin. Also stabilized emulsion droplets can under some circumstances form particle gels. Though the macroscopic rheological behavior of the two types of gels is very similar, the underlying microscopic mechanisms appear to be very distinct. Various model

studies, both experimental and by simulation, have been performed to distinguish these mechanisms for particle gels. Here we will discuss mainly simulation studies, and we will refer to the experiments as the “real” systems, to which the simulations must be validated. Actual protein particle systems usually are too complex to be accessible for direct modeling, but simplified colloidal particle suspensions provide good model systems. Next to colloidal particle gels we will also describe the modeling of destabilized suspensions forming the aggregates that can lead to gelation of the system.

There is a large body of published material about the simulated rheological behavior of colloidal particle suspensions. Early reviews on the subject are by Heyes [3,4], a very recent one is by Frenkel [5]. A recent review milk protein stabilized oil in water emulsions is by Dickinson [6]. Much less is available about the behavior of particle gels, on both the gelation process itself and the gel properties. One important reason is that particle gels are essentially non-equilibrium systems, while most of the standard statistical physical theories apply to systems in thermodynamic equilibrium. An important application of the model gel systems is that they can be used as test systems for non-equilibrium statistical mechanics theories. Our interest here is in the gel properties themselves, and numerical simulation models are quite useful for that purpose too. As there is much research on particle suspensions, many type of models have been developed to capture the essential features of such systems. The main two categories are continuum models, and discrete (particle) models. In the continuum models, such as the finite element or difference schemes used in computational fluid dynamics, the flow of material in the system is described in terms of densities defined on a discrete grid of points in space [7-11]. Also the Lattice Boltzmann [12-14] and Dissipative Particle Dynamics [15,16] techniques belong to this category. Though this doesn't seem to be the most obvious way to describe discrete particles, some interesting results have been obtained with these techniques [17]. Still, because both the particles and the suspended fluid are modeled at the same level of detail in this approach, a substantial amount of computational resources is used for the fluid motion, which in general is of less interest. In the category of discrete models the main techniques are Molecular Dynamics (MD) and Brownian Dynamics (BD) [3,4], and more recent Stokesian Dynamics (SD) [18-23]. In all cases the numerical equations solved apply to the dynamic variables that describe the colloidal particles themselves, interacting with and through a continuous suspending fluid. In the MD approach the fluid is essentially absent, and the dynamical equations are just the Newtonian equations of motion for a set of interacting particles, where an effective potential can be used to incorporate solvent effects. In the BD approach the effect of the solvent is a drag force on the moving particles, and a random Brownian force mimicking the many collisions of the solvent molecules with the colloidal particles. In general only single body

interactions are considered to fall within the scope of this technique, but several authors also incorporate two body hydrodynamic effects, such as lubrication, into BD. Incorporation of many body hydrodynamic interactions, also the long range interaction, is pursued in SD.

It is clear that hydrodynamic interactions are important in models for flow in colloidal suspensions. An important excuse that they have been neglected in the earlier simulations [24-32] is that no efficient models were available at that time, and computers simply were not fast enough to treat sufficiently large systems. Several approaches have been developed to make SD more efficient [33-35], and consequently there is an increasing interest in the application of the more sophisticated models [36-39]. The simpler BD models, without many body hydrodynamics, could at least be used to investigate trends, and develop further insight into the systems. These BD models are not suited as more or less ab-initio models to predict the behavior of real suspensions from model calculations, as is presently possible for molecular systems and even small proteins or parts of proteins, by using validated MD models. For aggregation BD models may be more appropriate, provided the aggregation takes place in a system sufficiently at rest, for instance for calculating phase diagrams for colloidal systems [40,41]. In real experiments that latter requirement will not often be satisfied, for somewhat larger colloidal particles the rate at which collisions, possibly leading to aggregation, occur can easily be low compared to the mixing effect because of small thermal disturbances to the sample. That implies that even for small colloidal particles, once they have formed larger clusters, aggregation is likely to be orthokinetic rather than perikinetic. Even for perikinetic aggregation, when the flow pattern in the suspending fluid can be neglected, and diffusion of the particles is the main mechanism, lubrication forces at close range during collision influence the aggregation possibility. As particles approach one another, this lubrication produces an effective repulsion. On the other hand, when they move apart again, the flow of fluid into the widening gap produces an effective attraction. Also Vanderwaals attraction between the surfaces of the particles will compensate the repulsion due to the fluid flow from the gap between the particles. In practice these effects may well cancel, and the overall result from including lubrication effects into a detailed model will be just a slowing down of the actual binding process. For an aggregation process that is diffusion dominated, that will only influence the formation of the smaller clusters, which will become somewhat more compact. Once larger clusters are formed, diffusion slows down anyhow and always is the limiting process. Later reorganization of aggregates will also lead to more compact structures, and it remains to be seen whether inclusion of hydrodynamics will lead to substantially different gel structures in model calculations.

For simulations that investigate the rheological properties of the gels themselves, after they have formed, it is an open question whether the gel kinetics is strongly influenced by that of the suspending fluid. Particle gels are enthalpic, rather than entropic, as are polymer gels. That means that the kinetics of the gel is dominated by that of the bonds between the particles, while in a polymer gels the dynamics of the polymer strands is the dominant feature. For local structure evolution in relatively dense gels simple models may be well suited [42-45]. Only in very dilute gels, with relatively long strands, will the kinetics of the strands in the suspending fluid be important, but otherwise the kinetics of the gel is the kinetics of the connected network. A second question is how the external forcing of the gel is transferred to the bulk. At low volume fractions the flow patterns in the suspending fluid will provide the dominating mechanism through which stresses are mediated. At higher volume fraction it will be the network itself that is responsible. In the latter case the hydrodynamic effects will probably not be very important. More relevant is that in medium and high volume fraction particle gel networks, when the network is mediating the external stresses, the motion of the bulk material will not be affine. For instance an external shear deformation imposed on a sample will not lead to a linear deformation profile of all particles of the gel, as if it is behaving as a Newtonian fluid. Only the stress-carrying network strands can be expected to follow the external forcing, and any inhomogeneities in that network will result in non-affine deformation. Hydrodynamic interactions between the individual particles in the gel will of course be present, and they may even be important for the actual dynamics, but it is unclear if they can be separated from the direct chemical and physical interactions that describe the bonds between the particles. In reality external stresses will be mediated both by the network and the suspending fluid, and only a full hydrodynamic model can adequately describe that coupled motion. In large deformation rheology, when macroscopic fracture occurs, the fluid flow inside the cracks needs hydrodynamic modeling, simplified models can only be expected to give a more or less reliable description of the earlier stages of fracture.

In this thesis we will restrict ourselves to the simplified Brownian Dynamics models neglecting all but single particle hydrodynamics, the Stokesian drag force of a particle moving through the suspending fluid. As explained the rheological properties of a colloidal suspension should be modeled using the available more extended models, for the gel properties, especially for higher volume fraction as we consider here, they probably can be neglected more easily. Using a simpler model still allows for studying larger systems on relatively simple computers. For a proper investigation of large-scale system failure samples with a large number of particles are necessary. In our calculations we have used samples of up to 10,000 particles. In practice the large deformation behavior of gels is often much more important than the small

deformation behavior, which often is studied more extensively [46]. We have earlier developed a model in which colloidal particles can form flexible but irreversible bonds between their surfaces, and form a network capable of reorganization [44,45]. With this model we have studied the reorganization within particle gels, and discovered that contrary to expectation, the generic fractal structure of the networks is not due to the generic nature of the fractal aggregation model itself, but to the reorganization. Freshly formed gels at different volume fractions have different fractal dimensionalities, and only upon aging of these gels do the dimensionalities converge [47-51]. Some of these results and a large overview of more recent literature is reviewed in [52]. Here we use this same model to study the kinetics of the aggregation process and the dynamics of the gels formed under external forcing, both for small amplitude periodic shear deformation, as large deformation rheology in shear and tensile mode. The main new aspect is that we explicitly consider non-affine deformation, in which the network itself is mediating the external stresses. As indicated above the overall neglect of many-body hydrodynamics in our calculations renders the results useless as a prediction for actual quantitative gel properties of materials with the given specifications. The main value of these model calculations is in shedding light on the details of the mechanism underlying the macroscopic rheological behavior of the model materials investigated. Also trends can be obtained from the results, on what the effect on the model system behavior of changing of parameters such as fluid viscosity.

In chapter 2 we discuss the aggregation kinetics of the destabilized model suspension within the context of our model. In the earlier simulations performed with this model we never tested whether the aggregation rates in the model are consistent with the simple model predictions of the Schmoluchowski model. It turns they are not. We present an explanation of the observed discrepancies in a Schmoluchowski model including a description of the transient effects associated with the initial particle distribution.

In chapter 3 we investigate the response of a simulated gel sample to small amplitude external sinusoidal shear deformation. In this chapter we introduce the non-affine simulation model, where the deformation is exerted at the external surface of the sample only, and mediated into the bulk by the gel structure itself. This approach is able to distinguish between different types of global gel structure. The more usual affine deformation, in which the gel deformation is assumed to be fluid mediated, mainly shows the local properties. Moreover the non-affine method can simulate surface load experiments. The non-affine model is also used in the large deformation simulations.

In chapter 4 we use our model to investigate large deformation shear rheology, the break-up of the gel due to continued shearing. Polymer gels can show a probably reversible transition from an elastic material to a viscous material under prolonged shear deformation. Due to the shear the gel network

breaks, but it reforms at the same rate. We do not observe that behavior for our particle gel model. Increasing local stresses do lead to breaking of bonds, and rupture of the network, but instead of reforming a similar global network, reorganization increases, leading to local compactification. Eventually the network is destroyed, and a dense suspension of large clusters remains. At that point our simple description of hydrodynamics is no longer valid.

In chapter 5 the same model system is considered in the context of large deformation tensile behavior. The effect of different notches is investigated and in all cases we find that within the parameter range investigated ductile fracture behavior is observed. That means that if at any point of the simulation the extension of the sample is stopped, the process of rupture also stops immediately. This is the case even for samples close to total rupture. We argue that with simulation models in general it will be difficult to study brittle fracture, because of the large difference in time scale between the process of the breaking of an individual bond, at atomic or molecular level, and that of the whole gel, at mesoscopic level.

1.1 References

- [1] P.Walstra, T.J.Geurts, A.Noomen. A.Jellema and M.A.J.S.van Boekel, *Dairy technology, principles of Milk Properties and Processes* (Marcel Dekker, New York, 1999).
- [2] P.Walstra, *Physical Chemistry of foods* (Marcel Dekker, New York, 2002).
- [3] D.M.Heyes, *J.Non-Newt.Fl.Mech.* **27** (1988) 47-85.
- [4] D.M.Heyes, *Adv.Coll.Int.Sci.* **51** (1994) 247-268.
- [5] D.Frenkel, *Physica A* **313** (2002) 1-31.
- [6] E.Dickinson, *Coll.Surf.B* 20 (2001) 197-210.
- [7] Q. Hassonjee, R. Pfeffer and P. Grantos, *Int. J. Multiphase Flow.* **18** (1992) 353.
- [8] S. Kim and S. J. Karrila, *Microhydrodynamics : principles and selected applications* (Butterworth-Heinemann, Stoneham MA 1991).
- [9] M. Lowenberg and J. Hinch, *J. Fluid Mech.* **321** (1996) 395.
- [10] E.M.Toose, D.van den Ende, B.J.Geurts, J.G.M.Kuerten, and P.J.Zandbergen, *J. Eng. Math.* **30** (1996) 31-150.
- [11] E.M.Toose, B.J.Geurts, J.G.M. Kuerten, *J.Non-Newt. Fluid Mech.* **60** (1995) 129-154.
- [12] A. J. C. Ladd, *J. Fluid Mech.* **271** (1994) 285.
- [13] A. J. C. Ladd, *J. Fluid Mech.* **271** (1994) 331.
- [14] A. J. C. Ladd, *Phys. Rev. Lett.* **76** (1996) 1392.
- [15] J. M. V. A. Koelman and P. J. Hoogerbrugge, *Europhys. Lett.* **21** (1993) 363.

- [16] J. M. V. A. Koelman and P. J. Hoogerbrugge, *Europhys. Lett.* **19** (1992) 155.
- [17] E. S. Boek, P. V. Coveny, H. N. W. Lekkerkerker, P. van der Schoot, *Phys. Rev. E* **55** (1997) 3124.
- [18] G. Bossis and J. F. Brady, *J. Chem. Phys.* **80** (1984) 5141.
- [19] G. Bossis and J. F. Brady, *J. Fluid Mech.* **155** (1985) 105.
- [20] L. Durlofsky, J. F. Brady and G. Bossis, *J. Fluid. Mech.* **189** (1987) 21.
- [21] J. F. Brady, R. J. Phillips, J. C. Lester and G. Bossis, *J. Fluid. Mech.* **195** (1988) 257.
- [22] J. F. Brady and G. Bossis, *Ann. Rev. Fluid Mech.* **20** (1988) 111-157.
- [23] G. Bossis and J. F. Brady, *J. Chem. Phys.* **91** (1989) 1866.
- [24] J. R. Melrose and D. M. Heyes, *J. Colloid Interface Sci.* **157** (1993) 227.
- [25] J. R. Melrose and D. M. Heyes, *J. Chem. Phys.* **98** (1993) 5873.
- [26] J. R. Melrose, *Europhysics Lett.* **19** (1992) 51.
- [27] J. R. Melrose, *Phys. Rev.* **44** (1991) R4789.
- [28] A. A. Potanin, *J. Chem. Phys.* **96** (1992) 9191.
- [29] A. A. Potanin, *J. Colloid Interface Sci.* **157** (1993) 399.
- [30] M. Doi and D. Chen, *J. Chem. Phys.* **90** (1989) 5271.
- [31] D. Chen and M. Doi, *J. Chem. Phys.* **91** (1989) 2656.
- [32] J.M.van der Veer, J.H.J.van Opheusden en R.J.J.Jongschaap, in *Proceedings Third European Rheology Conference*, D.R.Oliver ed. (Elseviers Science Pub., 1990, Amsterdam) pp.489-491.
- [33] A.S.Sangani and G.Mo, *Phys. Fluids* **8** (1996) 1990.
- [34] A.Satoh, G.N.Coverdale, and R.W.Chantrell, *J.Coll.Int.Sci* **231** (2000) 238-246.
- [35] R.C.Ball and J.R.Melrose, *Physica A* **247** (1997) 444-472.
- [36] R.B.Jones, *J.Chem.Phys.* **115** (2001) 5319.
- [37] L.E.Silbert and J.R.Melrose, *J.Rheol.* **43** (1999) 673.
- [38] L.E.Silbert, R.S.Farr, J.R.Melrose and R.C.Ball, *J.Chem.Phys.* **111** (1999) 4780.
- [39] A.A.Catherall and J.R.Melrose, *J.Rheol.* **44** (2000) 1.
- [40] K.G.Soga, J.R.Melrose, and R.C.Ball, *J.Chem.Phys.* **108** (1998) 6026.
- [41] K.G.Soga, J.R.Melrose, and R.C.Ball, *J.Chem.Phys.* **110** (1999) 2280.
- [42] M.Whittle and E.Dickinson, *Mol. Phys.* **90** (1997) 739-757.
- [43] M.Hütter, *J.Coll.Int.Sci.* **231** (2000) 337-350.
- [44] B.H.Bijsterbosch, M.T.A.Bos, E.Dickinson, J.H.J.van Opheusden, and P.Walstra, *Farad. Disc.* **101** (1995) 51-64.
- [45] M.T.A.Bos and J.H.J.van Opheusden, *Phys. Rev* **E53** (1996) 5044-5050.
- [46] T.van Vliet and P.Walstra, *Farad. Disc.* **101** (1995) 359-370.
- [47] M.Mellema, J.H.J.van Opheusden and T.van Vliet, in *Food Emulsions and Foams*, E.Dickinson and J.M.Rodriguez-Patino eds., The Royal Chemical Society, Cambridge, 1999, 307-317.

-
- [48] M.Mellema, J.H.J.van Opheusden and T.van Vliet, *J.Chem.Phys* **11** (1999) 6129-6135.
 - [49] M.Mellema, J.W.M.Heesakkers, J.H.J.van Opheusden and T.van Vliet, *Langmuir*. **16** (2000) 6847-6854.
 - [50] M. Mellema, J. H. J. van Opheusden, and T. van Vliet, *J.Rheol.* **46** (2002) 11-29.
 - [51] M. Mellema, P. Walstra, T. van Vliet, and J. H. J. van Opheusden, *Adv Coll. Int. Sci.* **98** (2002) 25-50.
 - [52] E. Dickinson, *J.Coll.Int.Sci.* **225** (2000) 2-15.

Chapter 2

Brownian Dynamics simulation of aggregation kinetics of hard spheres with flexible bonds¹

Brownian Dynamics simulations have been performed on the aggregation dynamics of colloidal particles within the context of a ball-and-string model. Particles are treated as hard spheres that can bind irreversibly through a string attached to their surface. The model is set up to mimic some aspects of the aggregation of casein micelles in renneted milk. In this study we test the model of Smoluchowski by comparing it with our BD simulation model. Aggregation kinetics was studied by models in a range of volume fractions from $\phi = 4 \times 10^{-6}$ to 0.20. We found aggregation rates close the Smoluchowski rates at the low volume fractions, increasing sharply at higher concentrations. Simulations for simpler models also give rates slightly above theoretical values, but only at very high dilution. We show that only when a large fraction of the particles have already clustered is the quasi-stationary solution used in Smoluchowski theory attained. This partially explains the increase of the rate with volume fraction. The steep increase in the rate with volume fraction also explains why fractal aggregation, in which the effective volume fraction of the clusters increases with cluster size, leads to gelation.

2.1 Introduction

Aggregating colloidal systems consist of two phases. One is the suspending fluid, the other is the colloidal particles, which on aggregation may form a percolating network. Its structure largely determines the mechanical properties of the sample. The aggregation of an initially stable system can be induced by a number of different factors, such as heating and enzyme action. Conditions used during aggregation strongly affect kinetics and the mechanism of aggregation and so the texture, porosity, and rheology of resulting gel. An example from the food domain is yogurt, in which the particles forming the network are casein micelles [1, 2].

¹ A.A. Rzeplia, J.H.J van Opheusden and T. van Vliet, *J.Coll.Interf.Sci.* **244** (2001) 43-50.

In recent years, several Brownian Dynamics simulation studies have been published on the formation and properties of particle gels [3 - 5]. The resulting structure of the gels is analyzed through fractal models [6, 7] which have stimulated understanding of aggregation processes [8].

Analytical models on particle aggregation attempt to describe the process in a strongly simplified form [9, 10]. Differences between the size and shape of particles and their geometrical distributions are neglected to be able to derive analytical results. In simulations approximations still have to be made, but fewer ones. One important advantage of simulations is that the positions and, if relevant, the orientations of all particles can be included in the model. The effect of particle distributions is especially important when the aggregates become space filling. Then a crossover occurs between models for aggregation in very dilute systems and percolation models for gel formation.

In earlier work, some of us [2, 3, 5] studied the gelation process within the context of a simple Brownian Dynamics (BD) simulation model of hard spheres that bind irreversibly through flexible strings. The model includes both translational and rotational diffusion of the particles involved. Because of the simplicity of the model the dynamics can be followed over large time intervals, also allowing the study of gel aging phenomena in reasonable CPU times. We use the same model to study aggregation kinetics in the early stages. We compare the simulation results with predictions from Smoluchowski theory.

A theoretical framework to classify the wide variety of growth processes in coalescing systems was introduced in 1917 by Smoluchowski [11] and has been used extensively since. It uses a mean field approach to the kinetics of aggregation. It has received great attention in earlier studies and has been explicitly solved numerically for some forms of coagulation kernels [12], especially for a constant coagulation kernel [13, 14], where the aggregation rate is independent of cluster size or mass. Meakin [9, 10] has extensively discussed calculations of coagulation kernels through different existing theories. The theory with a constant coagulation kernel cannot describe gelation; only when the rate increases substantially fast with cluster size, may gelation occur.

The theory of Smoluchowski with a size scaled coagulation kernel may adequately describe the early aggregation stages in a dilute system, but still fails to take into account the effects of various cluster shapes, which are formed during the coagulation process. A second shortcoming is that the model uses a mean field approximation, implying that the system must be within limitations of ideal mixing, geometrical correlations are largely ignored. A third approximation is that the sol must be so dilute that collision between more than two clusters can be neglected. Finally it assumes that the process is in its asymptotic quasi-stationary state, where effects of the initial configuration have relaxed. It has been shown before [12] that the model of Smoluchowski nevertheless can describe aggregation processes taking place in some specific

aggregating systems with quite good agreement. Very good agreement was found by Puertas [15] between constant coagulation kernel from theory and BD simulation. However, very little detail is given about the simulation method used. Diffusion-limited aggregation of an initially monodisperse suspension is well modeled by a constant kernel during the early stages of the reaction [14, 16, 17]. In experiments one usually finds lower rates, by a factor of about 2, that could be attributed to short range hydrodynamic repulsion. The reasonable agreement between model and experiment might however, be due to a fortuitous cancellation of effects that are neglected in the model.

2.2 Brownian Dynamics Model

The model we are considering contains N hard spheres of radius a , placed in a three-dimensional cubic box. The particles move through the solvent due to random displacements. When two particle surfaces come within a bonding distance R_{bond} , a flexible bond or string is formed. The bond once formed is permanent. The attachment points are fixed on the surface, and rotate with the particle. The bond is completely flexible but can not be stretched beyond R_{bond} . Relative particle motion due to rotational and translational diffusion is possible as long as it does not result in bond stretching or particle overlap. Hence the model allows for cluster and gel reorganization.

A BD simulation model is based on the Langevin equation, the dynamical equation of motion for a system of diffusing particles. The total force here is the sum of the net force of interaction between particles, the random Brownian force and hydrodynamic interactions. The solvent is regarded as continuous and the Brownian force mimics thermal collisions between the solvent and the dispersed particles. In the case of hard spheres (no direct interaction), the force on particle i is given by the equation

$$F = m \frac{d^2 r_i}{dt^2} = R_i + H_i, \quad (1)$$

where R_i is the random (Brownian) force and H_i is the force modeling hydrodynamic interactions, r_i is the position of particle i , and t is the time. We approximate H_i by simple Stokesian friction, neglecting hydrodynamic interactions between particles. The liquid drag force on a single particle, H_i , is proportional to the particle velocity,

$$H_i = \gamma \frac{dr_i}{dt}, \quad (2)$$

where $\gamma = 6\pi\eta a$ is the Stokes drag, η is the solvent shear viscosity, and a the particle radius. Furthermore the model uses constraint forces for the stretching of the bonds and the hard core repulsion of the spheres.

The size of the simulation box determines the volume fraction of the particles. Periodic boundary conditions are used to avoid edge effects. All parameters corresponding to sizes or distances are normalized to the radius of a particle ($a = 1$) and all parameters corresponding to energies are normalized to units of $k_B T$ ($k_B T = 1$).

Equation (1) is solved numerically, enabling us to follow the movements of each particle through the system in consecutive constant time steps. By choosing the time step much larger than the relaxation time of the particle velocities we can neglect the second order term in (1), so

$$\frac{dr_i}{dt} = -\frac{1}{6\pi\eta a} R_i. \quad (3)$$

This is called the large damping limit. To solve the remaining first-order differential equation of motion we use the Euler forward method, which gives us

$$\Delta r_i(t + \Delta t) = \frac{\Delta t}{6\pi\eta a} R_i(t). \quad (4)$$

The effect of the random force R_i is a translational displacement that, on average, obeys Einstein's law for an isolated particle. For instance in the x direction this gives us

$$\Delta x_i^R(t + \Delta t) = N_s \sqrt{6D_T \Delta t}, \quad (5)$$

where $D_T = 1 / 6\pi\eta a$ ($k_B T = 1$) is the translational diffusion coefficient, which is normalized to unity. The parameter N_s is a random number, which has a uniform distribution on the interval $(-1, 1)$, and its average square is given by

$$X^2 = \frac{1}{2} \int_{-1}^1 x^2 dx = \frac{1}{3}. \quad (6)$$

The dimensionless root-mean-square displacement in the x direction, in the absence of interactions is equal to $\sqrt{2D_T \Delta t}$. At each time step three independent uniform random numbers are drawn to calculate the stochastic displacement vector for each particle. This implies that in the absence of interactions, the displacement vectors for different particles at each time step are uncorrelated. The number of steps that the simulation has passed, is given by the parameter $N_{\Delta t}$. It is a direct measure of time.

Apart from the translational diffusion the individual particles also undergo rotational diffusion. The rotational motion is governed by the diffusion coefficient D_R (note that $a = 1$):

$$D_R = \frac{3D_T}{4}. \quad (7)$$

The implementation of rotational diffusion in the model is similar to that of translational diffusion. Rotational diffusion of clusters results from combined translations and rotations of the individual particles.

The hard core repulsion and the finite length strings lead to constraints, which when violated are being removed iteratively by moving and rotating the involved particles using the SHAKE procedure [18]. The motion of a particle within a cluster results from combined translational and rotational diffusion and removal of the constraints.

2.3 Aggregation Kinetics

The theory of Smoluchowski, originally designed for coagulation of spherical droplets, can also be used to describe particle cluster formation. It assumes that aggregating particles and clusters behave in a similar fashion. The theory is given in the form of a set of differential equations describing the rate at which the concentration, z_n , of clusters of size n changes with time, t , during an aggregation process:

$$\frac{dz_n}{dt} = \frac{1}{2} \sum_{i+j=n} K_{ij} z_i z_j - z_n \sum_{j=1}^{\infty} K_{nj} z_j. \quad (8)$$

The first term gives the rate of creation of clusters of size n by aggregation of two smaller clusters, and the second term gives the rate at which clusters of size n are eliminated by further aggregation. The coagulation kernel K_{ij} gives the rate constants for these processes. Eq. (8) does not include bond-breaking processes. Furthermore, for (8) to apply, the solution must be so dilute that collisions between more than two clusters can be neglected.

The kinetics of the model is largely contained in the coagulation kernel. It determines the number of collisions per time unit between an i -mer and a j -mer that result in bonding. The original Smoluchowski approach uses a single constant kinetic kernel, which is assumed to be independent of the form or size of the aggregates that are coagulating. A more general description incorporates a power law scaling of the kinetics kernel with volume fraction [19].

The standard coagulation kernel for rapid coagulation Eq. (8) is calculated as:

$$K_{ij} = 4\pi R_{ij} D_{ij} \quad [m^3 s^{-1}], \quad (9)$$

where R_{ij} is radius of a sphere of action and D_{ij} is the relative diffusion coefficient. For monomers with $R_{ij} = a_i + a_j$ and $D_{ij} = 2D_T$, this results in the standard Smoluchowski rate constant:

$$k_S = 8\pi D_c a. \quad (10)$$

In the case of Stokes friction the diffusion constant, D_c , will scale inversely with cluster size, leading to almost constant kernels. In the free draining limit we apply, the diffusion constant scales with cluster mass N as $1/\sqrt{N}$, while fractal scaling gives $N \propto R^D$, with D the fractal dimensionality. For fractal clusters with $D = 1.45$, the value we find for translational and rotational diffusion-limited cluster aggregation without reorganization, results in $k_S \propto N^{-0.2}$; for $D = 2.2$, with much reorganization, one finds $k_S \propto N^{-0.05}$. In view of these coefficients no large effect of the cluster size on k_S can be expected.

Equation (8) with constant coagulation kernel can be analytically solved to give equations for the change of the total number of clusters, single particles, doublets, and n -mers [20]:

$$\sum z = z_1 + z_2 + z_3 + \dots = \frac{z_0}{1 + k_S z_0 t}, \quad (11)$$

$$z_1 = \frac{z_0}{(1 + k_S z_0 t)^2}, \quad (12)$$

$$z_2 = \frac{z_0 (k_S z_0 t)}{(1 + k_S z_0 t)^3}, \quad (13)$$

$$z_n = \frac{z_0 (k_S z_0 t)^{n-1}}{(1 + k_S z_0 t)^{n+1}}. \quad (14)$$

Here z_0 is the initial number of primary particles per unit volume.

To describe the aggregation process, we calculated different coagulation kernels, k_S , by fitting simulation results for the total number of clusters, and for clusters of size up to six particles, to the equations above (see Table 1). Thus, we compare the evolution of the aggregating systems obtained from our BD model with that predicted by the theory of Smoluchowski. Curves representing the number of clusters as a function of time obtained from the model and the theory will be compared for various values of particle volume fraction ϕ .

2.4 Results

Our Brownian Dynamics simulations start by placing primary particles in the simulation box in random fashion but avoiding particle overlap. The particles diffuse through the box due to the random Brownian force, and form clusters through strings between fixed points on their surfaces. A string is formed when a particle surface comes within the specified bonding range of $R_{\text{bond}} = 0.1$, one-tenth of the particle radius. That value is also the maximal length of the string. Up to 12 bonds can be attached to one particle, fixed on its surface. In practice for these short string lengths that number is rarely obtained.

The BD simulation model has two parameters that may be optimized to quickly give results without affecting the accuracy. To obtain fast results one would like to consider a system with a small number of particles and simulate it with large time steps. We tested our BD simulation model in a range of particle numbers from 100 to 10,000, to check whether the size of the system was influencing calculated results, the kernel k_s , and its precision, Δk_s . We observed (Fig. 1) that curves for the number of clusters of given size as a function of time, have less statistical noise for big systems. We chose to use a system size of 1000, which allows relatively fast calculations and gives statistically smooth results. Earlier results from gelation simulations, moreover, have shown that such a system size is needed to have clusters grow to their appropriate dimensions, and become space spanning. For the lower densities we had to use larger systems because of the large statistical error due to the low collision rate.

The BD model was also tested to find an optimal time step. The random numbers for the translational and rotational displacements generated at each

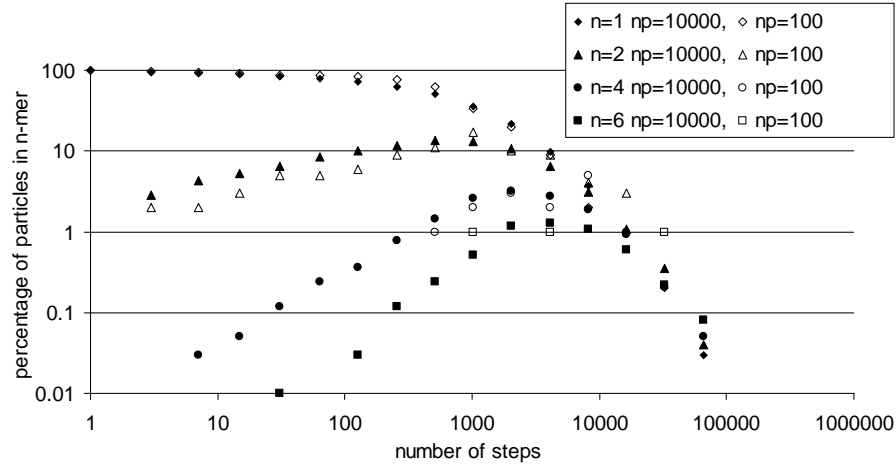


Fig. 1. Percentage of particles in n -mers ($n = 1, 2, 4, 6$) as a function of simulation time for two system sizes. Full symbols: system of 10,000 particles, empty symbols: system of 100 particles. Volume fraction is 3% simulation time step, $\Delta t = 0.001$.

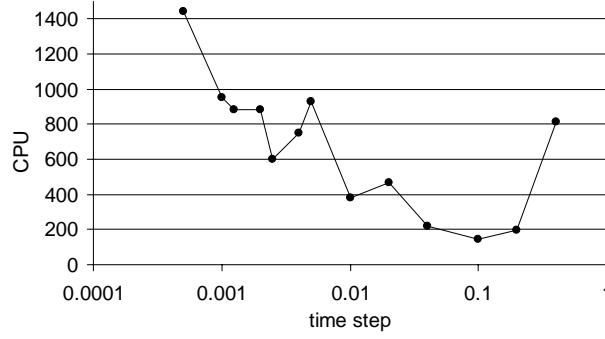


Fig. 2. Computer CPU time of a simulation run as a function of time step. The number of steps, $N_{\Delta t}$, times the time step, Δt , is constant for all the runs. Maximal number of SHAKE iterations is set to 5000. System of 3% volume fraction, 1000 particles, and on average one bond per particle.

time step for all the particles are relatively unimportant, as they are all uncorrelated. Their number scales simply with the inverse time step and the number of particles. More important are the model constraints, bond stretches and particle overlaps. Those constraint violations are detected by checking all (relevant) pairs, and are removed iteratively. Increasing the simulation time step results in larger, or even more constraint violations per step, while too large a step may produce unphysical results. For larger time steps the pair list mechanism we used is less efficient, and in general, larger time steps result in more iterations. Fig. 2 shows that above $\Delta t = 0.1$ simulation times increase due to the many SHAKE iterations necessary. In this study we chose to use a time step of 0.001, well below the point where constraint removal becomes a problem. We set the maximal number of SHAKE iterations to 100, leaving the remaining constraint violations, if present, to be removed by the Brownian motion in the next step. For systems that have not formed gels, as we study here, this limit is rarely reached. With this time step and system size even the longest of the simulation runs can be ran overnight on a simple PC (500MHz Pentium).

The BD model was used to study aggregation kinetics as a function of volume fraction, ϕ , in the range of 4×10^{-6} to 0.20. Figure 3 shows three stages of aggregation of a 3% system generated by the BD model. The evolution of the number of clusters during simulation time for the same system is presented in Fig. 4. The drawn curves represent the fitted values according to Smoluchowski theory. The constant coagulation kernels, k_s , were calculated for each curve separately, through nonlinear regression, to fit the theory. A dynamic scaling of kernels was found in earlier studies *e.g.* [21]; here since differences between obtained kernels were not systematic and within statistical error we took their weight average. Table 1 gives the kernels for the total number of clusters, for the clusters of size up to six particles and their weight average. The analysis

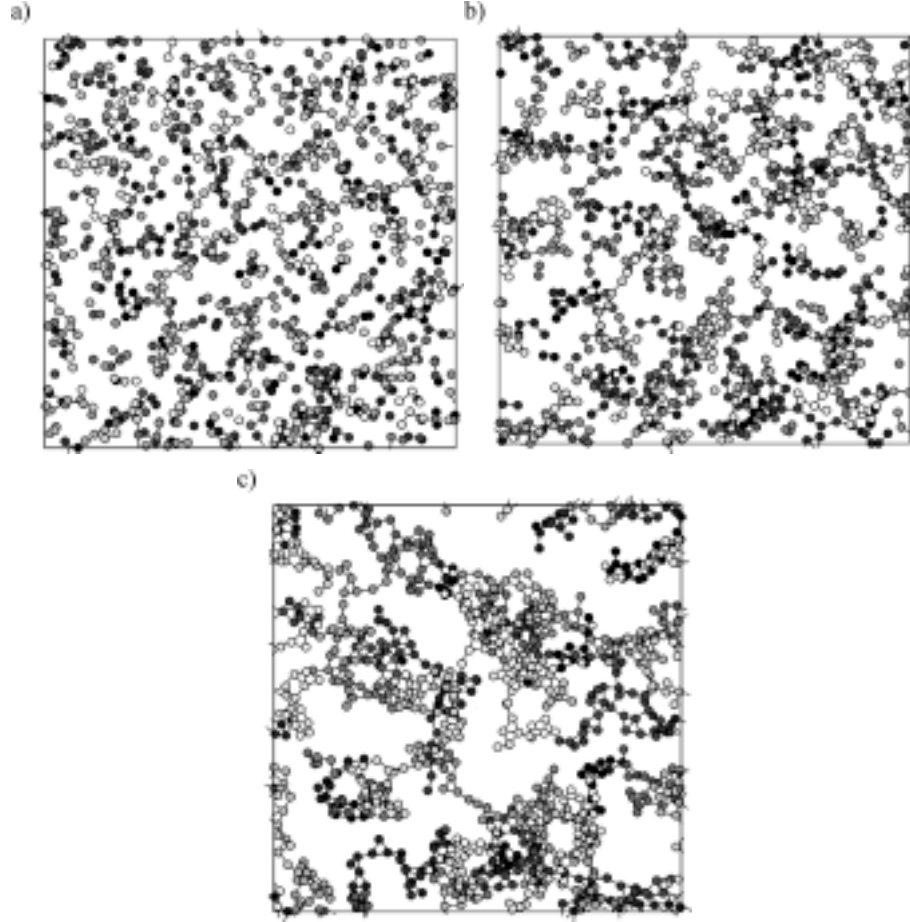


Fig. 3. Two-dimensional representation of 3D aggregating system in three stages as simulated with BD model. Shading indicates the depth of the picture; for clarity particle size is reduced to half of its actual size, so bonds are much longer than in reality. System of $\phi = 3\text{vol}\%$ at simulation stages: a) $N_{\Delta t} = 1750$, $N_{\text{agg}} = 468$; b) $N_{\Delta t} = 9250$, $N_{\text{agg}} = 159$; c) $N_{\Delta t} = 65500$, $N_{\text{agg}} = 21$; ($\Delta t = 0.001$, N_{agg} = number of all aggregates).

included only an intermediate time range of the curves. Data points at early times, with high statistical noise, which we took to be the points where the number of clusters of given size was less than 4 were omitted. Moreover, for late times, gelation occurs. The gel-point was defined somewhat arbitrarily as the moment at which 50% of all particles build the largest aggregate. Data points beyond “gelation” were omitted as well. We also checked this by plotting $1/z$ and $1/\sqrt{z_1}$, with z and z_1 the cluster density and monomer density, as a function of time. According to Eqs. (11) and (12) these produce linear curves if Smoluchowski theory applies. The linear parts of these curves indeed roughly corresponded with the intervals we used, be it with a too steep slope at higher ϕ .

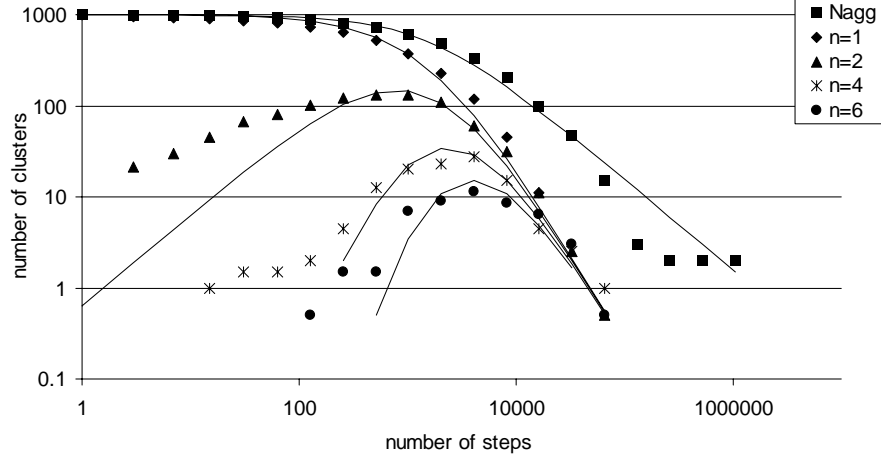


Fig. 4. Number of clusters, n -mers, as a function of simulation time. $\phi = 3\text{vol}\%$, $N = 1000$, $\Delta t = 0.001$. Points represent BD simulation results; lines represent theory results with $\langle k_S \rangle = 88.14$. (N = number of particles).

For the system of $\phi = 0.03$ the calculated value of k_S is 88. That is considerably above the value predicted by theory: $k_S = 4\pi R D_T$, where $R = 2a$ is the radius of action and D_T is the diffusion coefficient for a single particle. As we use reduced units of $D_T = 1$, and $a = 1$ in our simulations, we expect to find a value of $8\pi \approx 25$. For dilute systems of 0.01% we find values slightly above this result, but with quite a large statistical error. For systems of higher volume fraction the values of k_S rapidly go up. The calculated kernels are plotted as a function of ϕ in Fig. 5 with the \bullet symbol.

Theoretical fits to simulation results are presented for three volume fractions: $\phi = 3\%$ (Fig. 4), $\phi = 16\%$ (Fig. 6), and $\phi = 0.1\%$ (Fig. 7). For the 3% system the early stage of aggregation in the BD model was even faster than reported above. This is due to the homogenous random initial configuration,

	0.01 vol%	0.1 vol%	1 vol%	3 vol%	10 vol%	16 vol%	20 vol%
k_S for Σz	26.9	30.4	50.6	81.0	314.1	635.6	1124.7
k_S for z_1	29.2	33.5	55.9	107.4	366.7	717.4	1121.8
k_S for z_2	26.2	30.4	58.6	123.4	494.7	740.3	1220.8
k_S for z_3	27.1	28.1	39.5	93.6	406.1	705.2	1593.1
k_S for z_4	27.5	28.1	59.2	87.2	312.6	577.7	1909.8
k_S for z_5	22.1	27.8	45.9	85.4	384.6	765.9	1794.6
k_S for z_6	19.2	22.6	38.8	91.6	293.0	874.9	1250.2
$\langle k_S \rangle$	25.2	31.3	49.0	88.1	342.4	691.9	1409.9

Table. 1. k_S value for the total number of clusters, for clusters of size up to six particles and their weight average.

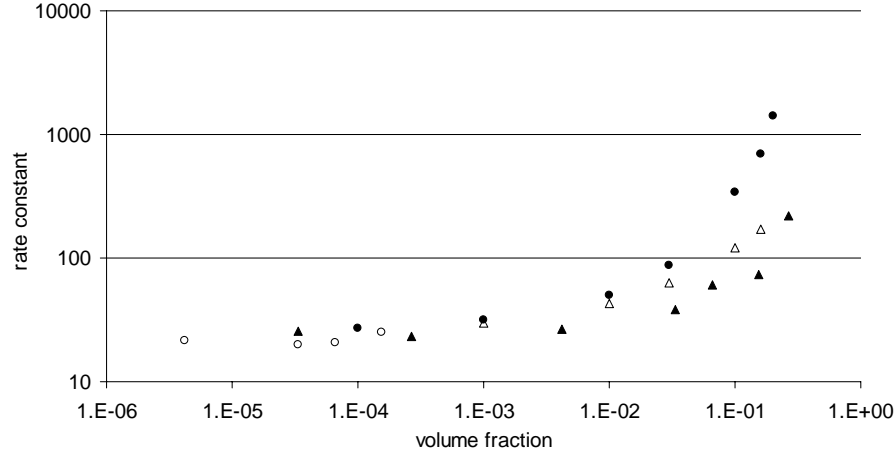


Fig. 5. Weighted average of kernels from ball-and-stick model (●, ○) and effective rate constant from coalescence model (▲, △) as a function of volume fraction. ○, Results from ball-and-string model for volume fractions below 0.01%; △, results from coalescence model for fixed measurement point at 50% particle disappearance.

with constant pair correlation function. Before the quasi-stationary pair correlation function profile is formed many particles have clustered. We discuss this point in detail later, as it may be a partial explanation for the increasing effective rate constant.

In the 16% system (Fig. 6) the aggregate growth is so fast that the early regime, where we still see the effects of the random initial distribution, and the late regime, where a gel has formed, could have overlapped. We were still able to derive some results from the center parts of the curves, giving very high effective rates.

2.5 Discussion

Before we discuss the results in more detail we take a somewhat closer look to Smoluchowski theory. The rate constant $k_S = 4\pi R D_T$ is calculated for the stationary state situation, where the density around a center of aggregation is a solution of the diffusion equation with boundary conditions zero at the radius of action and the homogeneous density at infinity. As all particles are centers of aggregation that applies to the pair correlation function rather than the density. One point to note is that we start our simulations with a uniform pair correlation function, which according to Fick's first law gives a large flux for a short period before the asymptotic state is reached. According to *e.g.* Overbeek [22] the time needed to reach steady state is of the order $t = 8\phi T_f$, where the flocculation time T_f is the time needed for the number of clusters to decrease half the original number. For $\phi = 3\%$ that implies about 30% of the original particles are joined

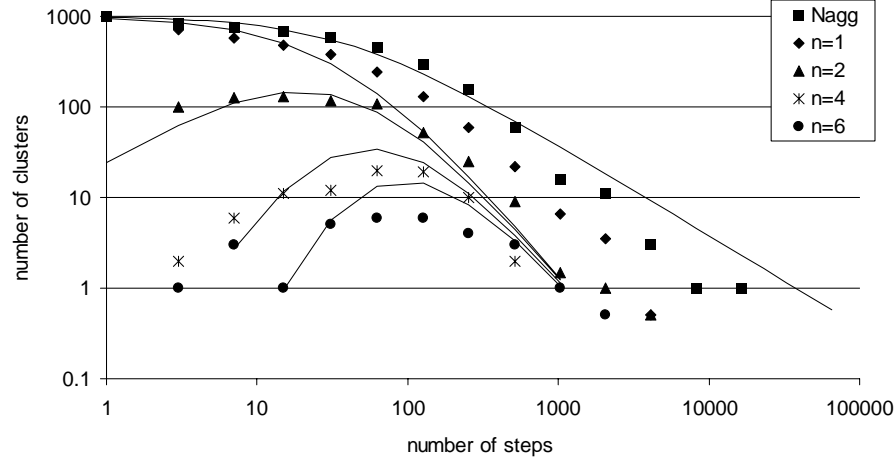


Fig. 6. Number of clusters, n -mers, as a function of simulation time. $\varphi = 16\%$, $N = 1000$, $\Delta t = 0.001$. Points represent BD simulation results, lines represent theory results with $\langle k_S \rangle = 691.86$.

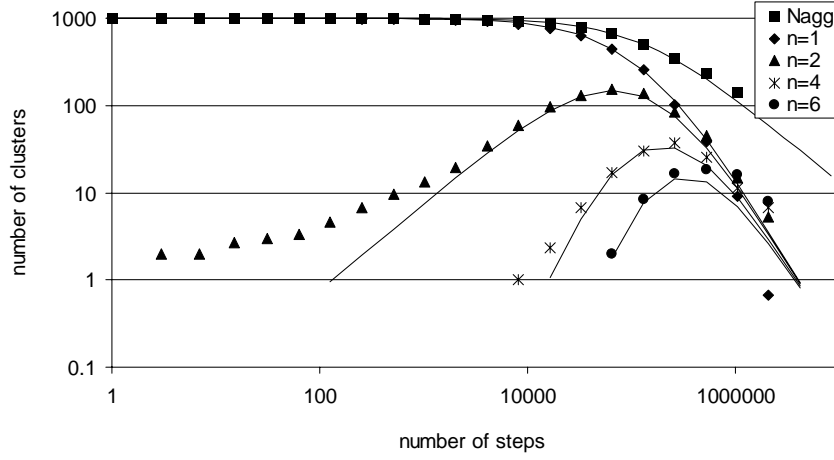


Fig. 7. Number of clusters, n -mers, as a function of simulation time. $\varphi = 0.1\%$, $N = 1000$, $\Delta t = 0.001$. Points represent BD simulation results, lines represent theory results with $\langle k_S \rangle = 31.60$.

into larger clusters before we should expect our curves to level off, and for higher densities the situation could become even worse. We will come back to this point below.

For one of the lower volume fractions we have investigated, $\varphi = 10^{-4}$, our result is still slightly above the theoretical value. This may be due to the fact that the radius of interaction for the BD model (at least for monomer-monomer bonds) should be taken $R = R_{\text{bond}} = 2.1$, bringing the theoretical prediction to

approximately 26, where we find 27, a fair agreement. Simulations at still lower volume fractions become increasingly troubled by statistical noise, due to the low absolute rate of aggregation. In model calculations down to $\phi = 4 \cdot 10^{-6}$ we have found values for k_s around 20 (see Fig. 5, symbol \circ), but we have no trustful estimate for the statistical error. Lower values for k_s are commonly found in experiments [16, 17, 23, 24], and are normally addressed to a remaining short-range (effective) repulsion between the aggregating particles, because of incomplete destabilization (*e.g.*, remaining charges) or hydrodynamic pair interaction (lubrication). As we have neither effect in our model, these cannot be the cause of the discrepancy found.

To investigate the discrepancy at higher volume fraction, we have performed calculations for both the reaction rate and for the pair correlation function in a modified BD model. In this second model the freely diffusing particles do not form bonds, but join to form a single particle of unit radius upon first contact (at $R = 2a$). This second simulation model hence remains as close as possible to the original rapid coagulation model of Smoluchowski. A similar particle coalescence model and its kinetics were studied before *e.g.* [25]. The difficulty in calculating the pair correlation function in the original model was that clustered particles make a large contribution at short distances. In the second model we always have only monomers. For this model we only investigated the development of total number of particles. Plotting $1/z(t)$ against t according to Eq. (11) gives a linear relation, which can be fitted to give k_s . The results are gathered in Fig. 5 (see symbol \blacktriangle). At low volume fractions we obtain the Smoluchowski value, and a rapid increase at higher concentrations, similar to what we found in the ball-and-string model.

The model as used by Smoluchowski is somewhat too simple, but it turns out that can be repaired relatively easily. We consider the density of particles around a single fixed sphere. This density is not described by the diffusion equation alone, but there is a sink term due to mutual collisions between the surrounding particles. Let the density of primary particles be z_0 ; then the density around a single primary particle satisfies

$$z_t = D_T \Delta z - k(t) z z_0, \quad (15)$$

where Δ is the Laplace operator, and the sink term describes the rate at which the surrounding particles are removed by collisions with other centers of attraction. At infinity the density is z_0 , at the interaction radius, the diameter d of the central particle, there is a (nonstationary) flux

$$j = 4\pi d^2 D_T z_r(d), \quad (16)$$

that describes their disappearance. As this is true for each particle, their overall disappearance is given by

$$z_0' = -z_0 j = -4\pi d^2 D_T z_0 z_r(d), \quad (17)$$

so the density at infinity around the central sphere is dropping. When we define $z(t) = z_0 g(t)$, substitute this in (15) and use (17), we find for the pair correlation function g :

$$g_t = D_T \Delta g - g z_0 [k(t) - 4\pi d^2 D_T g_r(d)]. \quad (18)$$

Now this system can be made consistent by considering the terms in square brackets to cancel. The function $g(r, t)$ then satisfies the diffusion equation without sink term, and the solution with $g(r, 0) = 1$ for $r > d$, $g(r, t) = 0$ for $r \leq d$, and $g(r, t) = 1$ for $r \rightarrow \infty$ becomes the standard result

$$k(t) = 4\pi d^2 D_T g_r(d) = 4\pi d D_T (1 + d/\sqrt{\pi D_T t}). \quad (19)$$

Note that this rate constant is singular due to the second term, the initial transient, at $t = 0$, but the number of particles that disappears remains finite. Using (17) and (19) we find $z_0' = -4\pi d D_T z_0^2 (1 + d/\sqrt{\pi D_T t})$, which can be solved analytically to give

$$z_0(t) = \frac{z_0(0)}{1 + 4\pi d D_T z_0(0)t (1 + 2d/\sqrt{\pi D_T t})}. \quad (20)$$

This suggests that for all volume fractions, we eventually arrive at Eq. (11), but it may take quite some time, during which a large fraction of the particles has clustered. From the above we can distinguish two time scales:

$$t_i = \frac{d^2}{\pi D_T}, \quad (21)$$

the time scale of the transient effect of the initial situation, and

$$t_a = \frac{1}{4\pi D_T d z_0(0)}, \quad (22)$$

the time scale of the aggregation process itself also called the aggregation time. Without the correction term for the transient, the number of particles decreases to half its original value over the aggregation time. The relation between the time scales is

$$t_i = 4d^3 z_0(0) t_a = \frac{24}{\pi} \varphi t_a, \quad (23)$$

with φ the initial volume fraction (note that $24/\pi \approx 8$, giving the estimate of Overbeek [22]). This means that for higher volume fractions the transient effect

is larger. Because of the correction term the number density at the aggregation time actually decreases with volume fraction according to

$$z_0(t_a) = \frac{z_0(0)}{2(1 + \sqrt{(24/\pi)\phi})} \quad (24)$$

For a volume fraction of 3% this implies that at the aggregation time the number density of the clusters is reduced to one-third the original density, rather than one half.

As the transient, especially for the higher volume fractions, after an initial rapid singular effect dies out so slowly (as $t^{-1/2}$), it is not correct to fit the observations to equation (11); rather, (20) should be used. The theoretical curve as given by (20), with $k_S = 8\pi$, fits simulation data points very well and better than a parameterized fit according to (11). An example plot for a dilute system $\phi = 0.1\%$ is given in Fig. 8. Just using visual inspection of the graphs of $1/z$ against time, as we have done in our analysis of the modified BD model, systematically gives too high values for the observed rate constant $k_{\text{eff}}(t) = 4\pi d D_T (1 + 2d/\sqrt{\pi D_T t})$. If we for instance fix the measurement point to where approximately 50% of the particles has disappeared, we find $k_{\text{eff}} = 30, 43, 63, 120$ and 170 for $\phi = 0.001, 0.01, 0.03, 0.10$ and 0.16 respectively. These values are larger than those reported above for the simplified model, but

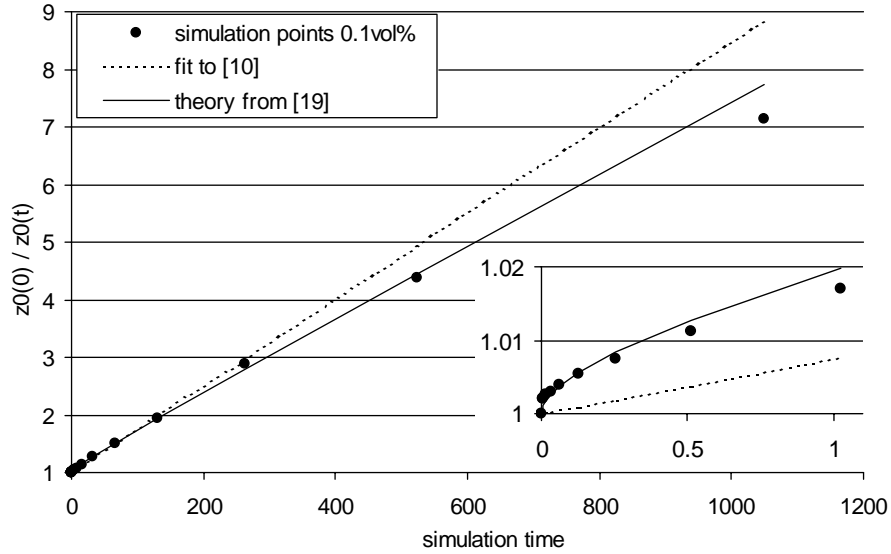


Fig. 8. Fit of equation (11) to simulation data points for total sum of clusters, and theory curve given by (20). Simulation data points for dilute system, $\phi = 0.1\%$.

generally smaller than those reported for the ball-and-string model see (Fig. 5, symbol Δ). Note that for the lower volume fractions, 50% is quite outside of our range; 10% aggregation is already a large fraction, for which at $\phi = 0.001$ an effective rate constant around 40 is calculated according to the modified model above. It appears the initial transient could be responsible for a large part of the effect of ϕ on k_s we observed, but for the more realistic system other aspects, such as cluster structure and many body collisions, probably are important too, especially at the higher volume fractions. For the lower volume fractions the transient correction as determined by the modified BD model above seems to overestimate the effect. The effect of the initial configuration on the observed kernel is discussed in more detail in a forth-coming paper [26].

2.6 Conclusion

We have found for a simple ball-and-string model for aggregation that the rate of aggregation for binding upon reaching the interaction distance in simulation exceeds the value as predicted by the Smoluchowski theory for fast aggregation. For volume fractions below about 0.1% the discrepancy is small, and might well be due to statistical error. There is a good agreement for cluster growth rates at several small cluster sizes. Calculations for a simplified model, where particles unite at collision, show a less pronounced increase in the effective rate constant with volume fraction. Analysis of the Smoluchowski theory shows that the increase in the observed aggregation rate may well be attributed to an initial transient from a fully random configuration to one with a pair correlation profile satisfying Fick's law for diffusion. For low volume fraction the transient correction seems to be too large. For the ball-and-string model the transient is only a partial explanation; other factors such as cluster shape and multiparticle collisions or (equivalently) multiparticle correlation functions are of importance.

2.7 References

- [1] M. Mellema, F.A.M. Leermakers, C.G. de Kruif, *Langmuir* **15** (1999) 6304.
- [2] M. Mellema, J.H.J. van Opheusden, and T. van Vliet, in "The Royal Chemical Society." (E. Dickinson and J.M. Rodriguez-Patino, Eds.), p. 307. Cambridge, 1999.
- [3] M.T.A. Bos, and J.H.J. van Opheusden, *Phys. Rev. E* **53** (1996) 5044.
- [4] M. Whittle, and E. Dickinson, *Mol. Phys.* **90** (1997) 739.
- [5] M. Mellema, J.H.J. van Opheusden, and T. van Vliet, *J. Chem. Phys.* **111** (1999) 6129.
- [6] E. Dickinson, *J. Coll. Int. Sci.* **225** (2000) 2.

- [7] J.H.J. van Opheusden, *Physica A* **252** (1998) 10.
- [8] P. Meakin, *J. Sol-Gel Sci. and Technology* **15** (1999) 97.
- [9] P. Meakin, *Adv. Colloid Interface Sci.* **28** (1988) 249.
- [10] P. Meakin, *Ann. Rev. Phys. Chem.* **39** (1988) 237.
- [11] M.Z.von Smoluchowski, *Phys. Chem.* **92** (1917) 129.
- [12] F. Family, and D.P. Landau, "Kinetics of Aggregation and Gelation." North Holland, Amsterdam, 1984.
- [13] R.M. Ziff, in "Kinetics of Aggregation and Gelation." (F. Family and D.P. Landau, Eds.), p. 191. North Holland, Amsterdam, 1984.
- [14] A. Puertas, J.A. Maroto, and F.J. de las Nieves, *Colloids Surf. A* **140** (1998) 23.
- [15] A.M. Puertas, A. Fernandez-Barbero, and F.J. de las Nieves, *Comput. Phys. Comun.* **121-122** (1999) 353.
- [16] H. Gedan, H. Lichtenfeld, H. Sonntag, and H.J. Krug, *Colloids Surf.* **11** (1984) 199.
- [17] J. Cahill, P.G. Cummins, E.J. Staples, and L. Thompson, *Colloids Surf.* **18** (1986) 189.
- [18] M.P. Allen, and D.J. Tildesley, "Computer Simulation of Liquids." Oxford University Press, Oxford, 1993.
- [19] C.J. Brinker, and G.W. Scherer, "Sol-Gel Science, The physics and Chemistry of Sol-Gel processing" Academic Press, San Diego, 1990.
- [20] H. Sonntag, and K. Streng, "Coagulation Kinetics and Structure Formation" Plenum Press, New York, 1987.
- [21] P.G.J. van Dongen, and M.H. Ernst, *Phys. Rev. Lett.* **54** (1985) 1396.
- [22] H.R. Kruyt, *Colloid Science*, Elsevier, Amsterdam, 1952 (Chapter VII).
- [23] J.W.TH. Lichtenbelt, C. Pathmamanoharan, and P.H. Wiersema, *J. Coll. Int. Sci.* **49** (1974) 281.
- [24] P.N.G. Penners, and L.K. Koopal, *Colloids Surf.* **28** (1987) 67.
- [25] K. Kang, S. Redner, P. Meakin, and F. Leyvraz, *Phys. Rev. A* **33** (1986) 1171.
- [26] J.H.J. van Opheusden, A.A. Rzepiela, and T. van Vliet, *in preparation*.

Chapter 3

Small non-affine shear deformation of particle gels studied by Brownian Dynamics simulations¹

We have studied the effect of small periodic shear deformation on a simulated sample of a model gel. The gel consisted of a network of spherical particles, irreversibly bound through non-central bonds at their surfaces. Brownian Dynamics simulations were performed at zero temperature, including only the Stokesian friction of the spheres in the suspending fluid. Many particle hydrodynamic effects were ignored. The shear deformation was imposed by moving the surfaces only, applying Lees-Edwards boundary conditions without the usual accompanying linear bulk fluid flow field. This led to a non-affine deformation of the sample, where the stresses were transferred to the bulk by the particle network instead of the fluid. This approach ensured that non stress carrying parts of the network did not contribute to calculated rheological parameters at all frequencies. Moreover we were able to observe a transition from a bulk load experiment at low frequencies, to a surface load setup at high frequencies. The associated theoretical response for a visco-elastic solid was derived, and used as an approximating method to calculate the loss and storage moduli from the observed stresses. It appeared that for high frequencies these approximations failed. The parameter choice for the simulations was such that the resonance frequency of the gel was at low frequencies. A more realistic parameter choice would have lead to prohibitively long simulations. The theoretical response derived can in principle be used as a basis to develop a better analysis method.

3.1 Introduction

Particle gels are colloidal, solvent rich materials that have become flocculated into a continuous three dimensional network structure. Aggregation kinetics and reorganization of the system determines strongly the structure of those gels [1, 2], which can often be characterized using fractal analysis. Particle gels are widespread in the food domain, examples are yogurt and cheese, in which the particles are casein micelles [3]. Most functional properties

¹ A.A. Rzepiela, J.H.J van Opheusden and T. van Vliet, *in preparation*.

of particle gels, such as shaping, handling, slicing and eating characteristics are related to their large deformation and fracture characteristics and only partly to their small deformation characteristics. Large deformation properties depend much more on the detailed structure of the gels than small deformation properties [4]. A previous study of particle gels under large shear deformation showed that those structures are not stable to shearing, they fracture into lumps that compactify due to local reorganization, resulting in a loss of their fractal character [5]. In these studies we have introduced non-affine simulation techniques, where the stresses are transferred from the surface to the bulk through the gel network, rather than the suspending fluid. It was found that at the slow deformation rates used in fracture simulations the distinction was not actually relevant.

Small deformation mechanical properties can account for some aspects of the undisturbed structure of the gel inaccessible by most other methods. They account for both the spatial distribution of the structural elements of the network, as well as the interaction forces between them. Small deformation is defined as such a small relative deformation that applying it does not affect the structure of the material studied. Mechanical properties of particle gels, as determined at small deformations, vary depending on the time scale considered. They behave as rather soft and deformable solids over short times, but as viscous liquids over long times. At intermediate time scales, their reaction to an applied strain will be partly elastic and partly viscous.

Application of homogeneous (affine) shear has been widely used in model studies. It has been used to study aggregating colloidal suspensions under a flow field [6, 7, 8] and model particle gels under both small [9] and large

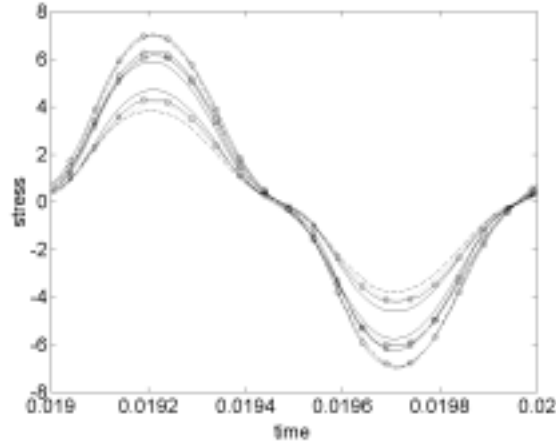


Fig. 1. Stress response in the layers 1 to 10 (see scheme fig 6) to affine strain oscillation. High damping model, $f = 10,000$. (—○—) layer 1 & 10; (—□—) layer 2 & 9; (—) layer 3 & 8; (—) layer 4 & 7; (····) layer 5 & 6.

shear deformations [10]. In the affine model the interpenetrating fluid is moving with a linear velocity profile, and the stress is due to fluid movement rather than due to the network. By applying homogenous sinusoidal shear strain the system reacts with a homogenous sinusoidal stress. The resulting stress profile through the system is time independent and scales simply with the number of bonds in a slice (fig. 1). As expected at high shear oscillation frequency, short deformation time scale, the system response is mainly elastic (the stress is in phase with strain, see figure 1) and at lower shear oscillation frequency, longer deformation time scale, the response is viscoelastic. The storage and loss moduli for an affinely deformed particle gel are plotted in figure 2. The thus obtained rheological parameters of the material reflect only its local structure and do not describe the global character of it. Simple relationships between the rheology and number density of bonds for affine deformation have been previously reported by others [9]. The affine technique may be a correct approach to study shear deformation in some systems but is ineffective for particle gel systems as will be shown later.

Real systems are actually sheared by moving boundaries, and the resulting strain profile through the system may be both time-dependent and non-linear. In this non-affine shear application the evolution of the stress profile depends on the structure and the time scale of shear wave propagation. Non-uniform materials may shear in an inhomogeneous way, reflecting the global character of the material.

In real experiments stress in a deformed test piece is measured at the surface and it is assumed that the stress is homogenous over the material. To ensure that, thin test pieces are used for materials where inertia effects play a

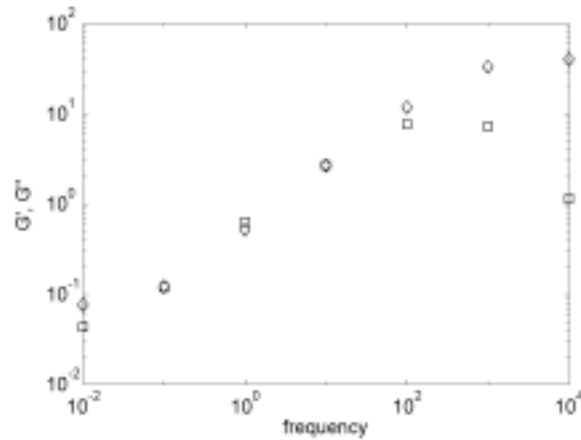


Fig. 2. Storage modulus G' (\diamond) and loss modulus G'' (\square) as a function of oscillation frequency f . Affine deformation, strain amplitude, $\gamma_0 = 0.1$.

role [11]. In those experiments too, the measured rheological properties account for the local character of the material, but the structural information is lost. For some materials omitting the structural term in calculations of the modulus from particle-particle interactions may give large errors and unrealistic results. Scaling relations for particle gels have been developed to account for the structural information of some geometry of structural elements [12, 13].

Experimentally it is difficult to measure the stress in different layers of a material under deformation and so techniques ensuring homogenous stress response have to be used. In simulations detailed data on stress distribution through a test piece are available and no such restrictions are necessary.

The scope of this paper is to study particle gels under small sinusoidal shear deformation, applied by moving the boundaries and discharging the flow profile of the incorporated fluid. This non-affine gel-mediated deformation is hence the opposite of the affine deformation, which is fully fluid-mediated. In real systems both components will be instrumental in the stress transport.

3.2 Simulation Details

The model contains N elastic spheres of radius a placed in a cubic box. All simulations are fully three-dimensional. Prior to gel formation the particles move through the solvent due to random displacements, and they form a bond when two particle surfaces come within a bonding distance R_{bond} . The attachment points are fixed on the surface, and rotate with the particle. The bond is completely flexible for lengths below R_{bond} and it is Hookean beyond this value.

3.2.1 Particle interactions

The particles interact through potentials which consist of the core potential V_C , equation 1, and the bonding interaction V_B , equation 2, both represented by a harmonic force,

$$V_C(r_{ij}) = \begin{cases} \frac{1}{2}K(2a - r_{ij})^2; & r_{ij} < 2a \\ 0; & r_{ij} \geq 2a \end{cases} \quad (1)$$

$$V_B(b_{ij}) = \begin{cases} \frac{1}{2}K(b_{ij} - b_0)^2; & b_{ij} > b_0 \\ 0; & b_{ij} \leq b_0 \end{cases} \quad (2)$$

where $r_{ij} = |r_i - r_j|$ is the distance between particle positions r_i and r_j , and $b_{ij} = |b_i - b_j|$ is the distance between bond attach points b_i and b_j on the particle

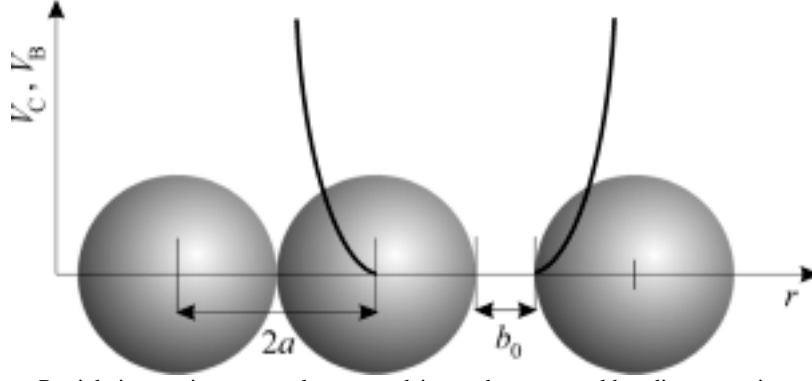


Fig. 3. Particle interactions: central core repulsion and non-central bonding attraction.

surfaces. Further b_0 is the maximum unstretched bond length, in fact $b_0 = R_{\text{bond}}$, and K is the force constant. This can be represented graphically as in figure 3. The force on particle i due to j , F_{ij} , is then simply:

$$F_{ij} = -\nabla_i (V_C(r_{ij}) + V_B(b_{ij})). \quad (3)$$

The total potential force on a particle is the sum of the pair forces.

3.2.2 Brownian Dynamics

The Brownian Dynamics (BD) simulation model used in gel formation, and in a modified form in oscillatory shear, is based on the Langevin equation of motion for a system of diffusing particles. The total force here is the sum of the net force of interaction between particles, the random Brownian force and hydrodynamic interactions. The solvent is regarded as continuous and the Brownian force mimics thermal collisions between the solvent and the dispersed particles. The force on particle i is given by the equation:

$$F_i = m \frac{d^2 r_i}{dt^2} = \sum_j F_{ij} + R_i + H_i, \quad (4)$$

with F_{ij} given by equation (3), R_i the random (Brownian) force and H_i the force modeling hydrodynamic interactions. We approximate H_i by simple Stokesian friction, neglecting hydrodynamic interactions between particles. The liquid drag force on a single particle, H_i , is proportional to the particle velocity,

$$H_i = \zeta \frac{dr_i}{dt}, \quad (5)$$

where $\zeta = 6\pi\eta a$ is the Stokes drag, with η the solvent shear viscosity, and a is the particle radius. The size of the simulation box determines the volume fraction of the particles. Periodic boundary conditions are used to avoid edge

effects. All parameters corresponding to sizes or distances are normalized to the radius of a particle ($a = 1$) and all parameters corresponding to energies are normalized to units of $k_B T$ ($k_B T = 1$).

3.2.3 Numeric models

In our calculations we will consider two limits of the model, one in which the time step in the simulation is shorter than or comparable to the relaxation time of the particles (inertia model), and one in which it is much longer (high damping limit). Taking particle velocities and positions as variables the second order differential equation (4) is written in the form of two, coupled first order equations:

$$\begin{cases} \frac{dv_i}{dt} = \frac{1}{m} \left(R_i - \zeta v_i + \sum_j F_{ij} \right), \\ \frac{dr_i}{dt} = v_i \end{cases}, \quad (6)$$

which system is solved numerically as follows:

$$\begin{cases} v_i(t + \Delta t) = v_i(t) + \frac{\Delta t}{m} (F_{ij}(r_{ij}) - \zeta v_i(t)) \\ r_i(t + \Delta t) = r_i(t) + \frac{1}{2} (v_i(t) + v_i(t + \Delta t)) \Delta t + s_i(t) \end{cases}, \quad (7)$$

where m is particle mass and v_i is particle velocity. The effect of the random force R_i gives uncorrelated particle displacements $\langle \Delta s_i^2 \rangle = 2D_T \Delta t$ with $s = x, y, z$, with $D_T = k_B T / 6\pi\eta a$ the translational diffusion coefficient. The particles similarly undergo rotational motion and diffusion, with a rotational diffusion coefficient $D_R = 3D_T / 4a^2$. This description applies to systems with low damping (ζ). In the limit of high damping the time step is much larger than the relaxation time of the particle velocities, so $m(d^2 r / dt^2)$ is zero in equation 4. This is true in a highly viscous system:

$$\frac{dr_i}{dt} = -\frac{1}{\zeta} \left(\sum_j F_{ij} + R_i \right) \quad (8)$$

This leads to a model, in which only particle positions have to be solved, which is done with the Euler forward method:

$$r_i(t + \Delta t) = r_i(t) + \frac{\Delta t}{\zeta} \left(\sum_j F_{ij}(t) + R_i(t) \right) \quad (9)$$

A more detailed description of the high damping limit model is given in an earlier paper [1]. The high damping limit was used in gel formation, where the simulation time was large. Both the high damping and inertia model will be used in the oscillatory shear calculations reported in this paper.

3.2.4 Rheology

A convenient way to study the viscoelastic properties of gels is by using dynamic tests, in which the structure is subjected to a sinusoidal varying strain, and the resulting stress is measured or vice versa. To simulate such a test, it is customary to include affine shear flow into the equations of motion (7) or (9), and an extra term is added to the particle positions:

$$\Delta S = y_i(t) \dot{\gamma}_{xy} \Delta t, \quad (10)$$

where $\dot{\gamma}_{xy}$ is shear rate. In the high damping limit calculations $a = 1$, $D_T = 1$, and $k_B T = 1$, so the shear rate equals the Péclet number in the units used ($Pe = \dot{\gamma} a^2 / D_T$). In the inertia model D_T depends on the viscosity, so $Pe = \dot{\gamma} a^3 6\pi\eta$ ($a = 1$ and $k_B T = 1$). Lees-Edwards boundary conditions [14] are used to get a continuous shear profile in the periodic system.

Affine deformation involves a linear flow profile obtained by the addition of position dependent gains. Shear is applied by imposing flow in the x -direction, with the shear gradient in the y -direction. This model description assumes that the interpenetrating fluid flows due to the applied shear with a linear profile, and the gel network is in fact deformed by the fluid movement. To model shear in a stagnant solution we omit the bulk flow field (ΔS), and apply shear deformation to the particle network. The deformation of the network will then be non-affine below a certain length scale, while affine deformation above this length scale is the result of the homogeneity of the network at larger length scales, instead of being externally forced. Application of the shear deformation leads to shear forces acting on the two parallel surfaces of the material. They are applied by using the Lees-Edwards boundary conditions, and are transported further in the system through displacement of the particles in the network. Both models, affine and non-affine deformation can be represented graphically as in figure 4.

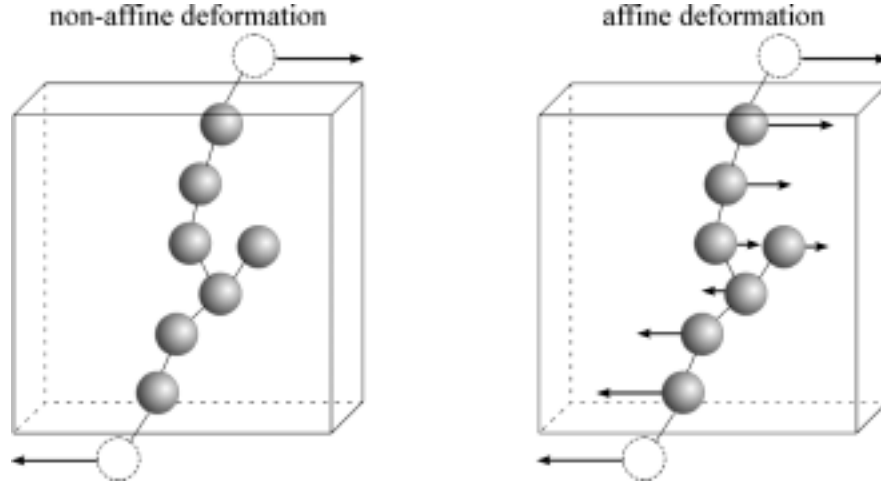


Fig. 4. Affine and non-affine deformation for a gel structure.

The interparticle stress tensor $\sigma_{\alpha\beta}$ is determined from the virial:

$$\sigma_{\alpha\beta} = -\frac{1}{V} \sum_{i=1}^N \sum_{j>i}^N r_{\alpha ij} F_{\beta ij}, \quad (\alpha, \beta = x, y, z), \quad (11)$$

where V is the investigated volume (in our case volume of a layer).

Using equation (10) and the Lees-Edwards boundary conditions, the system and its images will be subjected to a time-dependent strain $\gamma(t)$. The resulting stress response will be analyzed to reveal rheological characteristics. The technique bears a deliberately close relationship to experimental oscillatory shear rheometry, and the applied strain should be small enough not to disrupt the structure if we are to examine the linear response. A small sinusoidal strain input experiment preserves the overall structure, particularly if no further bonds are formed or broken. The resulting stress response is sinusoidal and phase shifted with respect to the input strain. A sine input of the strain at frequency $f = \omega / 2\pi$,

$$\gamma(t) = \gamma_0 \sin(\omega t), \quad (12)$$

produces a stress response:

$$\sigma(t) = \sigma_0 \sin(\omega t + \delta). \quad (13)$$

The phase lag δ and the strain to stress amplitude ratio γ_0/σ_0 depend on the material and, under linear conditions, can be regarded as material properties although both will vary with frequency. For an elastic material the response will be proportional to the strain (stress and strain in phase) and for a viscous one to the strain-rate (stress and strain 90° out of phase). By measuring the stress and

strain amplitude and the phase difference, both storage, G' , and loss, G'' , moduli can be determined:

$$G' = \frac{\sigma_0}{\gamma_0} \cos(\delta), \quad G'' = \frac{\sigma_0}{\gamma_0} \sin(\delta) \quad (14)$$

so that:

$$\sigma(t) = \gamma_0 (G'(\omega) \sin(\omega t) + G''(\omega) \cos(\omega t)). \quad (15)$$

The time scale of the measurement can be adjusted by varying the oscillating frequency ω . The storage modulus is a measure of the energy stored during a periodic application of a strain, and the loss modulus a measure of the energy dissipated in the material. The tangent of the phase angle between stress and strain is:

$$\tan \delta(\omega) = G''(\omega) / G'(\omega). \quad (16)$$

Above equations are derived with the assumption that the test block of the material is sufficiently thin and we may neglect the inertia of the material. Implicitly this assumes that the stress is the same at all points in the material, at least at the scale over which averages are taken in eq. (11). More specifically, the test piece thickness should be small compared with the wavelength of shear waves at the test frequency.

The general description of a shear experiment considers two parallel boundary surfaces moving in the x direction, as shown in figure 5 with a displacement x . Sinusoidal strain means $x(\pm L, t) = \pm \gamma_0 e^{i\omega t}$, and for purely sinusoidal deformation the complex wave equation reduces to [11]:

$$x_{yy} = -\frac{\rho \omega^2}{G^*} x = \Gamma^2 x, \quad (17)$$

where ρ is the material density and G^* is the complex modulus,

$$G^* = G' + iG''. \quad (18)$$

The parameter Γ is called the propagation constant.

The general solution of equation 17 is

$$x(y, t) = (k_1 e^{\Gamma y} + k_2 e^{-\Gamma y}) e^{i\omega t}, \quad (19)$$

where k_1 and k_2 are constants with values chosen to fit particular boundary conditions.

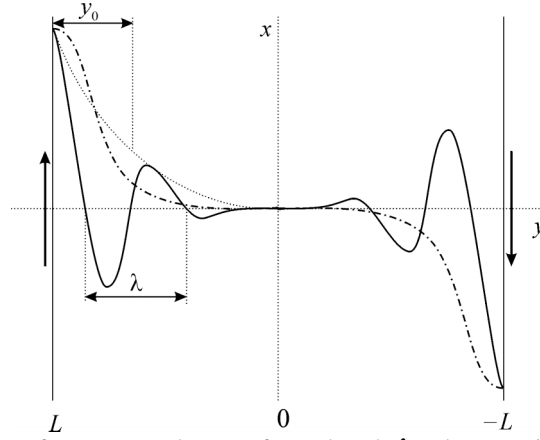


Fig. 5. Propagation of an attenuated wave of wavelength λ and penetration depth y_0 from two parallel oscillating surfaces at distance L and $-L$ from the center of the box. Propagating (—) and critically over-damped (---) wave.

The solution with the shear boundary condition is

$$x(y,t) = \gamma_0 e^{i\alpha t} \frac{(e^{\Gamma y} - e^{-\Gamma y})}{(e^{\Gamma L} - e^{-\Gamma L})} = \gamma_0 e^{i\alpha t} \frac{\sinh(\Gamma y)}{\sinh(\Gamma L)}, \quad (20)$$

The initial deformation inside the sample will of course not satisfy this relation. The discrepancy will lead to an initial transient, due to the internal friction in the material. Equation (20) describes the quasi-stationary solution of the deformation in the sample once the initial transient has relaxed. The strain is:

$$\gamma(y,t) = \frac{\partial x}{\partial y} = \gamma_0 \Gamma e^{i\alpha t} \frac{\cosh(\Gamma y)}{\sinh(\Gamma L)}, \quad (21)$$

and the observed stress defines as above the complex modulus G^*

$$\sigma' + i\sigma'' = \sigma = G^* \gamma = \gamma_0 G^* \Gamma e^{i\alpha t} \frac{\cosh(\Gamma y)}{\sinh(\Gamma L)}. \quad (22)$$

Equation (22) for the observed stress can be interpreted as a damped stress wave moving through the sample material, with penetration depth y_0 (distance over which the wave is damped to $1/e$) and wavelength λ (fig. 5). If these parameters can be determined from the data, G' and G'' can be calculated as [11]:

$$G' = \frac{\rho \omega^2 \left(\frac{4\pi^2}{\lambda^2} - \frac{1}{y_0} \right)}{\left(\frac{4\pi^2}{\lambda^2} + \frac{1}{y_0} \right)^2}, \quad (23)$$

and

$$G'' = \frac{\rho\omega^2 \frac{4\pi}{\lambda y_0}}{\left(\frac{4\pi^2}{\lambda^2} + \frac{1}{y_0}\right)^2}. \quad (24)$$

If the thickness of the sample is very large compared to the penetration depth, the simulation describes a surface load experiment on both sides of the sample. As the waves have attenuated before they reach the opposite end of the sample, there are essentially two independent simulations. If the thickness of the sample is not much larger, or smaller than the penetration depth the full description is needed. If the wavelength is large compared to the sample thickness, the simulation portrays a bulk load experiment.

3.3 Results

The BD simulations start with the preparation of percolating particle configurations. These were formed by randomly placing 1000 particles in a 3D periodic cubic box with volume fraction $\phi = 0.1$, and simulating aggregation at rest. This was done by using the described, high damping model and a simplified ball and string model, which resulted in aggregation and gel aging in short computing time [15]. This simple model does not incorporate explicit potentials, so it has no stresses. We used a gel configuration from the simple model, slightly aged, as a starting configuration for the model with potentials. This configuration was equilibrated by running it for a short period without external forcing, thus minimizing external stresses.

The prepared gels were subjected to oscillatory shear deformation. We have performed simulations using the non-affine deformation model for both the high damping and inertia model. For the inertia model simulations were performed with and without particle rotations included. During dynamical deformation tests, the structure of the gel sample should not change. Therefore in the simulations particle - particle bonds were not allowed to break and no new bonds could be formed during deformation. The lengths of the runs were chosen long enough for the initial transient to relax. For small input strains or high frequencies the stress response was buried in thermal noise. The random Brownian forces on the individual particles produced high amplitude stress waves through the network, which relaxed slowly. With thermal noise many cycles had to be recorded before good averages for the stationary conditions were reached and a harmonic stress signal was obtained. Thermal diffusion of the particles was found to be the main contribution to this noise, because it disappeared at zero temperature and hence that was applied in all simulations to

avoid lengthy runs. With zero temperature we indicate that the random thermal force R_i in eq. 4 is taken zero.

Run parameters that were varied were strain amplitude ($\gamma_0 = 0.05$ to 0.5) and frequency ($f = 0.001$ to $10,000$). At those amplitudes, 10 cycles were generally sufficient at low frequencies and 20 at high frequencies to achieve satisfactory statistics. The higher order frequencies were filtered out from the rough data through Fourier transform analysis. For all simulations we took as the characteristic unstretched bond length, $b_0 = 0.1$. The harmonic force constant, K , was taken 1000 in all the simulation runs. The harmonic constant controls the rate of relaxation of particle overlaps and bond stretches, the fastest motions in the system. The value used in the simulations was the largest one not leading to numerical problems for the given time step.

The reduced time step for the high damping model, at frequencies less than or equal to 100, was $\Delta t = 10^{-4}$, small enough to result in particle movements small with respect to particle radius and bond length. At higher frequencies of 1000 and 10,000 the time steps were $\Delta t = 10^{-5}$ and 10^{-6} respectively, small enough to obtain a sufficient number of data points for further analysis. For the inertia model, at frequencies less than or equal to 10, we took a time step $\Delta t = 10^{-4}$ and varied the viscosity, $\eta = 0.001$ to 2 and particle mass, $m = 0.0001$ to 1 . At higher frequencies, up to 1000, the time step was $\Delta t = 10^{-9}$. In both models the time step has to be related to the external shear force, which is system independent. In the high damping model the viscosity enters the equation through $\Delta t/6\pi\eta$ only, so there is little point in varying this parameter. Varying the shear frequency has the same effect.

For data analysis the results on detailed particle positions, bonds and stresses were used. Stress wave propagation through the gel structures was determined by calculating stress in layers parallel to the top and bottom layers, to which the strain was applied. For non-homogenous stress response the wave propagation theory was used to calculate the G' and G'' using equations 23 and 24. Instead of performing a full two real parameter fit of a complex valued Γ to the observed time dependent stress profile, we tried to approximate penetration depth and wavelength from those data, and use eqs. (23) and (24) to calculate the moduli. The penetration depth, y_0 , was estimated by fitting a function

$q + \cosh \frac{y}{y_0}$, where q is a constant, to a data set of stress amplitudes at adjacent

layers. The wavelength, λ , was estimated from the wave speed $c = \frac{\lambda\omega}{2\pi}$ as observed in the phase shift of the maxima between the adjacent layers. For homogenous stress response across the layers of the sample, G' and G'' can not be calculated from the wave propagation theory, and eq. (15) was used instead, with the observed stress simply averaged over the full system. At very high

frequencies the stress response was restricted to the outer layers of the sample and not enough data were available to reliably calculate the wavelength and penetration depth. The observed behavior as seen in several representative results selected from all the available data will be discussed. In the results section we will report on the high damping model, the inertia model without particle rotations and the inertia model with particle rotations.

For the calculations the simulation box was divided into layers parallel to the xz plane as shown on figure 6, and within each of these the stress and average bond length were calculated. The layers count from 1 to 10 from top to bottom of the box so layers 1 and 10 are the outer layers of the simulation box, where the deformation is applied. Bonds crossing from one layer to the other were included in the calculations for both layers. Bonds crossing the image boundary were excluded from most calculations, as we interpreted them as the points where the stress was imposed to the medium. It is not clear whether this interpretation and the ensuing omission is actually justified for all conditions studied, but because it was done before the data were written, we could not investigate this in detail without having to perform all simulations again. For some conditions studied, we investigated the effect of including the cross-boundary bonds and found it to be small (see below).

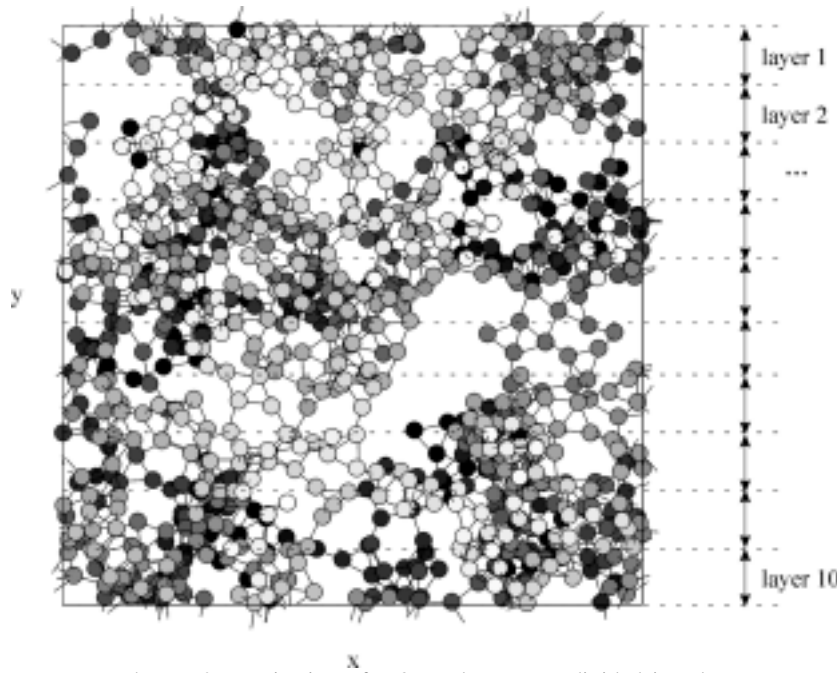


Fig. 6. Layer scheme. 2D projection of a 3D gel structure divided into layers across the xy plane. Gray scale is used as depth cue.

3.3.1 High damping model

In figure 7a the stress distribution over the layers is plotted for the high damping model. It shows a single, first strain oscillation from rest at low frequency, $f = 0.05$, with strain amplitude, $\gamma_0 = 0.3$. The first oscillation starts at zero strain and average zero stress in the whole system. The stress in the layer 1 and 10 (the outer layers of the box) increases upon deformation and reaches its maximum before $t = 5$, the strain maximum. The stress response in the lower layers has a lower amplitude and layers 5 and 6 (the most middle layers) show only a very small response upon deformation of the structure. In the high damping model the strain wave propagation through the structure is quickly damped out and we see surface loading occur even at this low frequency. Note that the stresses in the mirror layers at the same distances from the image boundary, from the top and the bottom, are not exactly the same. This is related

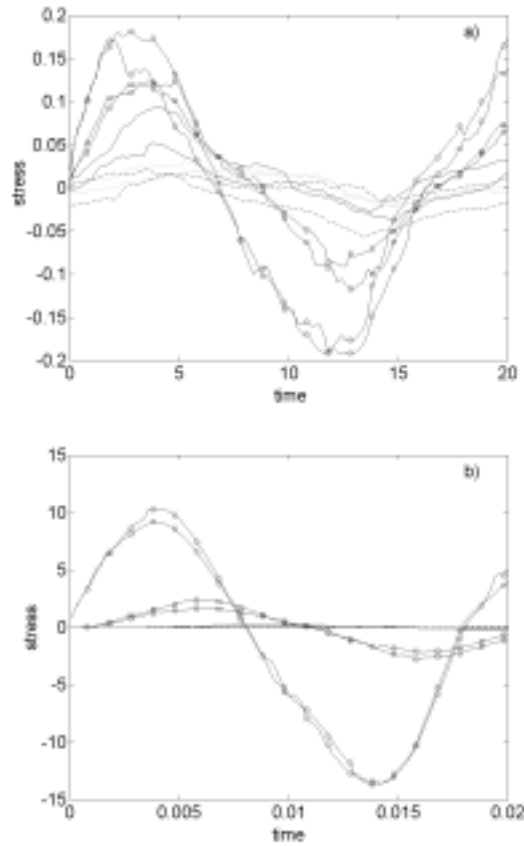


Fig. 7. Stress response in the layers 1 to 10 (see scheme fig 6) to strain oscillation for the high damping model. Strain amplitude, $\gamma_0 = 0.3$; oscillation frequency, $f =$ a) 0.05, b) 50. (—○—) layer 1 & 10; (—□—) layer 2 & 9; (—) layer 3 & 8; (—) layer 4 & 7; (—) layer 5 & 6.

to the small system size, 1000 particles, and the relatively large inhomogeneities in the structure.

In figure 7b the stress distribution is plotted for one strain oscillation at high frequency, $f = 50$, and strain amplitude, $\gamma_0 = 0.3$. The stress in the two outer layers of the box behaves similar to that at lower frequencies. There is a small stress response in the layers 2 & 9 but in the rest of the structure no measurable stress was observed. The penetration depth, of the order of one layer thickness, is too small to be determined from the simulation for this case.

In figure 8 the calculated storage modulus, G' , and loss modulus, G'' , are plotted as a function of oscillation frequency, f , for the high damping model.

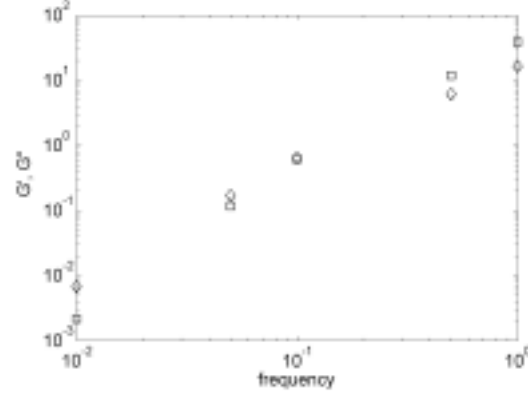


Fig. 8. Storage modulus G' (\diamond) and loss modulus G'' (\square) as a function of oscillation frequency f for the high damping model. Calculations excluding the cross-boundary layer of the sample. Strain amplitude $\gamma_0 = 0.3$.

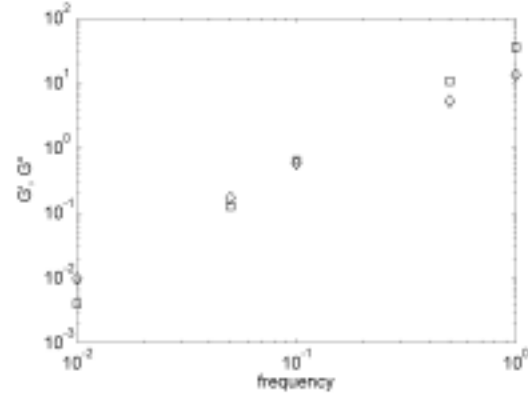


Fig. 9. Storage modulus G' (\diamond) and loss modulus G'' (\square) as a function of oscillation frequency f for the high damping model. Calculations including the cross-boundary layer of the sample. Strain amplitude $\gamma_0 = 0.3$.

Both G' and G'' increase about linearly with frequency, f , on a log-log plot. The curves do not differ much and their slope is approximately 2. The G' and G'' were calculated based on the wave propagation theory from equations 23 and 24. They could be calculated only for those frequencies where a stress wave was observed penetrating some distance in the sample. At higher frequencies only the outer layers of the material show a stress response and thus there is not enough information to calculate λ and y_0 . Results obtained from a rerun of these simulations, in which we included the boundary crossing bonds, are shown in fig. 9. All those bonds were added to layers 1 and 10. So values plotted in figure 9 are based on a stress response including the thin cross-boundary layer, while figure 8 presents the same calculations, but only based on the stress response in the simulation box, so excluding the cross-boundary layer. The results are very similar, only at low frequencies G' and G'' are slightly higher in figure 9. In this case the added stress from layer zero is small compared to that of the other bonds in the outer layers, and within the accuracy of our determination the resulting moduli are identical. We expect that will be the case for all our simulations. Only for rapid external changes, the stress wave does not penetrate the sample very much, and a large part of the stress in the outer layers comes from those boundary-crossing bonds. However, for those cases we can not reliably calculate the moduli and therefore, they are not presented.

3.3.2 Inertia model (without particle rotations)

In developing the computer code for the inertia model, a small programming error was made, with the effect that particle rotations were excluded. Before we corrected this error, we had already gathered all the necessary data, some of them we present below followed by data from calculations in which particle rotations was included. The model without rotations may physically not be very relevant, from the modeling viewpoint it is a valid model, with different properties from the model with rotations. In fact data obtained shows the same trends if rotation was included or not (see below). Moreover, comparison allowed us to discuss the effect of particle rotation.

In figure 10 the stresses as a function of time are plotted for the inertia model without particle rotations for the different layers (see fig. 6). For a frequency of 0.01 (fig. 10a) there is a very homogenous distribution of stress across the layers of the structure. At this relatively low viscosity the average stress response is the same in all the layers. There is no significant transient, all layers react in phase and at the same amplitude, and there is no sign of any damping towards the center of the sample. Note that the sample does not react sinusoidally. This is due to the fact that bonds in our model only carry stress when extended beyond $b_0 = 0.1$, putting an essential non-linearity at very small deformation. Only the bonds already stretched, that is extended beyond b_0 , at

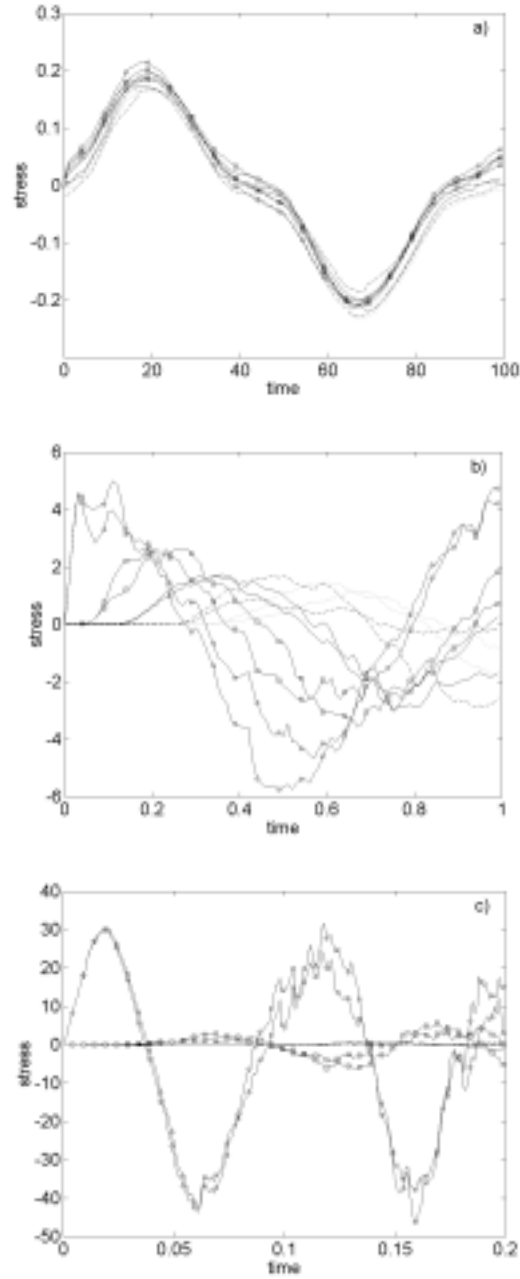


Fig. 10. Stress response in layers 1 to 10 (see scheme fig 6) to one (a and b), and two (c) strain oscillations for the inertia model. Viscosity, $\eta = 0.1$, particle mass, $m = 1$, strain amplitude, $\gamma_0 = 0.1$, oscillation frequency, $f =$ a) 0.01, b) 1, c) 10. $(-\circ-)$ layer 1 & 10; $(-\square-)$ layer 2 & 9; $(-)$ layer 3 & 8; $(--)$ layer 4 & 7; (\cdots) layer 5 & 6.

zero deformation contribute to the stress at very small deformation, but as deformation increases more bonds become stretched and the slope increases. The freedom of the bonds to stretch to a certain length without leading to a restoring force was introduced in the model to allow undisturbed gels to locally reorganize due to small thermal motion of the particles. With a finite value for the parameter b_0 we have implicitly incorporated some mild strain hardening in deformation of these gels. Once all the bonds in the backbone of the gel are actually stress carrying the system becomes linear, and strain hardening is the result of bond reorientation, as observed in large deformation rheology. In a test we set b_0 to zero, and found the normal sinusoidal response, see fig. 11.

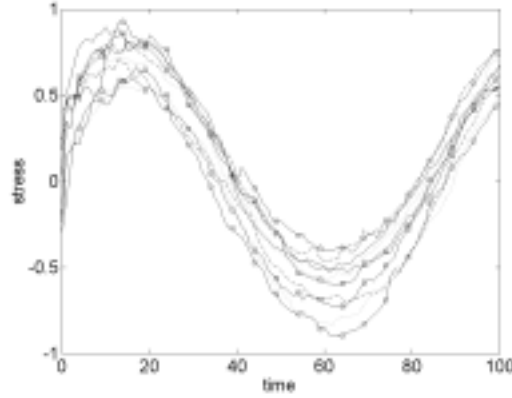


Fig. 11. Stress response in layers 1 to 10 (see scheme fig 6) to one strain oscillation for the inertia model. Unstretched bond length, $b_0 = 0$, viscosity, $\eta = 0.1$, particle mass, $m = 1$, strain amplitude, $\gamma_0 = 0.1$, oscillation frequency, $f = 0.01$ (—○—) layer 1 & 10; (—□—) layer 2 & 9; (—) layer 3 & 8; (—) layer 4 & 7; (—) layer 5 & 6.

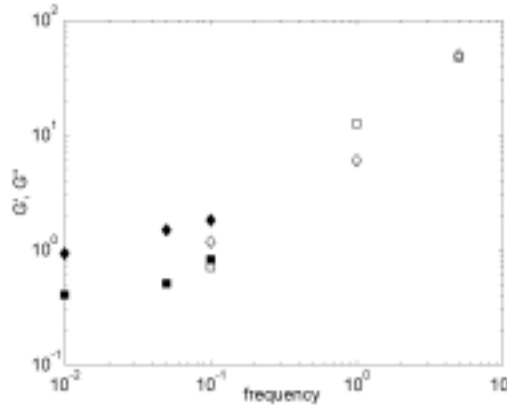


Fig. 12. Storage modulus G' (◇) and loss modulus G'' (□) as a function of oscillation frequency f . Empty symbols from eq. 23 and 24, full symbols from eq. 14. Strain amplitude $\gamma_0 = 0.1$, viscosity $\eta = 0.1$, particle mass $m = 1$.

The stress distribution over the layers at a strain frequency of 1 is plotted in fig. 10b. Distinct strain wave propagation can be observed in the layered stress response here. The layers 1 & 10 show an immediate stress response to the applied strain and the neighboring inner layers follow in time. Layers 5 & 6, the central ones, are the last to react and they oscillate about 150° out of phase with the strain input at the surface. At a frequency of 10 (fig. 10c) the stress response is mainly in the outer layers, while layers 2 & 9 oscillate about 180° out of phase. In the other layers no measurable stress response was observed.

In figure 12 the storage modulus, G' , and loss modulus, G'' , are plotted as a function of oscillation frequency, f , for the inertia model without rotations. For lower frequencies a homogenous stress response was found and G' and G'' were calculated using equation 14, while at higher frequencies they were calculated by using eqs. 23 and 24. At a frequency of 0.1 both methods for calculating G' and G'' were used and at this point the results differ by a factor 1.5 for G' and 1.2 for G'' . Both G' and G'' , increase roughly linearly with f on a log-log scale for $f \geq 0.1$. The slope is approximately 1 for $f > 10^{-1}$, so also on a linear scale the relation is linear. Beyond a frequency of 5 the stress response was only in the outer layer and G' and G'' could therefore not be calculated.

3.3.3 Inertia model (with particle rotations)

In figure 13 stress as a function of time is plotted for the layers 1 to 10 (see scheme fig. 6) for the inertia model including particle rotations. For frequency 0.01 (fig 13a) a quite homogenous stress distribution through the layers is observed, although less homogenous than in the inertia model without particle rotations, compare fig. 10a. There also is some transient behavior.

At frequency 1 (fig. 13b) layers farther from the outer face show consequently decreasing stress amplitudes. The middle layers show hardly any stress response at all upon deformation. The curves bear less noise than in the corresponding plot for the inertia model without rotations, compare fig. 10b, also less than in fig. 13a. This is still the case if we wait until the transients die out.

At frequency 50 (fig. 13c) the stress response is again mainly in the outer layers and layers 2 & 9 oscillate at about 90° out of phase. At this viscosity and particle mass and at this high frequency the time scale of the applied strain oscillation is high compared to the internal time scales of the system.

The resonance frequency of this system was found at frequency of about 0.001 (figure 14). The stress in the system oscillates with increasing amplitude with consecutive periods of strain application. The average bond

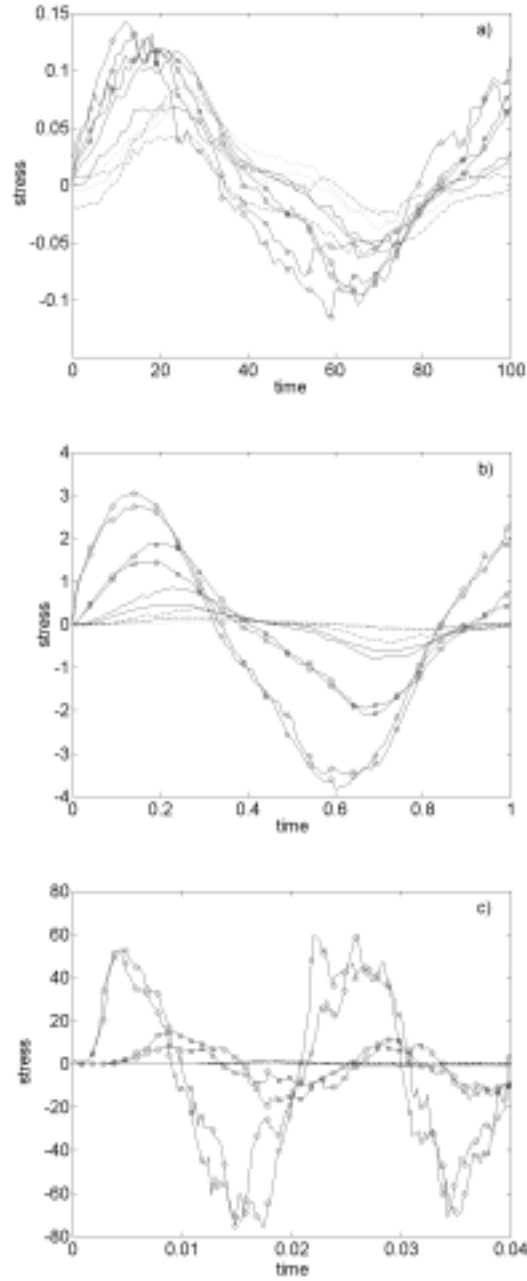


Fig. 13. Stress response in layers 1 to 10 (see scheme fig 6) to one (a and b) and two (c) strain oscillations for the inertia model including particle rotations. Viscosity, $\eta = 0.053$, particle mass, $m = 0.01$, strain amplitude, $\gamma_0 = 0.5$, oscillation frequency, $f =$ a) 0.01, b) 1, c) 50. (—○—) layer 1 & 10; (—□—) layer 2 & 9; (—) layer 3 & 8; (—) layer 4 & 7; (—) layer 5 & 6.

length shows also an increasing trend regarding the oscillation amplitude. The overall natural frequency of the gel structure is lower than the frequency of the external sinusoidal oscillation that we used in all our other simulations.

In figure 15 the storage and loss modulus are plotted as a function of frequency, for the inertia model with particle rotations. In a log-log plot, G'' increases about linearly with f with a slope of approximately 2 for the plotted range of f , while G' does not depend on frequency beyond $f = 0.1$.

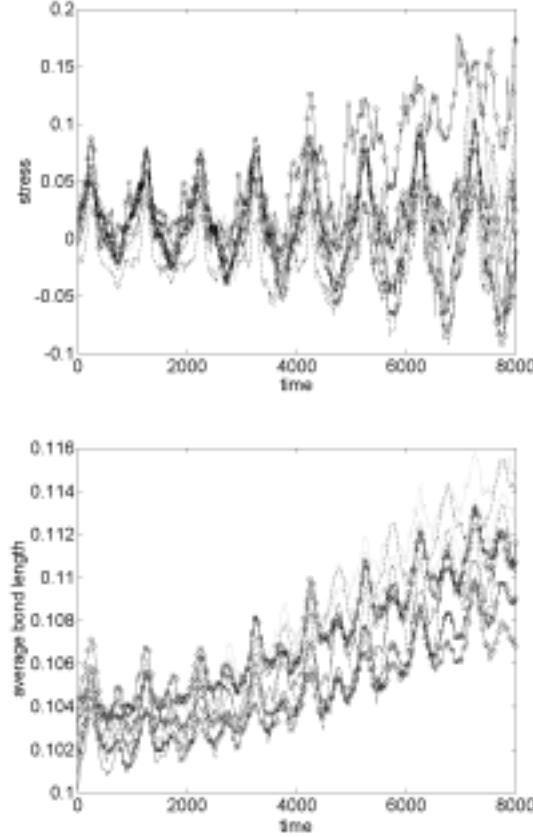


Fig. 14. Stress and average bond length during eight strain oscillations, both plotted in layers (see scheme fig 6). Viscosity, $\eta = 0.053$, particle mass, $m = 0.01$, strain amplitude, $\gamma_0 = 0.5$, oscillation frequency, $f = 0.001$. (-o-) layer 1 & 10; (-□-) layer 2 & 9; (—) layer 3 & 8; (- -) layer 4 & 7; (...) layer 5 & 6.

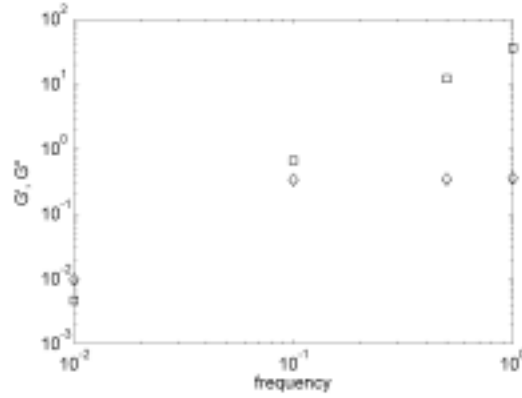


Fig. 15. Storage modulus G' (\diamond) and loss modulus G'' (\square) as a function of oscillation frequency f . Strain amplitude $\gamma_0 = 0.5$, viscosity $\eta = 0.053$, particle mass $m = 0.01$.

3.4 Discussion

If an affine deformation is applied in a simulation, the deformation of the gel sample will be due to interpenetrating fluid movement rather than due to straining of the network. The entire network is strained, both parts building the structures' backbone and dangling ends. The stress profile through the sample is homogeneous, the strain is by bulk loading. Differences in stress between layers in the gel will be due to specific aspects of local structure, such as the number of bonds or bond orientation. These differences are most clearly observed at low frequencies. Although the affine technique has been used before to study shear deformation of particle gels it has been proven to be ineffective to determine the global character of those systems [10].

In the non-affine technique the strain deformation is applied at the surface of the structure and propagates through the network to the middle layers. Only the structural elements of the network carry stress, the strain application is by surface loading. The stress profile depends on the structure at all length scales, it reflects the global character of the material. Experimentally it is difficult to measure stress in different layers of a test material during deformation and so techniques ensuring homogenous stress response have been used. In simulations detailed data on stress distribution through a test piece are available and no such restriction is necessary. With the approximate models available, the reverse of this observation is more important; simulations of the type we used, with simplified hydrodynamics, should preferably use surface loading in a non-affine shear mode. If affine deformation is applied, it should be tested at least whether it is justified.

In this paper we report on simulating oscillatory shear deformation tests. We determine the stress response in adjacent layers through a test piece and use these data to calculate the storage and loss modulus from the wave propagation theory. In most of our calculations we disregarded the stress from the cross-boundary layer, where the strain was applied. Within the accuracy of our calculations likely that does not significantly influence the results.

In the high damping model the stress response in the outer layer is always greater than in the rest of the box, regardless the strain amplitude or frequency, within the domain investigated. The stress propagates into the bulk of the box and is quickly damped out. For the lowest oscillation frequencies there is a just noticeable effect of the applied strain in the inner layers, see fig. 7a, but at higher frequencies the only measurable stress response is in the outer layers. Essentially for a macroscopic system the stress response will always be a surface effect only for this parameter regime. This is in agreement with what one would expect for the high damping limit, which implies high viscosity systems.

Inertia effects must be included to have a proper strain wave propagation through a gel structure. The time scale of strain wave propagation in the inertia model depends on the viscosity of the sample, mass of the particles and the strength of the bonds (harmonic constant). A parameter regime exists, for which at low frequency a homogenous stress profile is observed in response to the surface strain loading, fig. 10a. The time scale of wave propagation, the time needed for a wave to cross the sample, is much shorter than the time scale of deformation. The inertia model without particle rotations showed a more homogenous stress response of the structure for higher damping conditions than the model including particle rotations. Neglecting rotations appears to lead to a somewhat stiffer gel. This can be understood by noting that the bonds are fixed at the particle surfaces and are small relative to particle size. If the particles can rotate that will diminish the amount a bond will be stretched upon deformation of the structure.

In the inertia model there is a viscosity dependent frequency, at which the system starts to resonate. This is a peculiar effect of the choice of the parameters, especially the low value of the harmonic constant. The natural frequency of the structure in experiments is usually higher than that of the external oscillations. In our simulation model it is the opposite, a more realistic, higher value for the harmonic constant would have lead to a smaller time step, and inhibitive long simulations. Similarly simulations below the resonance frequency would have needed to be extremely long because of the low frequency and the long transient.

For the high frequencies, regardless of the model used, only the outer layers give a stress response due to the strain. The response of the first layer from the surface is mainly elastic, meaning that bonds stretch due to applied

force, but the adjacent layer of particles does not move at all. For the high damping model this is already the case at lower frequencies than in the inertia systems. Most differences between the models are observed at low frequencies, where the time scale of the wave propagation is sensitive to the detailed model and inertia parameters.

The estimated values of the wavelength λ and penetration depth y_0 , *c.f.* those of G' and G'' calculated from these, from our approximated analysis of the stress wave model may not be very accurate. More data points, *i.e.* more layers, larger samples, longer runs, would obviously help in increasing the accuracy, but the main thing that is needed is a better fitting procedure of the available data to the theoretical two parameter stress profile. We are currently developing such a procedure. At high frequencies only the outer layer is moving so there is no wave propagation from which we can estimate λ and y_0 . Thinner samples could be used with thinner layers to have data about wave propagation in those systems. On the other hand for very narrow samples, thinner than the fractal length measured, these properties would no longer be the material properties of a real sample.

3.5 Conclusions

We have shown that the standard procedure of simulating oscillatory shear strain or stress experiments, by using an affine deformation of the sample, is probably an incorrect method to determine the rheological properties of the gel structure. Not only does this method apply stresses to parts of the gel that are not stress carrying, but it also ignores effects of shear wave propagation through the sample. Especially at higher frequencies of the externally applied deformation these shortcomings become manifest. The non-affine method that we propose is equally simple to use as the affine method. The explicit determination of the time dependent stress profile in the gradient direction immediately shows whether the simulation should be identified as a bulk load or a surface load experiment. The approximate method we have used to analyze the surface load experiments is imperfect, and should be further developed.

3.6 References

- [1] A.A. Rzepiela, J.H.J. Opheusden and T. van Vliet, *J. Coll. Sci.* **244** (2001) 43-50.
- [2] M. Mellema, P. Walstra, J.H.J. van Opheusden, T. van Vliet, *Adv. Coll. Interf. Sci.* **98** (2002) 25-50.
- [3] L.G.B. Bremer, Ph.D. Thesis, Wageningen University, The Netherlands 1992.
- [4] T. van Vliet and P. Walstra, *Faraday Discuss.* **101** (1995) 359.

- [5] A.A. Rzepiela, J.H.J. Opheusden and T. van Vliet, submitted to *J. Rheol.*
- [6] D.M. Heyes, P.J. Mitchell, *J. Chem. Soc. Faraday Trans.* **90** (1994) 1931.
- [7] A.A. Catherall, J.R. Melrose and R.C. Ball, *J. Rheol.* **44** (2000) 1.
- [8] A.A. Potanin, *J. Coll. Int. Sci.* **157** (1993) 399.
- [9] M. Whittle and E. Dickinson, *Mol. Phys.* **90** (1997) 739.
- [10] M. Whittle and E. Dickinson, *Faraday Trans.* **94** (1998) 2453.
- [11] R.W. Whorlow, *Rheologica Techniques*, 2nd Edition, Ellis Horwood, Chichester, 1992.
- [12] L.G.B. Bremer, B.H. Bijsterbosch, R. Schrijvers, T. van Vliet and P. Walstra, *Colloids and Surfaces* **51** (1990) 159.
- [13] T. van Vliet, in Food Emulsions and Foams; Interfaces, Interactions and Stability, (E. Dickinson and J.M. Rodriguez Patino eds) *Proc. Int. Symp. Royal Soc. Of Chem.*, Cambridge (1999) 307.
- [14] M.P. Allen and D.J. Tildesley, "Computer simulation of liquids", Oxford Univ. Press, Oxford 1993.
- [15] M. Mellema, J.H.J. van Opheusden and T. van Vliet, *J. Chem. Phys.* **111** (1999) 6129.

Chapter 4

Large shear deformation of particle gels studied by Brownian Dynamics simulations¹

Brownian Dynamics (BD) simulations have been performed to study structure and rheology of particle gels under large shear deformation. The model incorporates soft spherical particles, and reversible flexible bond formation. Two different methods of shear deformation are discussed, namely affine and non-affine deformation, the second being novel in simulation studies of gels. Also two dynamic descriptions of the model are presented, with and without inertia effects. Non-affine deformation resulted in a slower increase of the stress at small deformation than affine deformation. At large deformation both models gave similar stress responses, although the inertia model resulted in lower stresses. The particle gels, regardless of the model used, were observed to fracture into lumps that compactified due to local reorganization. A reversible yielding transition, as observed in polymer gels, was not found. Fractal properties of the gels were irreversibly lost at large deformation.

4.1 Introduction

Particle gels are systems of colloidal particles that form weakly bonded percolating networks interpenetrated by a suspending fluid. They are characterized as soft, deformable, elastic solids. A wide range of particles may form this type of system. In many food gels the particles may themselves be complex and deformable. However, the unifying feature is that the entities forming the particle gel are roughly globular in shape and have relatively short-ranged bonding interactions with near neighbors. The structure of those gels is strongly determined by the aggregation kinetics and reorganization of the system [1] and can often be characterized using fractal analysis [2]. The concentration of particles in those systems can be quite low, but in spite of that, the mechanical properties are dominated by the network rather than by the interpenetrating fluid. An example of a particle gel from the food domain is

¹ A.A. Rzepiela, J.H.J. van Opheusden and T. van Vliet, *in revision for J. Rheol.*

yogurt in which the particles are casein micelles [3]. Particle gels should be distinguished from polymer gels, such as gelatin. Polymer gels consist of cross-linked long molecules with considerable conformational flexibility between the cross-links. The two types of gels strongly differ in their large deformation rheological behavior as a result of their different microstructures.

Most functional properties of gels are related to their large-deformation and fracture characteristics rather than small-deformation characteristics. Large deformation properties depend much more on the detailed structure of the gel than small deformation properties do [4]. When a colloidal gel is put under stress, its structure is first deformed and finally destroyed. Often gels do not exhibit clear macroscopic fracture, but show a transition from an elastic to a viscous regime.

Many models were previously developed to describe shear deformation and flow of aggregating viscous, colloidal suspensions over a wide range of volume fractions and shear rates. Whittle and Dickinson [5, 6] studied large strain rheology of gels whereby the bonding interactions were varied. Shear thinning and flow properties of concentrated colloid suspensions with depletion interactions were studied by Silbert *et al.* [7]. Potanin [8] studied deformation and breakup of colloidal aggregates due to shear flow as a function of the particle interactions.

In the studies quoted above and numerous other simulation studies an affine model for shear deformation of particle gels was used. In the affine model the interpenetrating fluid is moving with a linear velocity profile. The response of the particle network to this flow determines the rheology. We have developed a non-affine deformation model in which the network is subjected to shear in a stagnant bulk fluid. The shear forces now act only on the two opposite parallel surfaces of the material. A real system will be an intermediate of the two models. The non-affine model has, to our knowledge, not been used before for studying gel deformation in shear.

If the time scale of relaxation of the particle velocities is much smaller than the time steps used in the simulations the so called high damping limit can be used. This model only keeps track of particle positions, velocities are ignored. That means also the kinetic energy is ignored. To study crack propagation and brittle fracture we here have extended our model with calculations of the particle velocities, thus including the inertia effects. Models were previously developed to describe brittle versus ductile fracture behavior for crystal solids under strain [9]. In this paper we will try to identify yielding, ductile fracture and brittle fracture in particle gels. The main question we want to answer is whether we microscopically can distinguish macroscopic fracture from macroscopic yielding.

4.2 Simulation details

The model describes elastic spheres of a radius a , with a harmonic central repulsion, placed in a 3D cubic box. Before a gel is formed the particles move through the solvent due to random displacements. When two particle surfaces come within a bonding distance R_{bond} , an elastic string is formed. The attachment points of the strings are fixed on the surface, and rotate with the particle. The string is completely flexible for lengths below R_{bond} , it is Hookean beyond this value and breaks when stretched above a specified length for bond breaking, R_{split} . Relative particle motion is possible due to rotational and translational diffusion, which allows cluster reorganization.

4.2.1 Particle interactions

The particles interact through potentials which consist of the core potential V_C , equation 1, and the bonding interaction V_B , equation 2, both represented by a harmonic force,

$$V_C(r_{ij}) = \begin{cases} \frac{1}{2} K (2a - r_{ij})^2; & r_{ij} < 2a \\ 0; & r_{ij} \geq 2a \end{cases} \quad (1)$$

$$V_B(b_{ij}) = \begin{cases} \frac{1}{2} K (b_{ij} - b_0)^2; & b_{ij} > b_0 \\ 0; & b_{ij} \leq b_0 \end{cases} \quad (2)$$

where $r_{ij} = |r_i - r_j|$ is the distance between particle positions r_i and r_j , and $b_{ij} = |b_i - b_j|$ is the distance between bond attach points b_i and b_j on the particle surfaces. Further b_0 is the maximum unstretched bond length and K is the force constant. This can be presented graphically as in figure 1.

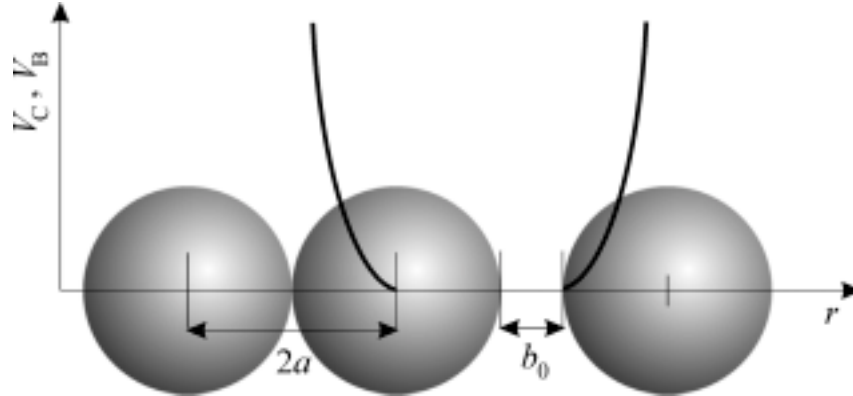


Fig. 1. Particle interactions: central core repulsion and non-central bonding attraction.

The force on particle i due to j , F_{ij} , is then simply:

$$F_{ij} = -\nabla_i (V_c(r_{ij}) + V_B(b_{ij})). \quad (3)$$

The total potential force on a particle is the sum of the pair forces.

4.2.2 Brownian Dynamics algorithm

The Brownian Dynamics (BD) simulation model is based on the Langevin equation, the dynamical equation of motion for a system of diffusing particles. The total force here is the sum of the net force of interaction between the particles, the random Brownian force and hydrodynamic interactions. The solvent is regarded as continuous and the Brownian force mimics thermal collisions between the solvent and the dispersed particles. The force on particle i is given by the equation:

$$F_i = m \frac{d^2 r_i}{dt^2} = \sum_j F_{ij} + R_i + H_i, \quad (4)$$

with F_{ij} given by equation (3), R_i the random (Brownian) force and H_i the force modeling hydrodynamic interactions. We approximate H_i by simple Stokesian friction, neglecting hydrodynamic interactions between particles. The liquid drag force on a single particle, H_i , is proportional to the particle velocity,

$$H_i = \zeta \frac{dr_i}{dt}, \quad (5)$$

where $\zeta = 6\pi\eta a$ is the Stokes drag, with η the solvent shear viscosity, and a the particle radius. The size of the simulation box determines the volume fraction of the particles. Periodic boundary conditions are used to avoid edge effects. All parameters corresponding to sizes or distances are normalized to the radius of a particle ($a = 1$) and all parameters corresponding to energies are normalized to units of $k_B T$ ($k_B T = 1$).

The Langevin equation (4) can be solved numerically, enabling us to follow the movements of each particle through the system in consecutive constant time steps.

4.2.3 The inertia effects model

Taking particle velocities and positions as variables this second order differential equation is written in form of two coupled first order equations:

$$\begin{cases} \frac{dv_i}{dt} = \frac{1}{m} \left(R_i - \zeta v_i + \sum_j F_{ij} \right), \\ \frac{dr_i}{dt} = v_i \end{cases}, \quad (6)$$

which can be solved numerically:

$$\begin{cases} v_i(t + \Delta t) = v_i(t) + \frac{\Delta t}{m} (F_{ij}(r_{ij}) - \zeta v_i(t)) \\ r_i(t + \Delta t) = r_i(t) + \frac{1}{2} (v_i(t) + v_i(t + \Delta t)) \Delta t + s_i(t) \end{cases}, \quad (7)$$

where m is particle mass and v_i is particle velocity. The effect of the random force R_i gives particle uncorrelated displacements $\langle \Delta s_i^2 \rangle = 2D_T \Delta t$ with $s = x, y, z$, and $D_T = k_B T / 6\pi\eta a$ the translational diffusion coefficient. The particles similarly undergo rotational motion and diffusion, with a rotational diffusion coefficient $D_R = 3D_T / 4a^2$. Algorithm (Eq. 7) is used if the simulation time step is smaller than the relaxation time of the particle velocity autocorrelation function. This relaxation time depends on the viscosity and is large for low viscosity systems. That implies that the description applies to systems with low damping (ζ).

4.2.4 The high damping model

In the limit of high damping the time step is much larger than the relaxation time of the particle velocities. This is true in high viscosity systems. To model this, we neglect the second order term in (4) to obtain:

$$\frac{dr_i}{dt} = -\frac{1}{\zeta} \left(\sum_j F_{ij} + R_i \right) \quad (8)$$

This first order differential equation for only particle positions, also is solved with the Euler forward method:

$$\Delta r_i(t + \Delta t) = \frac{\Delta t}{\zeta} \left(\sum_j F_{ij}(t) + R_i(t) \right) \quad (9)$$

A more detailed description of the high damping limit model is given in an earlier paper [1].

4.2.5 Rheology

To probe the rheology of the system, shear flow is included into the equations of motion (7) and (9). The widely used affine method involves a linear flow profile by addition of position dependent increments (Fig. 2). Shear is applied by imposing flow in the x -direction, and a shear gradient along the y -direction. In the equation of motion an extra term is added to the particle positions increment:

$$\Delta S = y_i(t) \dot{\gamma}_{xy} \Delta t. \quad (10)$$

where $\dot{\gamma}_{xy}$ is the shear rate. In the high damping limit calculations $a = 1$, $D_T = 1$, and $k_B T = 1$, so the shear rate equals the Péclet number in the units used ($Pe = \dot{\gamma} a^2 / D_T$). In the inertia model D_T depends on the viscosity, so $Pe = \dot{\gamma} a^3 6\pi\eta$ ($k_B T = 1$). Lees-Edwards boundary conditions [10] are used in the affine model to have a continuous shear profile in the periodic system.

Note that the high damping limit and the inertia model refer to different physical systems, rather than to different models that can be used for the same system. Which model one has to use depends on the values of the physical parameters, particle mass and size, viscosity and temperature.

In the non-affine model we omit the bulk flow field (ΔS) but still apply Lees-Edwards boundary conditions (Fig. 2). The shear forces act only on the two parallel surfaces of the material and are transferred further through the network. To allow this transfer and to avoid wall slip in the early stages of deformation, bonds are not allowed to break in a small layer of two particle diameters at both the top and the bottom of the box.

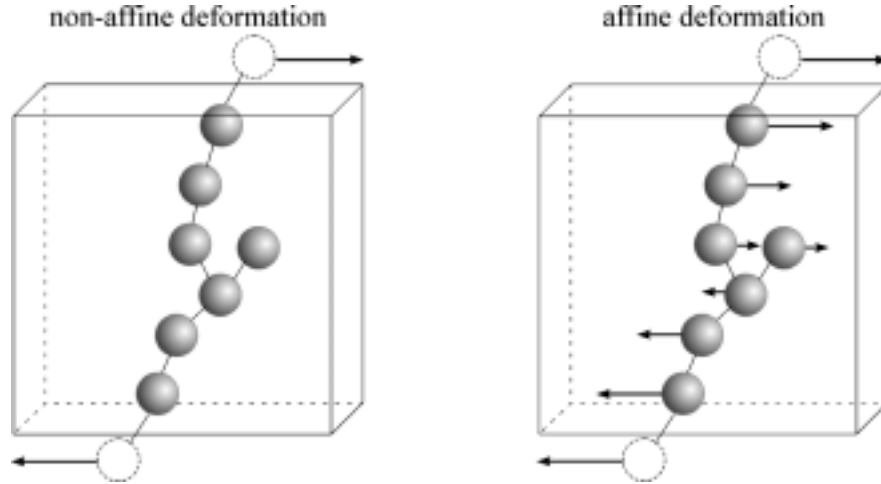


Fig. 2. Affine and non-affine deformation for a gel structure.

The interparticle stress tensor $\sigma_{\alpha\beta}$ is determined from the virial:

$$\sigma_{\alpha\beta} = -\frac{1}{V} \sum_{i=1}^N \sum_{j>i}^N r_{\alpha ij} F_{\beta ij}, \quad (\alpha, \beta = x, y, z), \quad (11)$$

where V is the volume of the simulation box.

Every iteration step in all models consists of: formation of new bonds between particles within the bonding range, moving of the particles due to the Brownian, external shear and interparticle forces, and breaking of stretched bonds.

4.3 Results

The BD shear simulations start from previously prepared percolating particle configurations. These were formed by randomly placing 10,000 particles in a 3D periodic cubic box at a volume fraction $\phi = 0.1$, and by simulating aggregation at rest. We used the high damping model and a simplified ball and string model for aggregation and gel formation [2]. The formed gels have a fractal dimensionality of approximately 2.3.

The prepared gels were equilibrated and subjected to shear deformation. Simulations were performed using affine and non-affine deformation for both the high damping and inertia model. The model parameters were varied, the shear rate ($Pe = 0.05$ to 0.5), and the bond breaking length ($R_{\text{split}} = 0.4$ and 0.7). For all simulations we took the particle distance for bond formation, $R_{\text{bond}} = 0.1$ as well as the unstretched bond length $b_0 = 0.1$. The harmonic force constant was taken $K = 1000$. The harmonic constant controls the rate of relaxation of particle overlaps and bond stretches, the value used in the simulations was the largest one not leading to numerical problems for the given time step. The reduced time step for the high damping model was $\Delta t = 10^{-4}$ in all the calculations. This was small enough to give particle movement small with respect to particle radius and bond length. For the inertia model we took a time step $\Delta t = 10^{-4}$ and varied mass, $m = 10^{-4}$ to 10^{-3} , and viscosity, $\eta = 0.053$ to 0.1 . Note that different reduced units are used in the models, and the absolute values of Δt cannot be compared directly. In both cases the time step is to be combined with the shear rate, giving the total shear, which is system independent. In data analysis results on detailed particle positions, bonds and stresses were used. We do not present here all available data but discuss the observed behavior for several representative results.

In the results section the high damping results will be first presented for affine and non-affine deformation. Next, we will compare results from the high damping model with those from the inertia model.

4.3.1 The high damping model

In figure 3 stress-strain relations are shown for affine and non-affine deformation of a given gel for the high damping model. For affine deformation the stress in the system steeply increases upon straining. Bonds carry stress, but do not break initially. New bonds are formed due to the ongoing process of local reorganization caused by Brownian motion and due to shear. About 70% of the bonds formed are due to the applied shear. The increase in the average bond length is for more than 90% strain driven. Thus the number of bonds per particle increases and continues to do so during the further simulation. Also the average bond length increases as a function of strain and only at the end of the simulation it starts to level off, see figure 4. At a strain of approximately 1.3 bonds break and the structure gains additional freedom for reorganization and relaxation. The stress reaches a plateau and does, for a certain strain range, not depend on strain, as bonding, breaking, stretching, and relaxation average out. From a macroscopic perspective, one would conclude that the system yields. However, at a strain of around 3.3 a phenomenon more alike macroscopic fracture was seen. Many bonds break, but many are formed as well, and the net result is still an increase in bonds. Stress relaxation due to bond breaking is apparently faster than stress increase caused by bond stretching, as the stress goes down. The system as a whole does not rupture yet, however.

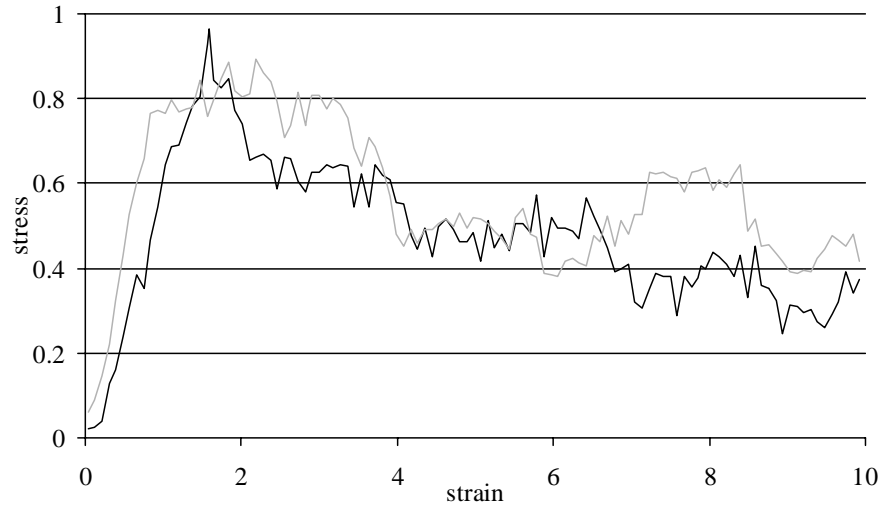


Fig. 3. Stress response of a gel structure as a function of strain. High damping model. For both systems $R_{\text{split}} = 0.4$ and $Pe = 0.1$. Gray curve: affine deformation, black curve: non-affine deformation.

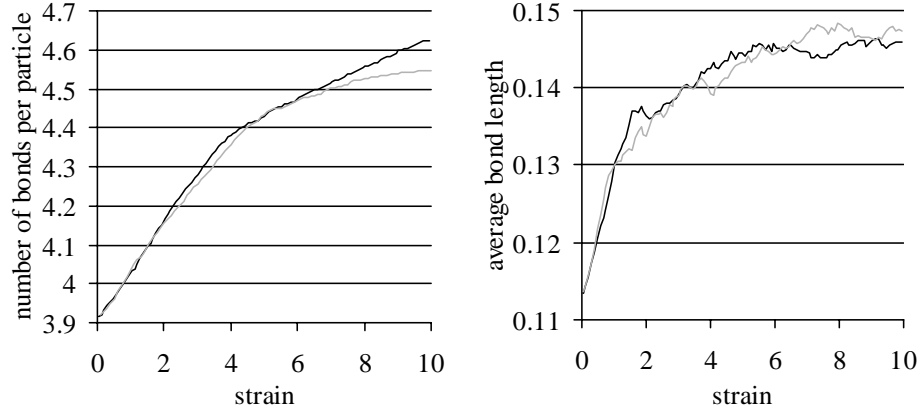


Fig. 4. Number of bonds per particle and average bond length as a function of strain. High damping model. For both systems $R_{\text{split}} = 0.4$ and $Pe = 0.1$. Gray curve: affine deformation, black curve: non-affine deformation.

If we look just at the stress-strain curve information, which can also be obtained in a macroscopic experiment, we could identify a yielding regime, after a partial fracture, between $\gamma = 4$ and $\gamma = 6$, followed by an elastic response, between $\gamma = 6$ and $\gamma = 7.5$, then yielding, fracture, yielding, etcetera. The obtained structural information such as presented in fig. 4, which generally cannot be obtained in a real experiment, shows no such regimes, but rather an ongoing process of compactification. For instance the "elastic" regime is not related to a significant increase in the average bond length and hence is probably related to an increase in number of bonds and bond orientation.

The non-affine deformation curve shows roughly the same stress-strain profile, with two differences. The initial slope of the curve is much smaller, and the stress reaches a maximum at strain of approximately 1.6 before decreasing to a yielding plateau. In the affine model all bonds are stretched, and the whole network carries stress. In the non-affine deformation only the backbone of the structure carries stress. Dangling side chains, or strands connected to the backbone in loops, generally will be stressless. Hence the affine model overestimates the actual initial stress. The stress overshoot in the non-affine model can be explained similarly. The backbone elements are the first to give way, leading to local fracture, and rapid stress relaxation, until the stress is transformed to new or other backbone elements. In the affine model stress is distributed much more homogeneously, inducing other elements than the backbone to break. Thus fracture also occurs much more distributed, and the effect is less singular.

The effect of the shear rate on the non-affine deformation stress-strain profile is shown in fig. 5. Over this range, all stress-strain curves show the same initial slope and similar behavior at larger strains. The stress overshoot seen in

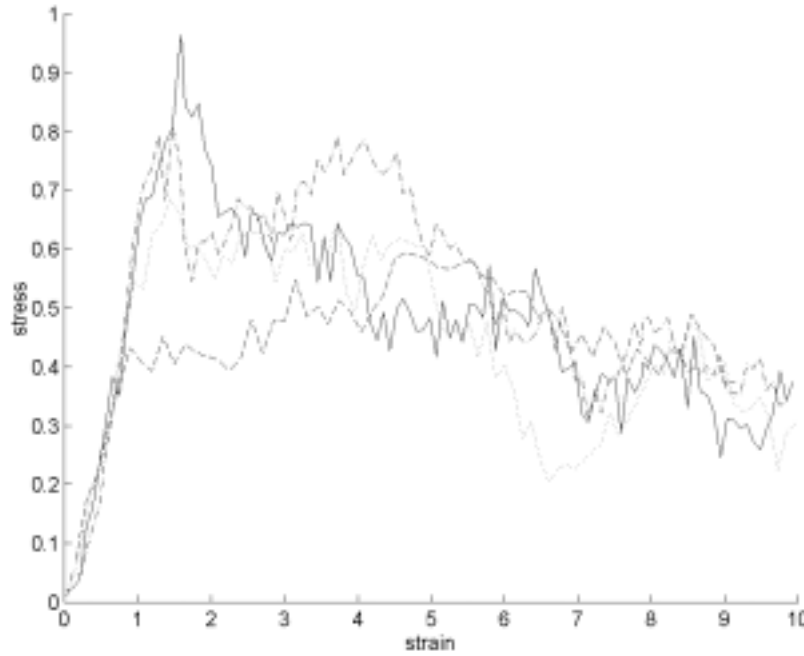
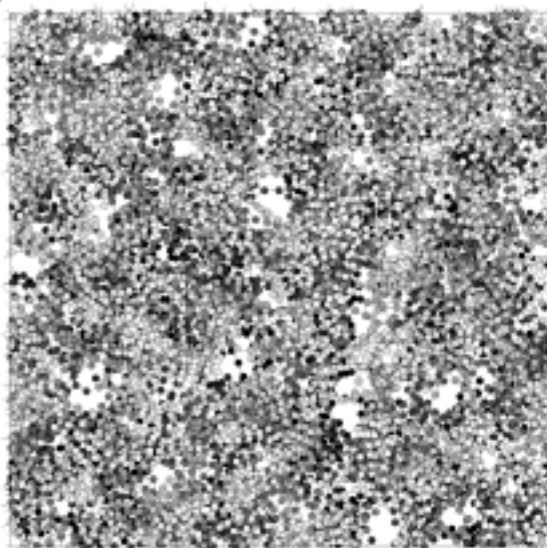


Fig. 5. Stress response of a gel structure as a function of strain. High damping model, non-affine deformation. For all systems $R_{\text{split}} = 0.4$. (—) $Pe = 0.1$, (---) $Pe = 0.05$, (···) $Pe = 0.2$, (-.-) $Pe = 0.5$.

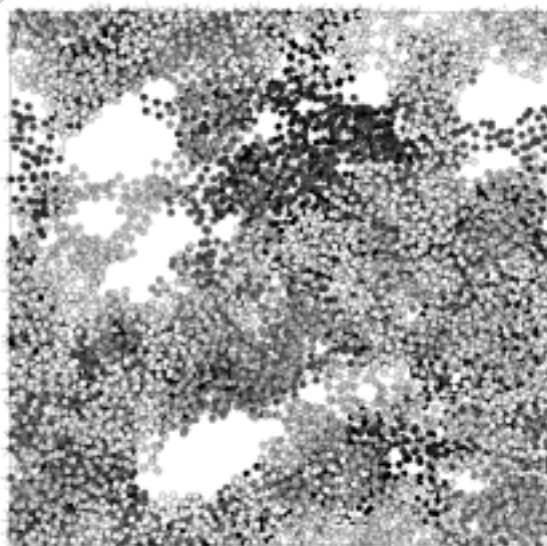
fig. 3 is less clear or absent, and maybe is no generic feature of the non-affine deformation. At $Pe = 0.5$ there is no overshoot at all, the initial increase in stress directly levels off to a plateau value. However at this and higher Pe numbers wall slip occurred during the non-affine deformation, implying that we could not investigate rheological behavior at large deformation for high shear rates with this simulation model. Note that the particle Pe number is rather low, but the cluster Pe number is considerably larger.

Figure 6 shows snapshots of: a) a starting gel configuration, b) a configuration of a non-affinely deformed gel, c) a stress distribution plot of the deformed gel, and d) the stress concentration plot with low values filtered out. In those plots the particle diameter is reduced to half of its real size and the bonds are much longer. A plot of the stress distribution (fig. 6c) in the deformed sample shows some stress concentration around the holes, in agreement with what one would expect from fracture mechanics [11]. The filtered out plot with only high stress values (fig. 6d) shows that stress carrying strands are aligned with the direction of the acting force.

a)



b)



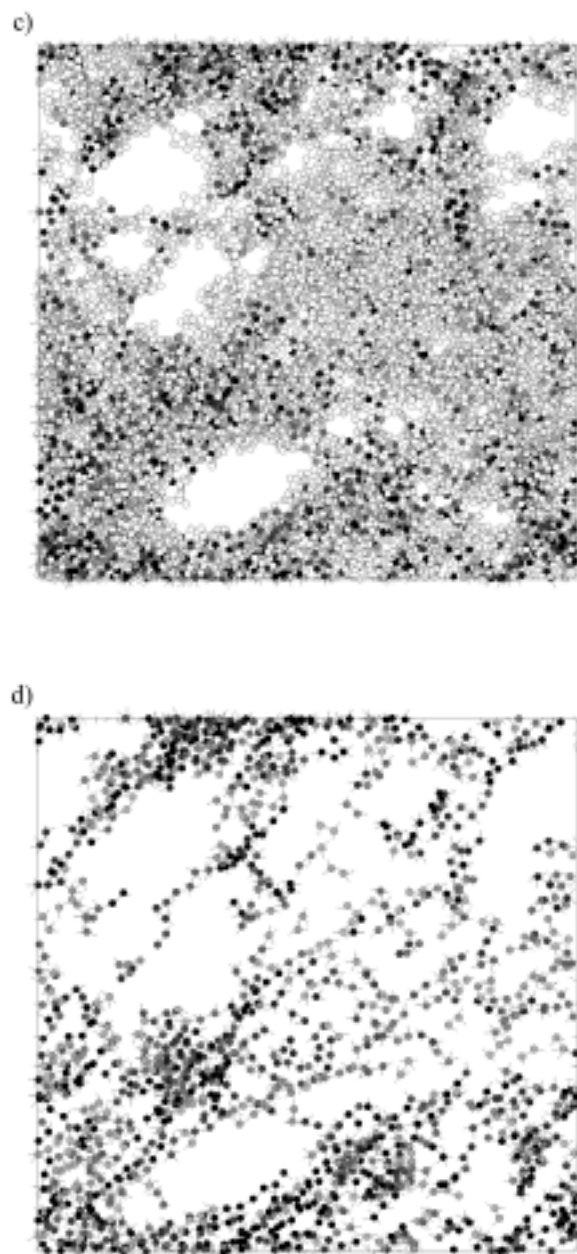


Fig. 6. A gel system under non-affine deformation: a) starting configuration, b) configuration plot at $\gamma = 8.35$ (gray scale is used as depth cue), c) stress distribution plot at $\gamma = 8.35$ (dark color denotes high stress), d) the stress distribution plot, low values filtered out.

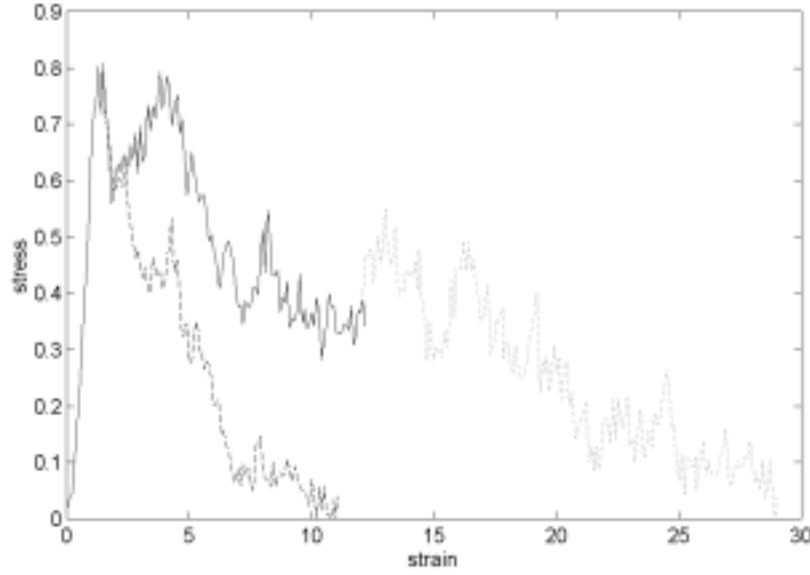


Fig. 7. Stress response of a gel system under non-affine shear deformation. High damping model. (—) $Pe = 0.05$ $R_{\text{split}} = 0.4$; (...) $Pe = 0.1$ continued from the configuration at $\gamma = 12$; (--) bonding disabled, starting from the configuration at stress maximum.

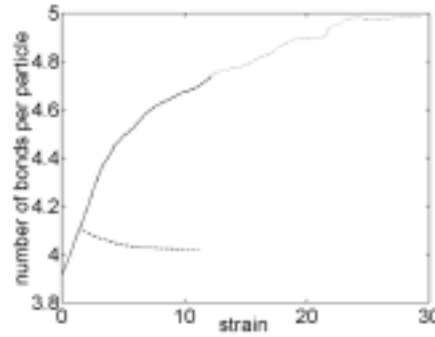


Fig. 8. Number of bonds per particle as a function of strain. High damping model. (—) $Pe = 0.05$ $R_{\text{split}} = 0.4$; (...) $Pe = 0.1$ continued from the configuration at $\gamma = 12$; (--) bonding disabled, starting from the configuration at stress maximum.

To substantiate the observed apparent macroscopic yielding, parameters were changed at certain points of the non-affine deformation run at $Pe = 0.05$ and $R_{\text{split}} = 0.4$, and the simulation was continued with the new parameter settings. Figure 7 shows the stress-strain profiles obtained, and figure 8 the number of bonds as a function of strain. At $\gamma \approx 12$ we increased the shear rate to $Pe = 0.1$. As expected the stress increases initially, but after repeated fractures,

the finite system finally ruptures completely. As the shear rate is not very much larger we can expect similar behavior if the simulation is continued at $Pe = 0.05$. The next test starts at the configuration near the stress maximum at $\gamma \approx 2$. If we prevent new bonds from forming the sample ruptures, but the stress does not decrease to zero monotonically, as weak spots still have to be loaded to their breaking point before they will fracture.

4.3.2 The inertia model

Figure 9 shows the stress-strain profiles of a particle gel as simulated using the two model approaches, the high damping limit and the inertia model. The dashed curve gives the stress response of a gel simulated with the inertia model but with parameters chosen such, to have the high damping limit apply. The curve shows more similarities than differences with the previous high damping result. The dotted curve of fig. 9 gives the stress-strain relation for the inertia model for a system where inertia effects are important. The initial slope of this curve is very similar to the former two. The stress increases as bonds stretch, with the same rate, in the direction of the acting force but bonds do not break yet. Meanwhile the pressure in the system is higher as in the relatively lower viscous system the particles move more rapidly than in the high damping system. Those rapid particle movements cause larger oscillations of the bond lengths, which at relatively low strains give higher value of average bond length (see fig. 10). The initial increase in average bond length up to the value of 0.123 is purely inertia effects driven. At a strain of about 0.4, many bonds break and the breaking rate is higher than in the high damping model due to the oscillations of the bond lengths. More bonds break, releasing more stress from the structure. At the same time new bonds form and the rate of bond formation is also higher than in the high damping model. Up to a strain of approximately 5 the resulting numbers of bonds per particle are very similar for both models. At strain of around 0.6 the stress reaches a plateau and does, for a certain strain range, not depend on strain. It seems the system simply yields. The yield stress for the inertia model is about half of the one for the high damping model.

After subsequent deformation the inertia system fractures at strain of about 3, yields, and fractures again at strain of about 6.8. From strain of approximately 3 the number of bonds per particle for the inertia model is lower than for the high damping system, the gap widens up from strain of about 5 and narrows down in the end. Those curves are results of a single simulation runs and were not tested for reproducibility. As the differences between the number of bonds per particle for different models are minor, no universal observations can be made. In general, one would expect that the lifetime of a bond is shorter in the inertia model and some evidence of it exists in the bond length distribution in the structure.

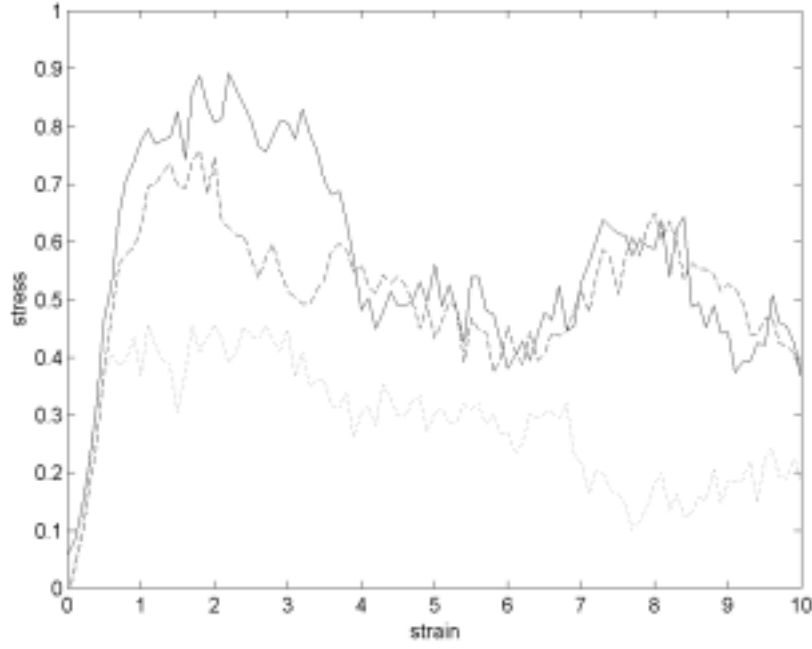


Fig. 9. Stress response of a gel system as a function of strain applying affine deformation $K = 1000$ and $R_{\text{split}} = 0.4$. (—) high damping, $Pe = 0.1$, $\Delta t = 10^{-4}$ (gray curve from fig. 3); (--) inertia model, $\dot{\gamma} = 0.1$, $\Delta t = 10^{-4}$, $\eta = 0.053$, $m = 10^{-4}$; (...) inertia model, $\dot{\gamma} = 0.1$, $\Delta t = 10^{-4}$, $\eta = 0.1$, $m = 10^{-3}$.

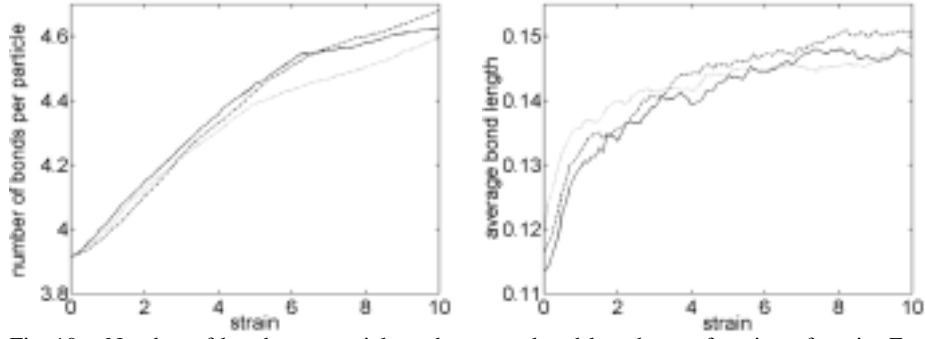


Fig. 10. Number of bonds per particle and average bond length as a function of strain. For all systems affine deformation $K = 1000$ and $R_{\text{split}} = 0.4$. (—) high damping, $Pe = 0.1$, $\Delta t = 10^{-4}$ (gray curves from fig. 4); (--) inertia model, $\dot{\gamma} = 0.1$, $\Delta t = 10^{-4}$, $\eta = 0.053$, $m = 10^{-4}$; (...) inertia model, $\dot{\gamma} = 0.1$, $\Delta t = 10^{-4}$, $\eta = 0.1$, $m = 10^{-3}$.

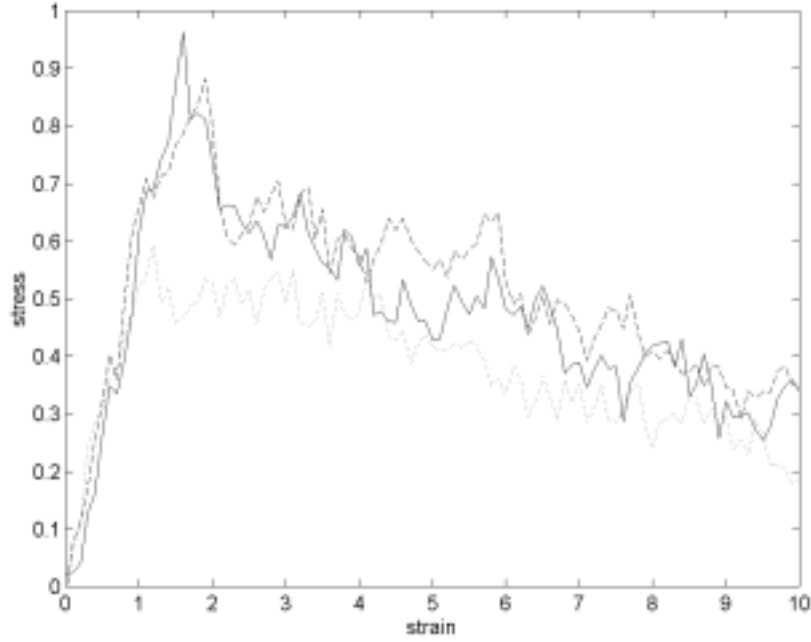


Fig. 11. Stress response of a gel structure as a function of strain. For all systems non-affine deformation $K = 1000$ and $R_{\text{split}} = 0.4$. (—) high damping, $Pe = 0.1$, $\Delta t = 10^{-4}$ (black curve from fig. 3); (--) inertia model, $\dot{\gamma} = 0.1$, $\Delta t = 10^{-4}$, $\eta = 0.053$, $m = 10^{-4}$; (...) inertia model, $\dot{\gamma} = 0.1$, $\Delta t = 10^{-4}$, $\eta = 0.1$, $m = 10^{-3}$.

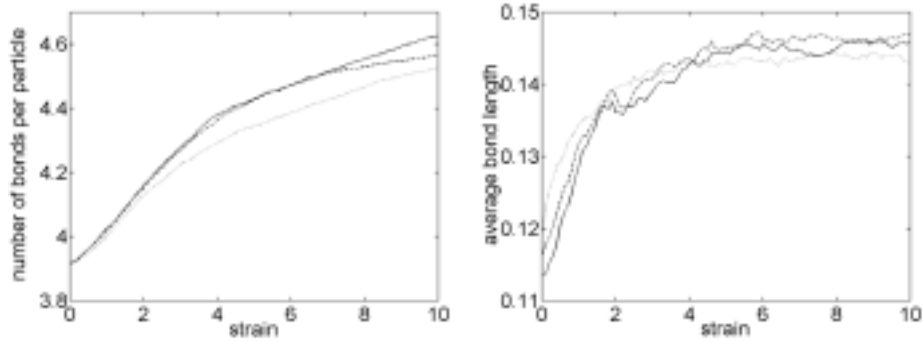


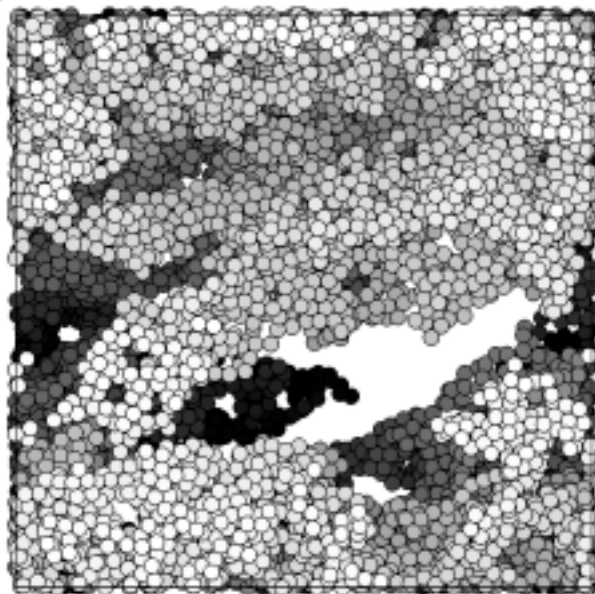
Fig. 12. Number of bonds per particle and average bond length as a function of strain. For all systems non-affine deformation $K = 1000$ and $R_{\text{split}} = 0.4$. (—) high damping, $Pe = 0.1$, $\Delta t = 10^{-4}$ (black curves from fig. 4); (--) inertia model, $\dot{\gamma} = 0.1$, $\Delta t = 10^{-4}$, $\eta = 0.053$, $m = 10^{-4}$; (...) inertia model, $\dot{\gamma} = 0.1$, $\Delta t = 10^{-4}$, $\eta = 0.1$, $m = 10^{-3}$.

Figure 11 shows the stress-strain profiles of a non-affinely deformed particle gel as simulated, using both the high damping and the inertia model. The dashed curve gives the stress response of a gel simulated with the inertia model but with parameters chosen such, to have the high damping limit apply. The curve rather closely follows the previous high damping result. The dotted curve of fig. 11 gives the stress-strain relation for the inertia model for a system where inertia effects are important. In general, the differences between the high damping and inertia model, for the non-affine deformation, can be discussed in similar lines as for the affine deformation. The stress maximum for the inertia system is roughly half of the one for the high damping. There is a large increase in the average bond length at relatively low strains, and the number of bonds is lower at lower strains. The stress overshoot of the non-affine deformation is present in the inertia model.

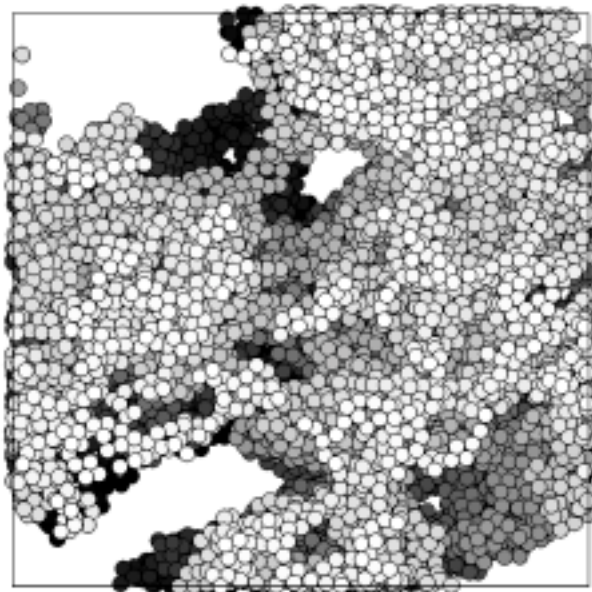
Figure 13 shows the end configurations of the deformed gels from the simulation runs of which results are presented in figures 9 and 11. All the pictures show structures with large holes surrounded by compact material. An affinely deformed gel using the high damping model (fig. 13a) in general results in a structure with a fracture in the xz plane in the bulk of the structure. A non-affinely deformed gel (fig. 13b) usually reorganizes to a compact structure in the center, which is connected through thick strands across the surface. In the end, when the structure breaks off from the surface, the percolating structure is lost. Fracture typically is initiated near the surface and continues into the bulk. The close to surface voids have a typical tilted shape due to movement of surrounding material. An affinely deformed gel using the inertia model (fig. 13c) results in a structure of smaller and more compact material lumps. Fracture occurs in the bulk of the structure rather than at the surfaces. It is often initiated in multiple fracture planes, where the material shows kind of a laminar flow in the early stages of deformation. A non-affinely deformed gel using the inertia model (fig. 13d) similarly as in the high damping model reorganizes to a compact structure in the center and voids by the surface. Again, in the inertia model the voids are smaller.

Using both models, inertia and high damping, the non-affine deformation often resulted in a wall slip. For high damping it happened mainly at high shear rates, $Pe \geq 0.5$ and bond length for splitting, $R_{\text{split}} < 1$. In the inertia model most of the gels deformed non-affinely resulted in a wall slip. It could be avoided only for a small range of parameters: viscosity, $\eta = 0.1$ to 0.053 , mass, $m = 10^{-4}$ to 10^{-3} , shear rate, $Pe = 0.1$, and bond length for splitting, $R_{\text{split}} = 0.1$. To be able to simulate non-affine deformation at relative lower viscosities we should probably go to much smaller time steps, this would make the calculations much more CPU expensive. The wall slip might also be avoided by taking a thicker layer at the top and the bottom of the box where bonds do not break. This way fracture can only take place in smaller fraction of the whole

a)



b)



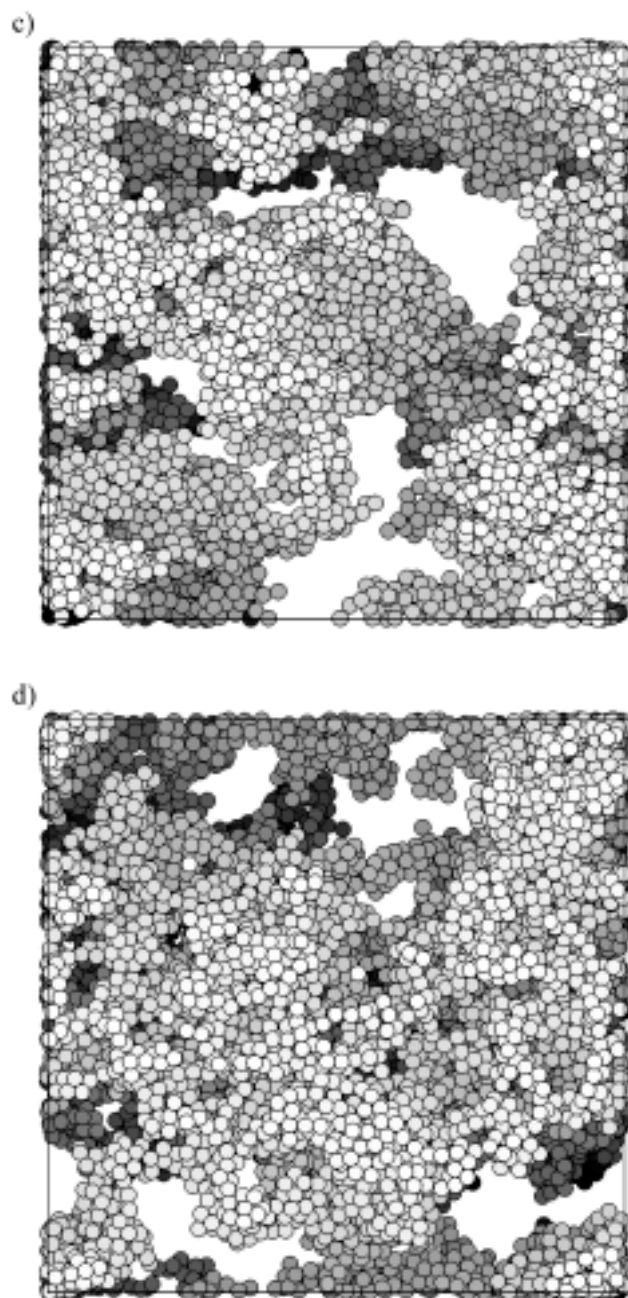


Fig. 13. Configurations of deformed structures from different models. All structures at a strain of approximately 10. a) high damping affine deformation, b) high damping non-affine deformation, c) inertia model affine deformation, d) inertia model non-affine deformation.

system and a larger absolute structure should be used to give satisfactory statistics.

In the end of most of our simulations a percolating structure remains, while most of the fractal characteristics have been lost. As we have shown in fig. 7, for the accelerated shear deformation, we can expect that such structures finally rupture completely, rather than showing a prolonged viscous regime.

The shear deformation used influence rotations of the lumps of the gel material. Affinely deformed structures show cluster rotations regardless of the position in the simulation box. Clusters in non-affinely deformed structures rotate only if they are positioned across the yz boundary plane. Single particles do not rotate in our model description, as it neglects most of the hydrodynamics. Clusters in the shear flow field rotate in the gradient plane due to shear induced bond stretches and subsequent bond relaxation. Any dimer in the shear field will rotate until it is aligned in the flow plane. In the affine deformation model there is a gradient profile in the whole box and clusters rotate regardless of their position. In the non-affine model an infinitely narrow shear gradient profile exists at the yz box boundary and only there clusters rotate.

4.4 Discussion

The underlying assumption behind our model is that we expect that the stress response in a real system is by the network rather than by the suspending fluid. For small strains the affine model overestimates the stress. This is because in this model all chains in the system, also dangling ones, are stretched. The non-affine model puts stress only at the structural part, the backbone of the gel. At somewhat larger strains, the moduli, the slopes of the stress versus strain curves, are more similar. This may be due to strain hardening, where bonds in the backbone of the gel matrix are directed in the shear direction, while side chains may still relax. Those stresses then primarily determine the resulting stress in the gel network. The stress contributions from bonds in the dangling ends become relatively small. The initial stress-strain curve did not depend on shear rate over the range investigated. For a non-affine deformation a stress overshoot could be seen. This overshoot was never observed in the affine model. The homogeneous stress distribution in affine models can explain the initial yielding behavior, where in non-affine models stress builds up around weak elements of the structure, inducing fracture at those spots. In the high damping model the transition of elastic deformation of the network to structural breakdown occurred at stress of approximately 0.8 regardless of the strain, strain rate, or deformation model used. This appears to be an intrinsic feature of the particle gel we used in the simulation. At higher volume fractions, higher yield stress was observed.

In the inertia model the initial stress response of a gel to a strain was very similar to the one found for the high damping model. The transition of elastic deformation of the network to structure breakdown occurred at a stress half of that obtained in the high damping model. The lower stress response in the inertia model is due to much stronger particle oscillations, which lead to bond stretching and increase in bond breaking. The particles move easier in the low viscosity "fluid" in the inertia model where in the damping model the viscosity was fixed by setting the diffusion constant and the particle radius at 1 giving $\eta = 1 / 6\pi$. In the inertia system, there are more short bonds and less intermediate bonds than in the high damping system. The bond lifetime is shorter. This leads to structures of smaller and more compact clusters. At large deformations the profile of the stress-strain curve in the inertia model is similar to the one in the high damping model.

In the investigated range of bond strengths, the stress maximum scales simply with the harmonic constant. For slower deformation rates the stress maximum is less pronounced, as to be expected, and for $\dot{\gamma} = 0.001$ there was no stress overshoot (data not included).

4.4.1 Yielding

Intuitively one would expect that during yielding the number of bonds between the particles stays constant, and during fracture it should decrease. However, in the simulations, the number of bonds always increased, and this phenomenon was rather independent of model or model parameters. Apparently external forces promote local reorganization, leading to compact regions surrounding empty holes, cracks, where a higher length for bond breaking, R_{split} , tends to give larger holes. It seems that the system does not break or yield but rather phase separates. Likely this is due to the fact that particles may form bonds at any position at their surface. In simulations allowing bond formation and breaking, with a high number of active sites on each particle, we will always get a compact, solid like structure in the end. This is a different behavior than the one observed for standard polymer gels. In particle gels new bonds may be formed with near neighbors while in some polymer gels an active site first has to travel a large distance before a new connection can be formed. Thus, particle gels may easily lose their fractal characteristics due to local reorganization while polymer gels will do that much less or not at all.

To prevent formation of compact structures in particle gels we would probably have to approach the limit of one bond per particle (two active sites per particle). In this limit only long, one particle thick chains are possible. They may form gels by physical cross looping or by incorporating a limited number of particles with three active sites, but these gels are not fractal. The increase in the number of bonds in the later stages of simulations was almost only due to

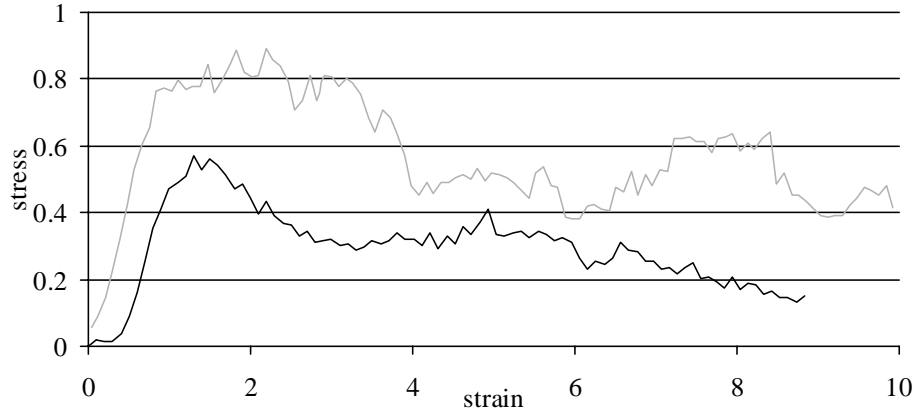


Fig. 14. Stress response of a gel system applying affine shear deformation, high damping model, $Pe = 0.1$ and $R_{\text{split}} = 0.4$. Gray curve: 12 active sites per particle (from fig. 3), black curve: 3 active sites per particle.

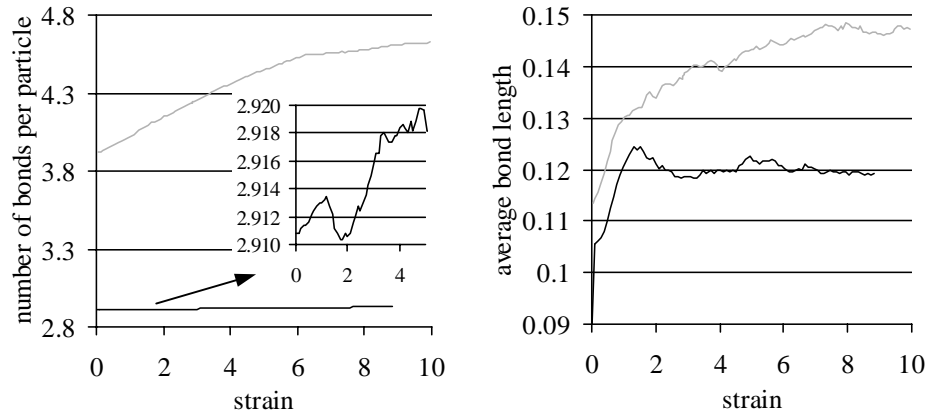


Fig. 15. Number of bonds per particle and average bond length as a function of strain. Affine shear deformation, high damping model, $Pe = 0.1$ and $R_{\text{split}} = 0.4$. Gray curve: 12 active sites per particle (from fig. 4), black curve: 3 active sites per particle.

formation of new bonds on particles, which already had 6 or more bonds attached to their surfaces. The possibility of formation of a large number of bonds, where we set the limit to 12 of active sites on each particle, can be the reason for formation of compact structures under strain. To test this a particle gel with the limit of three active sites was formed and deformed affinely in the high damping regime. Figure 14 shows the stress-strain profile of such a gel and fig. 15 shows number of bonds per particle and average bond length as a function of strain. In both figures, results are compared with the results shown before in fig. 3 and 4 for a gel with 12 active sites per particle.

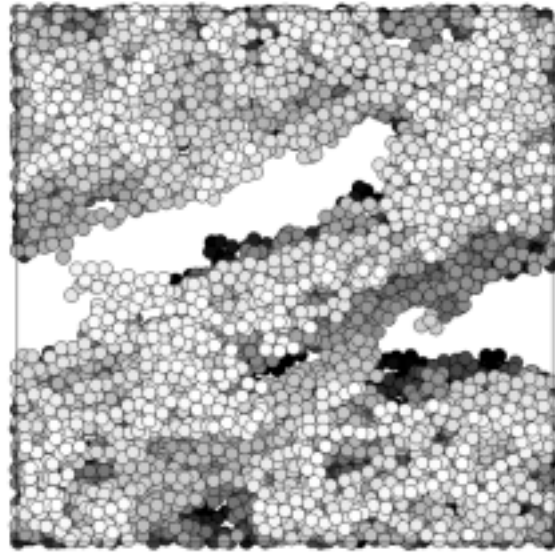


Fig. 16. Configuration plot of deformed gel build of particles with three active sites. Strain of around 5.

The stress in the three-active gel is lower during the whole deformation than in the twelve-active gel. There are fewer bonds cross-connecting the structure, thus also less stress carrying bonds. The structure fractures at strain of approximately 1.4 and the stress and number of bonds decrease. Still, the general slope of number of bonds per particle shows an increase, and in the end approaches the value of 3, which is the maximum in this system. Despite the limit of three bonds per particle, this gel also reorganizes to compact structures and empty holes. The deformed gel is plotted in figure 16.

Particle network gels do not exhibit typical yielding or breaking as, regardless of the model used, the number of bonds per particle increases under deformation. Instead, the system under large deformation undergoes fracture in many places of the network, which allows relaxation of the surrounding material and formation of new bonds. Consequently lumps of material are formed, which compactify due to local reorganization, rather than reforming the network. The size of the lumps depends on bond reversibility. Particle systems with truly reversible bonds can not form a stable fractal structure but will always phase separate, although the time scale may be very long. Structures with basically irreversible bonds, where bonds can brake but can not reform, will fracture in the classical way that they fall apart. To have yielding, bonds must be reversible, they must break and reform, but the structure may not

compactify on deformation, which is the case for the particle network systems investigated here.

A network of these compactified lumps will be formed, when the external deformation stops, but the structure of the gel has been irreversibly altered by the shearing. When such a gel is sheared again, it will probably break at the links between the lumps, and become a very viscous fluid with little further reorganization within the lumps. Upon re-gelling hence, little effect would be observed of the external shear. The coarse lumped network will not be fractal as the original gel, but have a structure as in percolation models. Still the internal structure of the lumps can be fractal, but due to the reorganization with a higher fractal dimensionality than originally. It can be expected that the gels formed this way are similar to those formed under shear.

4.5 Conclusions

The stress response of the particle gels in affine and non-affine deformation models showed differences at small strains. It was overestimated by the affine model, but similar for larger deformations. The transition stress, from the elastic to the viscous regime, in the inertia model was found to be half of that in the high damping model, can be measured due to the lower viscosity of the system.

Particle gel networks formed at rest, regardless the model, are not stable to shearing. They do not yield, but fracture into lumps that compactify due to local reorganization. The system is a highly viscous fluid instead of a continuously deformable solid. External shear alters the system properties irreversibly, though it may still form a different kind, non-fractal gel network at rest, similar to gels formed during shear.

4.6 References

- [1] A.A. Rzepiela, J.H.J van Opheusden and T. van Vliet, *J. Coll. Inerf. Sci.* **244** (2001) 43-50.
- [2] M. Mellema, J.H.J van Opheusden and T. van Vliet, *J.Chem.Phys.* **111** (1999) 6129-6135.
- [3] L.G.B. Bremer, B.H. Bijsterbosch, R. Schrijvers, T. van Vliet and P. Walstra, *Colloids Surf.* **51** (1990) 159.
- [4] T. van Vliet and P. Walstra, *Faraday Discuss.* **101** (1995) 359-370.
- [5] M. Whittle and E. Dickinson, *J. Chem. Phys.* **107** (1997) 10191-10200.
- [6] M. Whittle and E. Dickinson, *J. Chem. Soc. Faraday Trans.* **94** (1998) 2453-2462.
- [7] L.E. Silbert, J.R. Melrose and R.C. Ball, *J. Rheology* **43** 3 (1999) 673-700.
- [8] A.A. Potanin, *J. Coll. Int. Sci.* **157** (1993) 399-410.

- [9] S.J. Zhou, P.S. Lomdahl, R. Thomson, B.L. Holian, *Phys. Rev. Lett.* **76** 13 (1996) 2318-2321.
- [10] M.P. Allen and D.J. Tildesley, "Computer Simulation of Liquids", Oxford Univ. Press, Oxford, 1993.
- [11] A.G. Atkins and Y-W. Mai, "Elastic and plastic fracture", Ellis Horwood Limited, Chichester England, 1985.

Chapter 5

Tensile deformation of particle gels studied by Brownian Dynamics simulations¹

Brownian Dynamics (BD) simulations have been performed to study structure and rheology of particle gels subjected to tensile deformation. The model incorporates soft spherical particles, and reversible flexible bond formation. Two different dynamic descriptions of the model are discussed, one with high energy dissipation or high viscosity, the high damping limit, and one with low energy dissipation, the inertia model. Within both models the particle gels were found to be notch insensitive and resulting fracture was due to global material failure rather than crack propagation. The relation between fracture stress and notch size was found to be nearly linear regardless of the model used. Within the parameter range used in this paper particle gels were found to exhibit ductile fracture behavior under tensile deformation.

5.1 Introduction

Particle gels are colloidal, solvent rich materials that have become flocculated into a continuous three dimensional network structure. They are characterized as soft, deformable, visco-elastic solids. A wide range of particles may form this type of system. Aggregation kinetics and reorganization of the system determines strongly the structure of those gels [1], which can often be characterized using fractal analysis [2]. The concentration of particles in those systems can be quite low, while still the mechanical properties are dominated by the network rather than by the interpenetrating fluid. Particle gels are widespread in the food domain, examples are yogurt and cheese, in which the particles are mainly casein micelles [3].

Different materials break in different ways, for instance a crispy biscuit will snap when you bite it, while the same biscuit when dipped into a cup of tea too long will slowly tear apart under the force of gravity. In general behavior of

¹ A.A. Rzepiela, J.H.J. van Opheusden and T. van Vliet, *submitted to J.Rheol.*

materials have been classified broadly into two types of fracture, namely brittle and ductile [4]. Within this scope, many detailed fracture mechanisms can be distinguished for materials like for example foods [5]. Fracture behavior is sensitive to different conditions like temperature, deformation rate, and presence of cracks or notches in a material. Notches tend to encourage fracture owing to the increase in stress concentration near the notch tip. The relation between notch length and fracture stress may help in distinguishing ductile and brittle material. Typical relations between fracture stress and notch length are plotted for both ductile and brittle material in figure 1. For ductile material this relation is simply linear, for brittle material the fracture stress decreases more rapidly with increasing notch length.

In a ductile material, built of essentially parallel independent strings or fibers, the fracture stress simply scales with the size of the notch, the fewer connections to break the lower the fracture stress. The total stress needed is just proportional to the number of strings. In a brittle, highly cross-connected structure, fracture of one element influences the other elements and energy released from the fracture of one element can be transmitted to other elements, inducing fracture propagation. The overall fracture stress is then lower than that based on the reduction in the number of connections to break when a notch is formed. Crack initiation and propagation depend on the shape of the notch tip, blunt notches usually require greater fracture loads than sharp ones. Dynamics of crack propagation in tensile deformation experiments has been investigated through simulations on atomic level [6]. Compared to atomic systems particle gels have a much larger energy dissipation, and we do not expect to have problems with stress waves travelling through the system at sound speed, reflecting at the sample boundaries. In the viscous gel system these waves will damp out relatively quickly, and artificial damping is not needed.

Most functional properties of particle gels, such as shaping, handling, slicing and eating characteristics are related to their large deformation and

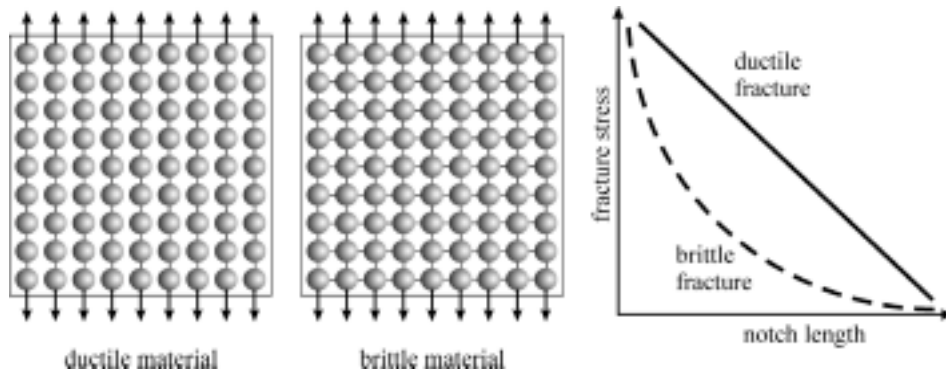


Fig. 1. Fracture stress versus notch length for ductile and brittle material.

fracture characteristics and only partly to their small deformation characteristics. Large deformation properties depend much more on the detailed structure of the gels than small deformation properties do [7]. Previous studies of particle gels under large shear deformation showed that those structures are not stable to shearing, they fracture into lumps that compactify due to local reorganization, destroying their fractal character [8].

Experimental tensile tests have been extensively performed in a range of materials from ceramic composite [9], through biscuit and pasta dough [10, 11], potatoes [12] up to polymer gels [13, 14]. Experimentally a large tensile deformation test on a gel is difficult to perform, particularly if the gel is weak. Particle aggregates have been studied under elongation flows by experiments [15] and simulations [16]. Tensile deformation has been used to study particle gels like cheese [17, 18], and more recently weak gels like yogurt [19]. Simulations do not share many of the practical problems of a laboratory experiment, and the available detailed data can help to explain the underlying mechanisms of tensile deformation and fracture.

5.2 Simulation Details

The simulation model contains N elastic spheres of radius a , with a harmonic central repulsion, placed in a three-dimensional box. Prior to gel formation the particles move through the solvent due to random displacements, and they form a bond when two particle surfaces come within a bonding distance R_{bond} . The attachment points are fixed on the surface, and rotate with the particle. The bond is completely flexible for lengths below b_0 , it is Hookean beyond this value and breaks when it is stretched above a specified length for bond breaking, R_{split} . After aggregation, relative particle motion is possible due to rotational and translational motion of the particles, which leads to cluster and gel reorganization.

5.2.1 Particle interactions

The particles interact through potentials which consist of the core potential V_C , equation 1, and the bonding interaction V_B , equation 2, both represented by a harmonic force,

$$V_C(r_{ij}) = \begin{cases} \frac{1}{2}K(2a - r_{ij})^2; & r_{ij} < 2a \\ 0; & r_{ij} \geq 2a \end{cases} \quad (1)$$

$$V_B(b_{ij}) = \begin{cases} 0; & b_{ij} \leq b_0 \\ \frac{1}{2} K (b_{ij} - b_0)^2; & b_0 < b_{ij} < R_{\text{split}} \\ 0; & b_{ij} \geq R_{\text{split}} \end{cases} \quad (2)$$

where $r_{ij} = |r_i - r_j|$ is the distance between particle positions r_i and r_j , and $b_{ij} = |b_i - b_j|$ is the distance between bond attach points b_i and b_j on the particle surfaces. Further b_0 is the maximum unstretched bond length, in fact $b_0 = R_{\text{bond}}$, and K is the force constant. This can be represented graphically as in figure 2. The force on particle i due to j , F_{ij} , is then simply:

$$F_{ij} = -\nabla_i (V_C(r_{ij}) + V_B(b_{ij})). \quad (3)$$

The total potential force on a particle is the sum of the pair forces.

This model using forces is a straightforward extension of a similar model with holonomic constraints for particle overlaps and stretched bonds, that was developed to investigate aggregation and reorganization [20].

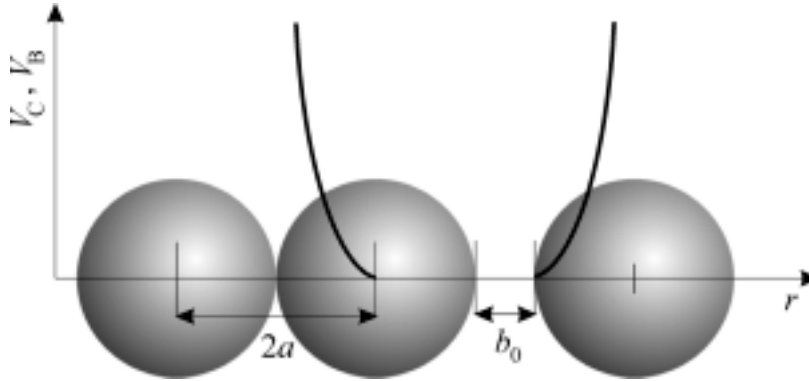


Fig. 2. Particle interactions: central core repulsion and non-central bonding attraction.

5.2.2 Brownian Dynamics

The Brownian Dynamics (BD) simulation model is based on the Langevin equation of motion for a system of diffusing particles. The total force here is the sum of the net force of interaction between particles, the random Brownian force and hydrodynamic interactions. The solvent is regarded as continuous and the Brownian force mimics thermal collisions between the solvent and the dispersed particles. The force on particle i is given by the equation:

$$F_i = m \frac{d^2 r_i}{dt^2} = \sum_j F_{ij} + R_i + H_i, \quad (4)$$

with F_{ij} given by equation (3), R_i the random (Brownian) force and H_i the force modeling hydrodynamic interactions. We approximate H_i by simple Stokesian friction, neglecting hydrodynamic interactions between particles. The liquid drag force on a single particle, H_i , is proportional to the particle velocity,

$$H_i = \zeta \frac{dr_i}{dt}, \quad (5)$$

where $\zeta = 6\pi\eta a$ is the Stokes drag, with η the solvent shear viscosity, and a is the particle radius. The size of the simulation box indirectly determines the volume fraction of the particles. Periodic boundary conditions in all three directions are used to avoid edge effects. All parameters corresponding to sizes or distances are normalized to the radius of a particle ($a = 1$) and all parameters corresponding to energies are normalized to units of $k_B T$ ($k_B T = 1$).

5.2.3 Numerical models

Taking particle velocities and positions as variables this second order differential equation is written in form of two coupled first order equations:

$$\begin{cases} \frac{dv_i}{dt} = \frac{1}{m} \left(R_i - \zeta v_i + \sum_j F_{ij} \right) \\ \frac{dr_i}{dt} = v_i \end{cases}, \quad (6)$$

which are solved numerically to give:

$$\begin{cases} v_i(t + \Delta t) = v_i(t) + \frac{\Delta t}{m} (F_{ij}(r_{ij}) - \zeta v_i(t)) \\ r_i(t + \Delta t) = r_i(t) + \frac{1}{2} (v_i(t) + v_i(t + \Delta t)) \Delta t + s_i(t) \end{cases}, \quad (7)$$

where m is particle mass and v_i is particle velocity. The effect of the random force R_i gives uncorrelated particle displacements $\langle \Delta s_i^2 \rangle = 2D_T \Delta t$ independently in all three directions $s = x, y, z$, with $D_T = k_B T / 6\pi\eta a$ the translational diffusion coefficient. The particles similarly undergo rotational motion and diffusion, with a rotational diffusion coefficient $D_R = 3D_T / 4a^2$. This description applies to systems with low damping (ζ). In the limit of high damping the time step is much larger than the relaxation time of the particle velocities. In a highly viscous system the equations of motion reduce to

$$\frac{dr_i}{dt} = -\frac{1}{\zeta} \left(\sum_j F_{ij} + R_i \right) \quad (8)$$

This leads to a model with only particle positions, which is solved with the Euler forward method:

$$\Delta r_i(t + \Delta t) = \frac{\Delta t}{\zeta} \left(\sum_j F_{ij}(t) + R_i(t) \right) \quad (9)$$

A more detailed description of the high damping limit model is given in an earlier paper [1]. The high damping limit, in combination with the constraint model, was used in gel formation, where the simulation time step used could be relatively big. First we used the high damping model for tensile deformation. The inertia model was used later to investigate possible brittle fracture.

5.2.4 Rheology

The uniaxial extension (tensile) tests are fundamental and probably most frequently used fracture tests, although for particle gels it is more often uniaxial compression that is applied. The obtained data, e.g. fracture or yield stress, can be exploited for quality control, material specification and development work. In a tensile test a material is subjected to a continuous increasing tensile strain, and the resulting stress is measured or vice versa. In experimental measurements sophisticated apparatus has been developed to grip a test piece and maintain an approximately constant extension rate, while it is assumed that the stress is uniformly distributed over the cross section of the sample. To simulate such a test, in affine deformation models extension is applied in the y direction, and an extra term is added to the particle positions:

$$\Delta S = y_i(t) \dot{\epsilon}_{yy} \Delta t \quad (10)$$

where $\dot{\epsilon}_{yy}$ is the extension rate. Also the length of the periodic image box in the y -direction is adjusted according to the applied tensile deformation. In this study the extension forces act only on two parallel (external) surfaces of the structure, omitting the gradient in the bulk, deforming only the box. The forces acting on the surface, and the stresses they give, are mediated into the bulk of the material by displacements of particles in the network itself, rather than by flow patterns in the interpenetrating solvent. The box adjustments we used are analogous to Lees-Edwards boundary conditions [21] for shear deformation.

The interparticle stress tensor $\sigma_{\alpha\beta}$ is determined from the virial:

$$\sigma_{\alpha\beta} = -\frac{1}{V} \sum_{i=1}^N \sum_{j>i}^N r_{\alpha ij} F_{\beta ij}, \quad (\alpha, \beta = x, y, z), \quad (11)$$

where V is the volume of the simulation box. Here it is assumed that the stress is homogeneously distributed on the length scales of the box size; equation (11) can also be applied to smaller volumes. Using equation (10) and the Lees-

Edwards boundary conditions, the system is subjected to a time-dependent extension. The Cauchy elongation strain is

$$\varepsilon(t) = \frac{y_{\text{box}}(t) - y_{\text{box}}(0)}{y_{\text{box}}(0)}, \quad (12)$$

where y_{box} is the simulation box dimension in the y direction. The resulting stress response can be analyzed to reveal rheological characteristics. The technique bears a deliberately close relationship to rheological tensile deformation experiments.

5.3 Results

We started by preparing particle gel configurations to be used for the tensile tests. The gels were prepared using the high damping BD algorithm with constraint dynamics. In this model N (where $N = 1,000$ or $10,000$ in some larger samples) particles are placed randomly, without particle overlaps, in a 3D periodic box with volume fraction $\phi = 0.3$, and aggregation at rest is simulated. This resulted in aggregation and gel aging in short computing time [2]. Rather than employing the cubic sample that we used for shear deformation [8], specific samples were developed for the tensile simulations. These samples were thin in the direction of the deformation, allowing fracture to occur in the relatively large perpendicular fracture plane.

From the continuous gel structures obtained in the above simulations notches of different shape and size were cut. The notch length was in the x direction (perpendicular to the tensile force), the notch thickness in the y direction (in the direction of the force), and in the z direction the notch stretched through the full gel sample). Thick notches were formed by removing all the bonds and particles from the notch space. The removed particles were randomly but without overlaps placed back in the simulation box. This configuration was equilibrated by running it for a short period without external forcing and allowing the box size to relax, thus minimizing stresses on sample walls. During equilibration the monomers were allowed to form new bonds outside of the notch, and more new bonds were formed due to relaxation and reorganization of the structure. This led to an increase of particle volume fraction in the gel structure, especially so around the cut out notch. Cutting only bonds in a specified xz plane was used to cut out narrow notches, with a thickness of the order of a bond length. Those structures were equilibrated while bonds were not allowed to form, as it could close the notch. Configurations with notches were used to investigate the impact of notch length and radius of the notch tip on fracture behavior.

The prepared gels, with and without notches, were subjected to a tensile deformation, which was applied in the y direction. In several test simulations, where x and z box dimensions were fixed there was an increase in stress components xx and zz as well. In simulations where the volume of the box was artificially kept constant up to and after fracture, compressive stresses developed; the stress components xx and zz had negative values. To avoid these unphysical effects in all final simulations we allowed the samples to shrink, by gradually relaxing the stresses in x and z directions, thus decreasing the size of periodical image box. The stress components xx and zz remained about zero during the whole deformation.

We have performed simulations using the non-affine deformation model for both the high damping and the inertia model. The model parameters we varied were the extension rate ($\dot{\epsilon} = 0.1$ to 1), and the bond breaking length ($R_{\text{split}} = 0.2$ to 0.4). The particle distance for bond formation was $R_{\text{bond}} = 0.1$ during both gel formation and aging. During deformation of structures with very narrow notches, bond formation was disabled to avoid closing up of the notch. In all simulations the characteristic unstretched bond length was $b_0 = 0.1$. The value of the harmonic force constant varied from $K = 1,000$ to $10,000$. The harmonic constant controls the rate of relaxation of particle overlaps and bond stretches, the values used in the simulations were the largest ones not leading to numerical problems for a given time step. The size of the time step we used is related to thermal translational and rotational diffusion. We come back on the relation between the harmonic constant and the time step in the discussion section.

The reduced time step for the high damping model was $\Delta t = 10^{-4}$, small enough to result in particle movements small with respect to particle radius and bond length. For the inertia model the time step varied, $\Delta t = 10^{-4}$ to $\Delta t = 10^{-7}$ as did the viscosity, $\eta = 0.01$ to 0.1 and particle mass, $m = 10^{-6}$ to 0.01 . In both

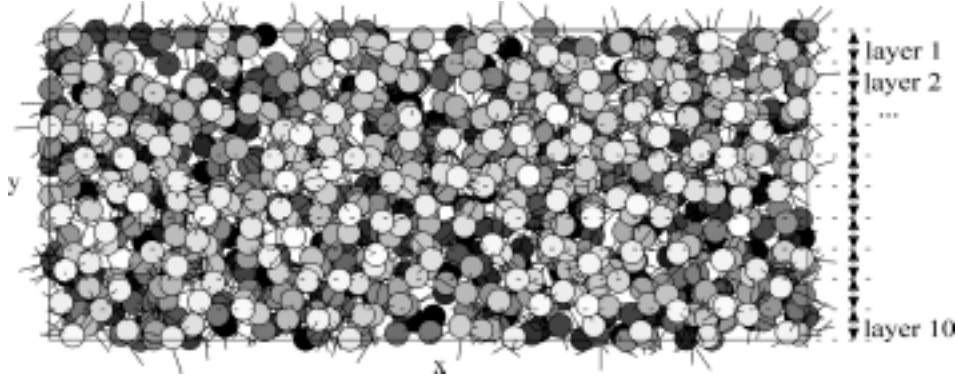


Fig. 3. Layer scheme. 2D projection of 3D gel structure divided into layers across the xz plane. Gray scale is used as the depth cue; for clarity particle size is reduced to half of its actual size, so bonds are much longer than in reality.

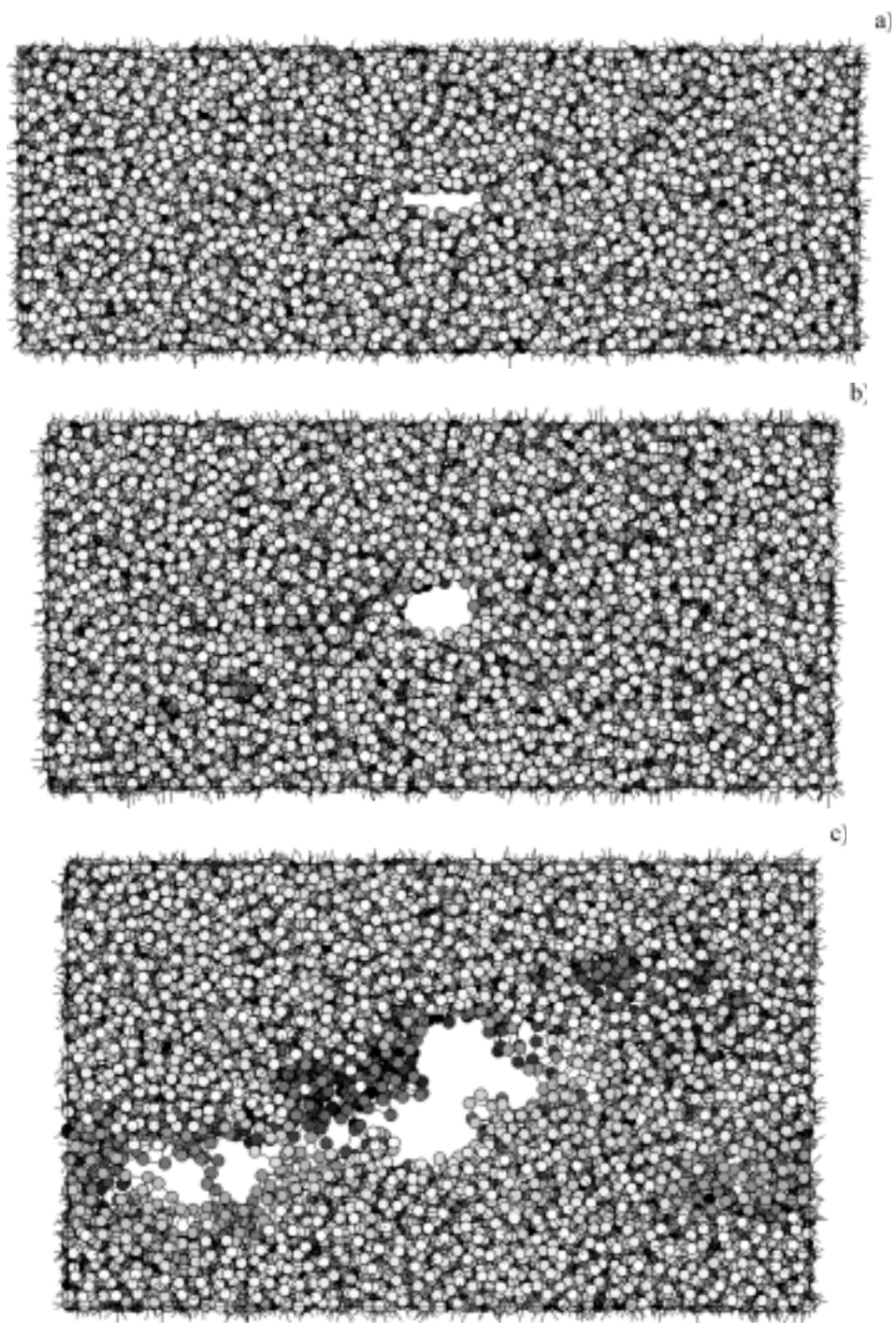
models the dimensionless time step has to be related to the external tensile force, which is system independent. In the high damping model the viscosity enters the equation through $\Delta t/6\pi\eta$ only, so there is little point in varying this parameter. Varying the extension rate, $\dot{\epsilon}$, which equals Pe in this approach, has the same effect.

For data analysis the results on detailed particle positions, bonds and stresses were used. Sample averaged stress tensor elements were plotted versus extension. For the simulation the computational box was divided into layers perpendicular to the y direction as shown in figure 3, and within each of the layers the stress and average bond length were calculated. The layers count from 1 to 10 from top to bottom of the box, so layer 1 and 10 are the outer layers of the simulation box, where the deformation is applied.

Several representative results selected from all the available data will be discussed to present the observed behavior. The behavior of particle gels under tensile deformation will be presented both for simulations with the high damping model and the inertia model.

5.3.1 High damping model

Figure 4 shows a typical set of configuration plots of a gel with a notch under tensile deformation. The starting structure plotted in fig. 4a contains a notch of $0.06 \times \text{box length}$ in the x -direction, $0.06 x_{\text{box}}$, and thickness of $2 \times \text{particle radius}$, $2a$. In the early stages of deformation the notch grows in thickness, changes shape and is roughly cylindrical at an extension of about 0.2, see figure 4b. Later both thickness and length increase, while simultaneously an independent void opens, originating from another naturally existing notch. This is shown in fig. 4c. The notch increases in length mainly due to joining of smaller voids, rather than to growth from the notch edge onwards. The stress does not seem to be concentrated around the notch, but stretched substructures are rather scattered over the sample, which is gradually being torn apart rather than cracking instantaneously. Breaking bonds are also scattered over the structure, and the ones breaking first are at a distance from the notch. Generally there are no breaking bonds directly above and below the notch, where the network is not box spanning in the direction of the tensile force. Stresses around the notch induce notch deformation instead of bond breaking. In the end the gel structure fractures in the xz plane. Fig. 4d shows a configuration just before that happened. While extending in the y direction, the whole gel sample shrinks in the x direction, see figures 4a through 4d, and it does so similarly in the z direction. This will be further illustrated in figures 7 and 8.



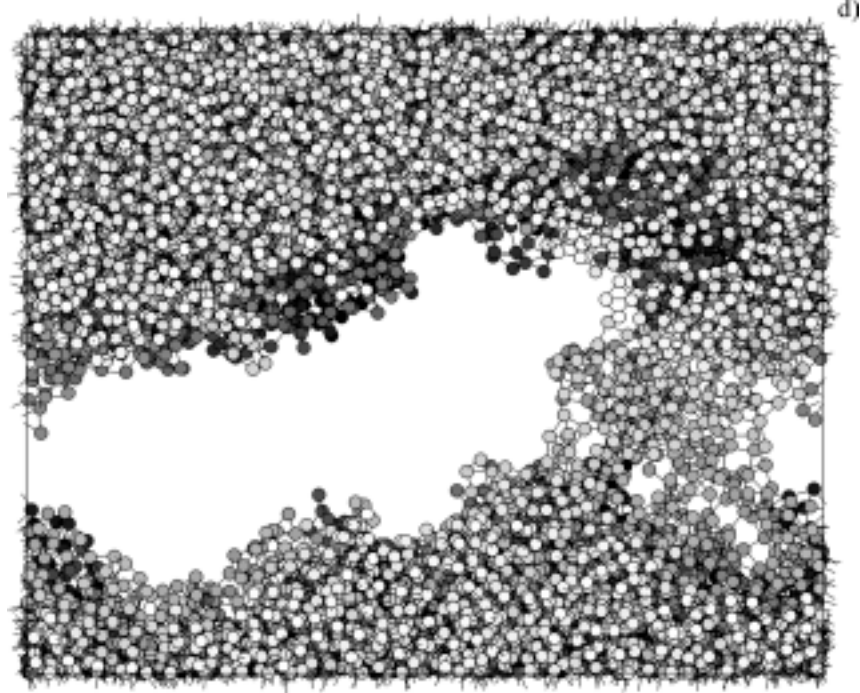


Fig. 4. Configuration plots of a gel structure, with a notch of $0.06 x_{\text{box}}$ by $2a$, under tensile deformation. High damping model, $\dot{\epsilon} = 0.1$, $R_{\text{split}} = 0.4$, $K = 1000$. Extension, $\epsilon =$ a) 0, b) 0.2, c) 0.5, d) 1.

In figure 5, the xx , yy and zz components of the stress tensor are plotted versus extension for the high damping model. The yy stress component steeply increases upon extension as bonds start to carry stress, but do not break initially. The xx and zz components of the stress tensor are approximately zero during the whole deformation, as the system is allowed to relax in those directions. New bonds are formed due to the ongoing process of local reorganization caused by thermal Brownian motion. Also the average bond length increases as a function of tensile strain. Bonds in the most outer layers at the top and bottom of the sample stretch first, which is quickly transmitted through the network to the middle layers. For the external extension rate chosen all layers stretch with roughly the same rate, see figure 6. At an extension of approximately 0.2 (*i.e.* a sample thickness of 1.2 times the initial thickness) bonds break and the normal stress starts declining, as the structure gains freedom for relaxation. The fracture does not seem to be local but global, as the stress release is the same in all layers. The average bond length decreases too, but it varies between different layers in a non-systematic way.

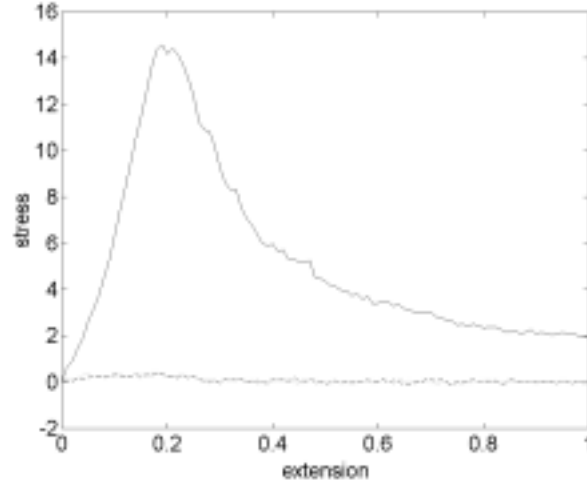


Fig. 5. Stress response of a gel structure, with a notch of $0.06 x_{\text{box}}$ by $2a$, as a function of extension. High damping model, $\dot{\epsilon} = 0.1$, $R_{\text{split}} = 0.4$, $K = 1000$. Stress tensor component: (--) xx , (—) yy , and (...) zz .

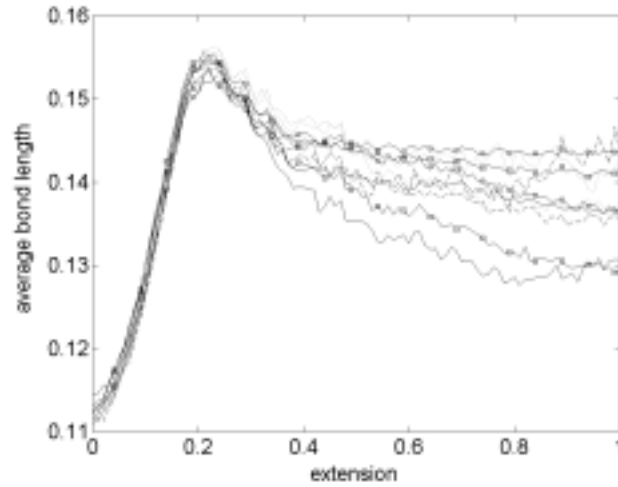


Fig. 6. Average bond length as a function of extension plotted in layers. Gel structure with a notch of $0.06 x_{\text{box}}$ by $2a$. High damping model, $\dot{\epsilon} = 0.1$, $R_{\text{split}} = 0.4$, $K = 1000$. (—○—) layer 1 & 10; (—□—) layer 2 & 9; (—) layer 3 & 8; (—) layer 4 & 7; (...) layer 5 & 6.

Upon tensile deformation the simulation box expands in the y direction and it shrinks in the x and z directions, see figure 7. At first there is some flexibility in the structure due to presence of unstretched bonds, the rate of increase of the thickness of the structures it is not matched by the rate of shrinking in the two perpendicular directions. The system takes up liquid as the

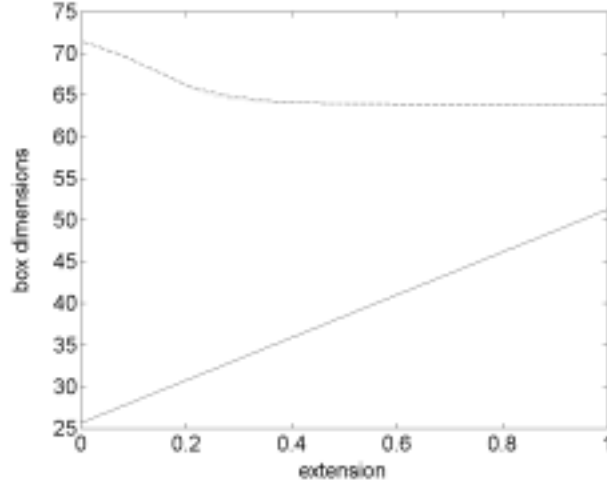


Fig. 7. Box dimensions versus extension in (--) x , (—) y , and (···) z direction. Gel structure with a notch of $0.06 x_{\text{box}}$ by $2a$. High damping model, $\dot{\epsilon} = 0.1$, $R_{\text{split}} = 0.4$, $K = 1000$.

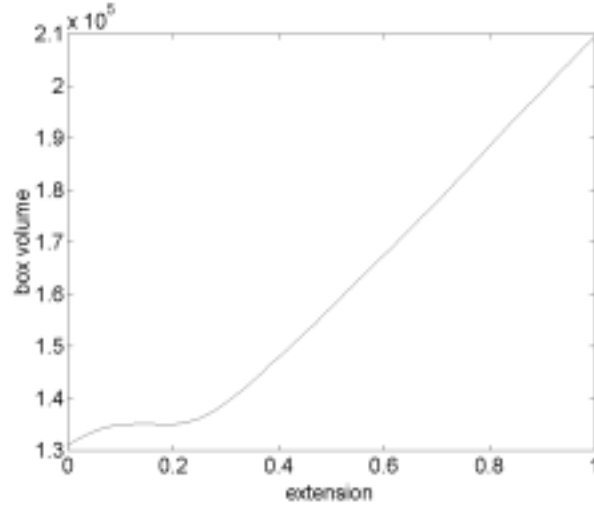


Fig. 8. Box volume versus extension. Gel structure with a notch of $0.06 x_{\text{box}}$ by $2a$. High damping model, $\dot{\epsilon} = 0.1$, $R_{\text{split}} = 0.4$, $K = 1000$.

volume of the box increases, see figure 8. Once the backbone of the network is stretched the extension in y is fully compensated by a contraction in the x and z direction. The sample behaves as a linearly elastic material, in the sense that the volume stays constant. At an extension of 0.2 the structure starts to break and the volume of the simulation box increases from this point on as the extension continues without much further effect on the x and z dimensions.

Under tensile deformation the relative size of the notch in the x direction remains approximately constant for extensions up to 0.4, see figure 9. The fracture occurring at tensile strain below 0.4 is not due to crack propagation from the notch. The simulation box shrinks in the x direction equally rapidly as the notch. At a strain of 0.4 the notch starts to grow in the x direction and it does so in a successive distinguished steps, when smaller voids

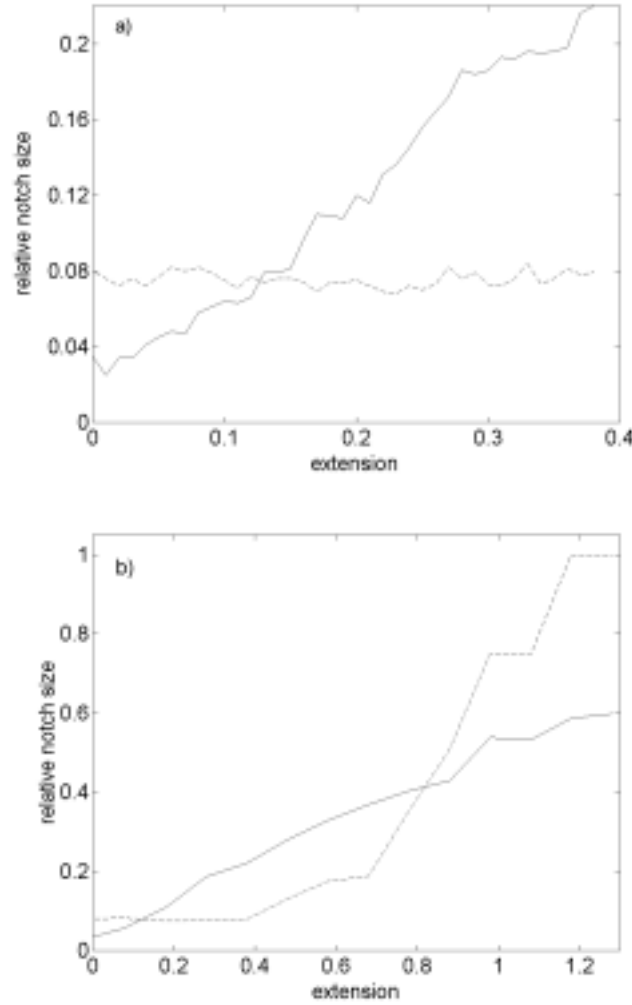


Fig. 9. Notch size relative to box size versus extension, in y dimension (—), and x dimension (---), a) small extension up to $\epsilon = 0.4$, b) large extension up to $\epsilon = 1.3$. Gel structure with a notch of $0.06 x_{\text{box}}$ by $2a$. High damping model, $\dot{\epsilon} = 0.1$, $R_{\text{split}} = 0.4$, $K = 1000$.

merge with the notch. At $\varepsilon = 1.1$ the notch is system spanning, and sample fracture is complete. The relative size of the notch in the y direction increases from the onset of the tensile deformation with a roughly constant rate. The whole extension of the gel in the column above and below the middle of the notch is accommodated by the increase in the thickness of the notch.

In figure 10 fracture stress is plotted for a range of systems with different notch lengths and radius of the notch tip. We observed almost linear relations between fracture stress and size of the notch for three different values of the notch tip radius. Fracture stress in structures without bond formation, which was used for very narrow notches, was lower than in structures with bond formation, compare the points for notch thickness $b_0 = 0.1a$ (\square) with those for notch thickness $2a$ (\diamond) in figure 10. The fracture stress for a system with a small and relatively thick notch (notch thickness $2a$ and relative notch length below 0.2) was found to be higher than for a system with no notch at all, the point indicated at relative notch length zero. The notch introduces some possibility for relaxation and if bonds are allowed to form, the structure can strengthen up, particularly around the notch. This does not happen in structures with very narrow notches, where no bond formation after notch formation was allowed, the fracture stress for notch thickness $0.1a$ and relative notch length 0.06 is lower than that the system without notch. The relation is nearly linear for the full range of notch lengths and for all notch thicknesses considered.

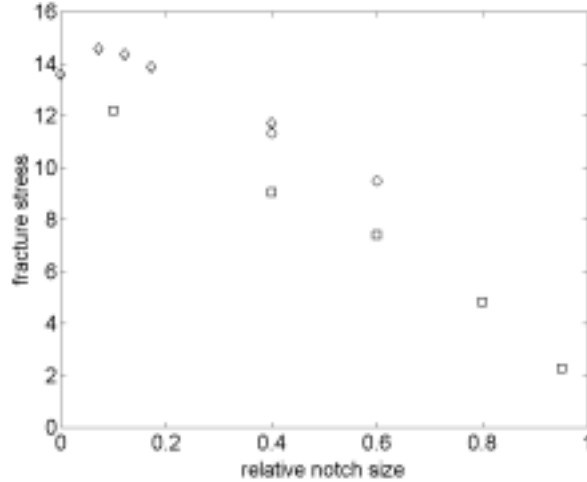


Fig. 10. Fracture stress versus relative notch size, notch tip $\diamond 2a$, $\circ 4a$, $\square 0.1a$. High damping model, $\dot{\varepsilon} = 0.1$, $R_{\text{split}} = 0.4$, $K = 1000$.

5.3.2 Inertia model

In figure 11 the xx , yy and zz components of the stress tensor are plotted versus extension for a simulated tensile strain experiment using the inertia model. The inertia model has a lower viscosity than a system in the high damping limit. All other parameters, such as notch size, radius of the notch tip, limit for bond breaking (R_{split}), harmonic constant (K), extension rate ($\dot{\epsilon}$), bonding probability, were identical in the two models. The initial slope of the stress-extension curve in the inertia model is the same as for the high damping model. The fracture stress is about 10% lower than in the high damping model 10 and 12, respectively, for the latter see point (\square) at notch thickness $0.1a$ and relative notch size 0.1 in fig. 10. The fracture strain is lower too.

The gel network in the inertia model breaks in similar fashion as in the high damping model. Breaking bonds are scattered throughout the sample. The notch becomes thicker due to the increasing tensile strain, while independent voids appear in the structure, see figure 12 (configuration at $\epsilon = 0.5$).

Most characteristics, box dimensions, box volume, and average bond lengths are similar between the high damping model and the inertia model with only a smaller viscosity. The main difference between the calculated data for the inertia and high damping model is the evolution of the bond breaking (figure 13). Fracture proceeds more rapidly in the inertia model. Bonds start to break sooner and the number of bonds per particle versus extension decreases faster. Moreover the curve for the high damping model levels off earlier then for

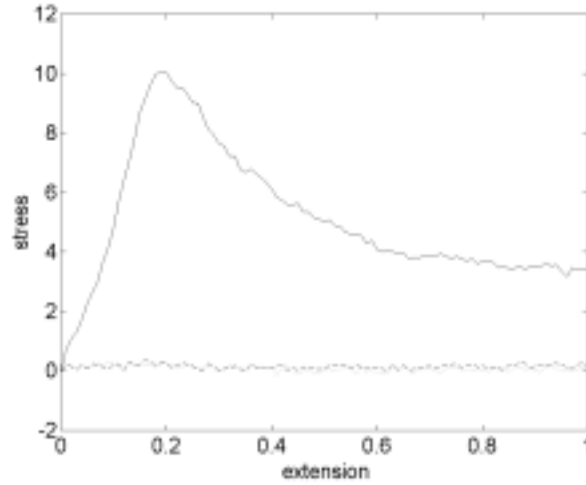


Fig. 11. Stress response of a gel structure, with a notch of $0.1x_{\text{box}}$ by $0.1a$, as a function of extension. Inertia model, $\dot{\epsilon} = 0.1$, $R_{\text{split}} = 0.4$, $K = 1000$, $m = 0.01$, $\eta = 0.1$. Stress tensor component: (--) xx , (—) yy , and (···) zz .

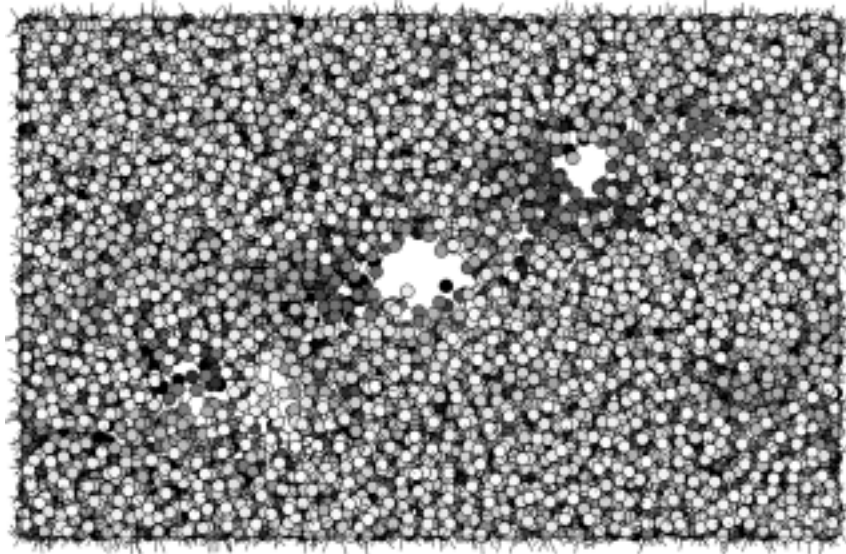


Fig. 12. Configuration plot of a gel structure, with a notch of $0.1x_{\text{box}}$ by $0.1a$, under tensile deformation at extension $\mathcal{E} = 0.5$. Inertia model, $\dot{\mathcal{E}} = 0.1$, $R_{\text{split}} = 0.4$, $K = 1000$, $m = 0.01$, $\eta = 0.1$.

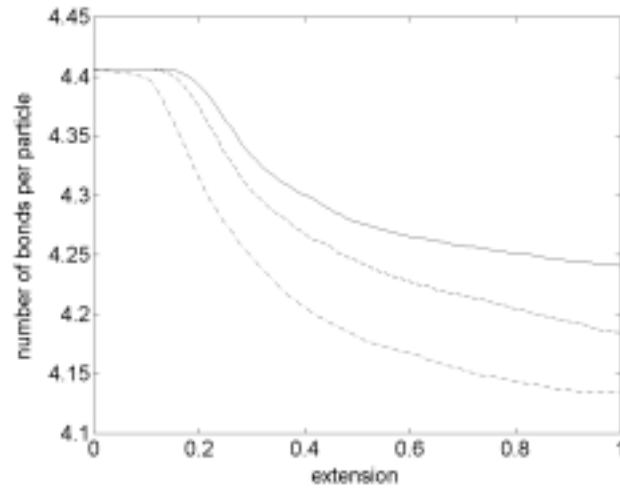


Fig. 13. Number of bonds per particle, in a gel structure with a notch of $0.1x_{\text{box}}$ by $0.1a$, versus extension, $\dot{\mathcal{E}} = 0.1$. Three systems: (—) high damping model, $R_{\text{split}} = 0.4$, $K = 1000$; (--) inertia model, $R_{\text{split}} = 0.4$, $K = 1000$, $m = 0.01$, $\eta = 0.1$; (-.-) inertia model, $R_{\text{split}} = 0.3$, $K = 10,000$, $m = 0.01$, $\eta = 0.1$.

the inertia model. Bond breaking proceeds increasingly rapidly on lowering the limit for bond breaking and increasing the harmonic constant.

Nevertheless, also for the inertia model, the relation between fracture stress and relative notch length is close to linear, see figure 14. Fracture stress in a structure with a notch of $0.1 x_{\text{box}}$ and $K = 1000$ in the inertia model is lower than in the high damping limit, while for a structure with a notch of $0.95 x_{\text{box}}$ and $K = 1000$ in the inertia model it is higher than in the high damping limit. The dependence of the fracture stress on relative notch length is weaker in the inertia model. Fracture stresses for the inertia model with a lower limit for bond breaking and a higher harmonic constant are higher because of this higher value $K = 10,000$. Results also appear to follow a linear relation.

Fracture strain is plotted as a function of relative notch size in figure 15. For two of the three different systems plotted here, fracture strain is roughly independent of the relative notch size except for the extreme system with a relative notch length of 0.95. At these very large notches, almost system spanning, the observed fracture strain is somewhat lower. In structures without any notch the fracture strain is lower than in structures with a small notch, both for the inertia and the high damping systems. A fracture strain decreasing with notch length is found for the inertia systems with $K = 10,000$ and $R_{\text{split}} = 0.3$, see symbols *, but this observation is based on only three data points. We were not able to distinguish the underlying mechanisms for the fracture strain dependence on relative notch size within these models and samples.

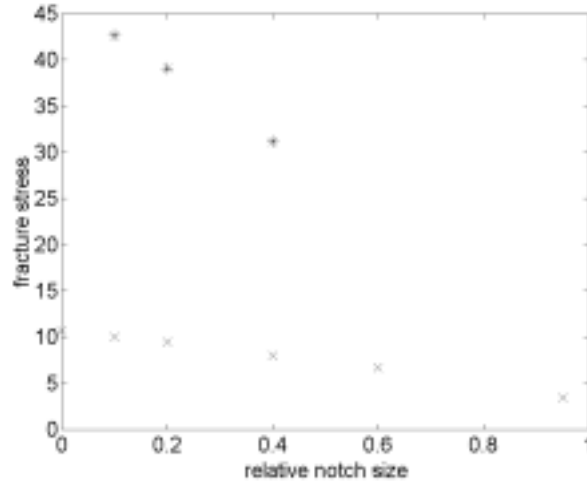


Fig. 14. Fracture stress versus relative notch size, notch tip $0.1a$, for two inertia models, $\dot{\epsilon} = 0.1$ $m = 0.01$, $\eta = 0.1$; $\times R_{\text{split}} = 0.4$, $K = 1000$; $* R_{\text{split}} = 0.3$, $K = 10,000$.

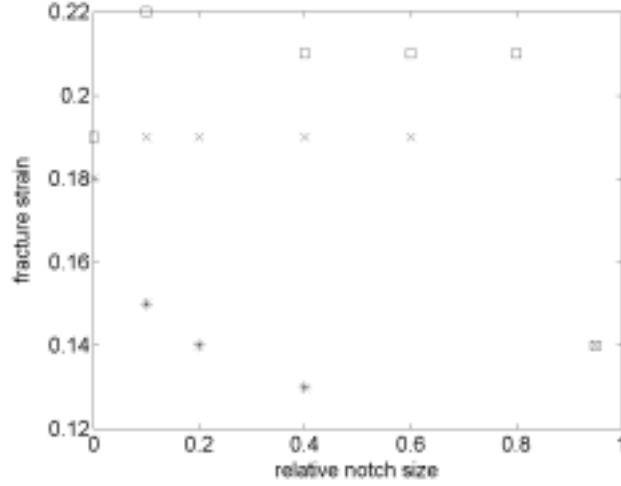


Fig. 15. Fracture strain versus relative notch size, notch tip $0.1a$, extension rate $\dot{\epsilon} = 0.1$. Three systems: \square high damping model, $R_{split} = 0.4$, $K = 1000$; \times inertia model, $R_{split} = 0.4$, $K = 1000$, $m = 0.01$, $\eta = 0.1$; $*$ inertia model, $R_{split} = 0.3$, $K = 10,000$, $m = 0.01$, $\eta = 0.1$.

5.4 Discussion

Some materials, when subjected to a tensile deformation at specific conditions, undergo brittle fracture. In a brittle material, released energy from the fracture of one element can be transmitted to other elements, inducing fracture propagation. The overall fracture stress is then strongly dependent on the size of notches in the material. In ductile materials fracture of one element does not directly influence other elements and the energy that comes free on bond fracture is dissipated as heat due to flow of material.

In this paper fracture behavior of particle gels was studied for tensile deformation. A linear relation was found between fracture stress and relative notch length from simulation runs within high damping limit, *i.e.* high viscosity systems. In this approximation the energy released from a broken bond is rapidly dissipated and as can be expected no fracture propagation was observed. To be able to describe low viscosity systems, which longer preserve kinetic energy, inertia effects were included in the simulation model. At lower viscosities the released energy from a broken bond gives particle accelerations and velocities that are not rapidly dissipated, and these may induce a chain of bond breaking events identified as spontaneous fracture. In the inertia models bonds were found to break more rapidly than in the high damping model, for the parameter range studied. The fracture stress and strain for a system with lower viscosity were found to be lower than for the high damping limit. The structure

breaks easier due to energy transmission through the network but possibly also due to larger particle diffusion in the low drag medium. Decreasing the friction effect by either lowering the viscosity or increasing the particle mass led to more rapid bond breaking. Lowering of the limit for bond breaking gave a similar effect. For systems of low viscosity ($\eta \leq 0.05$) and/or high mass ($m \geq 0.1$) and/or low limit for bond breaking ($R_{\text{split}} \leq 0.3$) strengthening of the bonds, *i.e.* a higher value of K , was necessary to avoid structure breakdown prior to tensile deformation. We have not been able to distinguish whether the increased ease of bond breaking in the low damping systems leads to fracture propagation. As we have not investigated correlation between bonds being disrupted, we do not know whether bond breaking is enhanced preferably near a broken bond or in the system in general.

Despite the effects on bond breaking, the relation between fracture stress and relative notch length for the inertia model was also found to be nearly linear, suggesting ductile fracture. It may be necessary to go to a system with much lower viscosity or higher particle mass or lower limit for bond breaking, to see brittle fracture in those particle gel systems. To avoid bonds being broken by random local stresses induced by thermal fluctuations, the bond stiffness, or harmonic constant needs to be increased substantially, possibly by a few orders of magnitude. As that leads to faster oscillations, a higher value for the harmonic constant, K , requires smaller simulation time steps to avoid numerical problems, thus making the calculations CPU expensive. The values of the harmonic constant used in this paper give rather weak gels, real bonds are stiffer, *i.e.* have higher K values. A further reduction of simulation time step, while maintaining the total deformation, would have made the calculations unfeasible on the computers to our disposition. Earlier simulation for crystalline atomic systems [6] were performed on supercomputers, where we used a simple top of the line PC. Moreover in crystalline samples the fracture strain is much smaller than in a fractal particle structure. The parameter regime for brittle fracture may be difficult to find or even non-existing in these types of gel structures, or for the approximated models we use. A somewhat artificial solution would be removing of the temperature effects when looking for brittle fracture behavior. That also removes the possibility of bond breaking through thermal fluctuations, and allows stress concentration to build up around a crack tip. Essentially removing temperature effects removes the diffusional timescale from the model, leaving only the time scale of the bond oscillation, associated with the value of K , and that of the tensile extension rate. In practice these values will still be far apart, leading to lengthy calculations.

Fracture initiation and propagation from a notch depends on the shape of the notch. A notch introduces a stress concentration at the notch tip, which is proportional to $1 + \sqrt{l/r_{\text{notch}}}$, where l is the notch length and r_{notch} is the radius of

the notch tip [4]. The stress concentration at the tip of a sharp notch is higher than at the tip of a blunt notch. Generally a notch is a weak spot in a structure, from which fracture can originate. However in the particle gels we have investigated, cutting out of a notch introduced possibilities for relaxation and reorganization in the structure, particularly in the vicinity of the notch. For some structures with thick notches, where new bonds could form, it resulted in strengthening of the structure instead of introducing a weak point. We have investigated structures with the widest range of notches possible in this geometry. Regardless of notch shape the stress was not concentrated around the notch, but distributed over the network. Bond breaking was scattered over the structure rather than concentrated at the notch tip. The fracture taking place did not originate at the notch but was a result of a global failure due to extensive tear.

The ductile character of particle gels may be a result of their structure. They are formed by a highly cross-connected network, which on a short length scale, at most two particle diameters, is fractal and on a longer length scale is random. Their structure is more that of an amorphous solid than of a crystalline solid.

5.5 Conclusions

Particle gels under tensile deformation as simulated by both a high damping and an inertia model were found to be notch insensitive. No fracture propagation from a notch could be observed and the material fracture was due to extensive tear. The relation between fracture stress and notch size was found to be nearly linear, regardless of the model used. Within the parameter range used in this paper particle gels were found to exhibit ductile fracture behavior under tensile deformation. This behavior could be explained by the fractal or random structure of the gel network on relevant length scales.

5.6 References

- [1] A.A. Rzepiela, J.H.J Opheusden and T. van Vliet, *J. Coll. Sci.* **244** (2001) 43-50.
- [2] M. Mellema, J.H.J van Opheusden and T. van Vliet, *J.Chem.Phys.* **111** (1999) 6129-6135.
- [3] L.G.B. Bremer, B.H. Bijsterbosch, R. Schrijvers, T. van Vliet and P. Walstra, *Colloids Surf.* **51** (1990) 159.
- [4] A.G. Atkins and Y-W. Mai, "Elastic and Plastic Fracture", Ellis Horwood Limited, England 1985.
- [5] P.J. Lillford, *J. Texture Stud.* **32** (2001) 397-417.

- [6] S.J. Zhou, P.S. Lomdahl, R. Thomson, B.L. Holian, *Phys. Rev. Lett.* **76** 13 (1996) 2318-2321.
- [7] T. van Vliet and P. Walstra, *Faraday Discuss.* **101** (1995) 359.
- [8] A.A. Rzepiela, J.H.J. Opheusden and T. van Vliet, submitted to *J. Rheol.*
- [9] O. Sbaizero, E. Lucchini, *J. Eur. Ceram. Soc.* **16** (1996) 813-818.
- [10] L. Piazza, A. Schiraldi, *J. Texture Stud.* **28** (1997) 523-541.
- [11] B. de Cindio, F. Celot, M. Migroli, C.M. Pollini, *J. Food Eng.* **48** (2001) 7-18.
- [12] D. Fahloul, M.G. Scanlon, *J. Texture Stud.* **27** (1996) 545-547.
- [13] A. Bot, I.A. van Amerongen, R.D. Groot, N.L. Hoekstra, W.G.M. Agterof, *Polymer Gels and Networks* **4** (1996) 189-227.
- [14] M. Teratsubo, Y. Tanaka, S. Saeki, *Carbohydrate Polym.* **47** (2002) 1-5.
- [15] S. Blaser, *J. Coll. Inter. Sci.* **225** (2000) 273-284.
- [16] K. Higashitani, K. Iimura, H. Sanda, *Chem Ing. Sci.* **56** (2001) 2927-2938.
- [17] H. Luyten, Ph.D. Thesis, Wageningen University, The Netherlands, 1988.
- [18] J. Visser, *Bulletin Int. Dairy Fed.* **269** (1991) 49.
- [19] G. Dimonte, D. Nelson, S. Weaver *et al.*, *J. Rheol.* **42** (1998) 727.
- [20] M.T.A. Bos and J.H.J. van Opheusden, *Phys. Rev. E* **53** (1996) 5044.
- [21] M.P. Allen and D.J. Tildesley, "Computer simulation of liquids", Oxford Univ. Press, Oxford 1993.

Chapter 6

Summary and conclusions

In this thesis we have investigated the rheological properties of a model particle gel using Brownian Dynamics simulations with different approximations. Particle gels are systems of colloidal particles that form weakly bonded percolating networks interpenetrated by a suspending fluid. They are characterized as soft, deformable, elastic solids. Examples in the food domain are yogurt and cheese, in which the particles are casein aggregates. We formulate our conclusions in the order of the chapters.

Chapter 2. The aggregation kinetics of the colloidal particle suspension into larger clusters has been investigated for different volume fractions, and compared with standard Schmoluchowski models. It was found that contrary to general practice, the initial particle distribution could not be neglected. The asymptotic aggregation rate is reached only when a substantial amount of the particles has already aggregated into larger clusters. A modified description, taking into account the homogeneous random particle distribution at destabilization of the suspension, was shown to follow the numerically obtained aggregation curves extremely well over a large range of volume fractions. Deviations occur only when really large clusters form, and the system is close to forming a gel or a space spanning cluster. The uniform nature of the models does not allow for a description of the fractal structure of the clusters, which is necessary to explain the fact that a gel can be formed.

Chapter 3. For small periodic shear deformation of a model gel sample we have tried to determine the storage and loss moduli as a function of frequency. We conclude that an affine or a non-affine description of the sample deformation leads to very different results. In the affine deformation mode the gel is sheared homogeneously, and the rheological behavior is very similar to that of a single damped oscillator. Details of the network play no important role, except at very low frequencies. In the non-affine mode, there is an inhomogeneity in the deformation of the network as certain parts of the network carry stress whereas other parts do not. Much more important is that with increasing frequency a transition can be observed from a surface load

experiment to a bulk load experiment. For the parameter values used in the calculations it turned out that the resonance frequency of the gel sample was below the range that we investigated.

Chapter 4. Large shear deformation of simulated particle gels within our model shows that the space spanning structure of the system is eventually lost at larger shear. Rather than yielding and maintaining its gel structure, the sample shows progressive ductile fraction by which the network is finally destroyed, and a still highly viscous suspension of large clusters is obtained. Prolonged shearing of the system leads to reorganization and irreversible compactification within these clusters. The cluster volume fraction within the sample is very high, and when the shear deformation is stopped, the individual clusters rapidly form a space-spanning network again, but with substantially fewer connections than the original gel formed at rest. The external distortion has irreversibly altered the microscopic structure of the model material. In general fractal particle gel networks probably do not yield, but fracture. At large deformations little difference has been found between affine and non-affine model calculations, probably because the rate of deformation was slow compared to the internal reorganization rate of the gel.

Chapter 5. Tensile deformation of simulated gels has only been performed in the non-affine mode. Allowing the sample to shrink in the directions perpendicular to the tensile deformation resulted in a material with an almost constant volume, apart from a small initial volume increase. Experiments with different notches, regarding size and shape, indicate that fracture behavior is always ductile. The random fractal structure of the gel apparently results in a large number of naturally occurring voids that act as notches, and fractures start in the bulk of the material, instead of near the prepared notch. Investigation at a lower suspension viscosity, where the limit on the viscosity was set by limits of the computational facilities, indicate still ductile fracture behavior. Probably brittle fraction in particle gels occurs only at very low viscosity of the suspending fluid, for instance when that fluid is a gas.

Samenvatting

Gelen zijn in het algemeen zachte, vervormbare, elastische vaste stoffen. Het is echter niet eenvoudig een sluitende definitie voor gelen te geven. Vanuit het gezichtspunt van de fenomenologische reologie kan een gel worden gedefinieerd als een materiaal dat zich gedraagt als een vaste stof wanneer het wordt geobserveerd over een korte tijd, of met een hoge frequentie bij een oscillerende belasting en zich gedraagt als een vloeistof over een lange tijdschaal, of bij een lage frequentie. Om discussie over de precieze afbakening tussen lange en korte tijdschalen te voorkomen, zullen we in dit proefschrift een meer structurele definitie hanteren. We gebruiken de term gel om materialen aan te duiden die bestaan uit een min of meer willekeurig netwerk van mechanische elementen in een continue vloeistoffase en met bindingen tussen de elementen die eenvoudig kunnen worden gevormd of verbroken.

We kunnen twee hoofdtypen gelen onderscheiden: polymeergelen en deeltjesgelen. Polymeergelen bestaan uit lange ketenmoleculen, waarbij fysische of chemische interacties verantwoordelijk zijn voor de verbindingen tussen de ketens. Deeltjesgelen bestaan in het algemeen uit netwerken van vaak min of meer bolvormige deeltjes, die met elkaar verbonden zijn door fysische of zwakke chemische interacties. Voorbeelden van dit type zijn standyoghurt en jonge kaas, waarbij de deeltjes caseïneaggregaten zijn.

In dit proefschrift hebben we de reologische eigenschappen van gemodelleerde deeltjesgelen onderzocht door gebruik te maken van Brownse Dynamica. Hieronder geven we een kort overzicht van de verschillende hoofdstukken van het proefschrift.

Hoofdstuk 2. In dit hoofdstuk is de kinetiek van de aggregatie van colloïdale deeltjessuspensies tot grotere clusters onderzocht voor verschillende volumefracties, en vergeleken met de standaard Smoluchowski modellen. Gebleken is dat, in tegenstelling tot wat algemeen verondersteld wordt, de aanvangsverdeling van de deeltjes niet kan worden verwaarloosd. De asymptotische aggregatiesnelheid zoals beschreven door de Smoluchowski vergelijking wordt pas bereikt als een aanzienlijk deel van de deeltjes al is geaggregeerd tot grotere clusters. In het hoofdstuk is aangetoond dat een aangepaste beschrijving, die rekening houdt met een homogene deeltjesverdeling bij de destabilisatie van de suspensie, de numeriek verkregen aggregatiecurven zeer goed beschrijft over een ruim gebied van volumefracties. Afwijkingen treden pas op als zeer grote clusters worden gevormd, en het

systeem op het punt staat een gel of een ruimtespannend cluster te vormen. De uniforme aard van de modellen staat geen beschrijving toe van fractale clusterstructuur, hetgeen noodzakelijk is om de mogelijkheid dat een gel wordt gevormd te verklaren.

Hoofdstuk 3. Getracht is de opslag- en verliesmoduli van deeltjesgelen te bepalen als functie van de frequentie waarmee een kleine oscillerende vervorming in afschuiving opgelegd werd. Zowel affiene als niet-affiene vervormingen werden opgelegd. Hierbij hebben we kunnen concluderen dat het gebruik van een niet-affiene vervorming leidt tot resultaten die sterk afwijken van resultaten die verkregen worden voor een affiene vervorming.

Voor affiene vervorming is de schuifvervorming van het gel homogeen en is het reologische gedrag sterk gelijkend op het gedrag van een gedempte enkelvoudige oscillator. Details met betrekking tot het netwerk spelen in dit geval geen belangrijke rol, behalve bij zeer lage frequenties. Voor niet-affiene vervorming is de vervorming van het netwerk inhomogeen als gevolg van het feit dat sommige delen van het netwerk belast worden en andere niet. Daarnaast werd bij toenemende frequentie een overgang waargenomen van een oppervlaktebelastingsexperiment naar een volumebelastingsexperiment.

Hoofdstuk 4. In dit hoofdstuk gebruiken we ons model om grote schuifvervormingen van deeltjesgelen te onderzoeken. Hierbij is gebleken dat de ruimtespannende structuur van het systeem uiteindelijk verdwijnt bij het opleggen van een toenemende schuifspanning. De gelstructuur blijft dus niet behouden, het monster breekt ductiel. Hierbij ontstaat een suspensie van grote clusters die nog steeds hoogvisceus is. Aanhoudende vervorming van het systeem leidt tot herschikking van de deeltjes binnen het cluster en tot een onomkeerbare compactie van de clusters. De volumefractie van de clusters in het monster is zeker aanvankelijk nog hoog, en wanneer dan de schuifvervorming wordt gestopt, vormen de individuele clusters weer snel een ruimtespannend netwerk, zij het met aanzienlijk minder onderlinge verbindingen dan in het oorspronkelijke gel. De externe verstoring heeft de microscopische structuur van het modelmateriaal onomkeerbaar veranderd. Voor grote vervormingen hebben we weinig verschil gevonden tussen affiene en niet-affiene modelberekeningen, waarschijnlijk omdat de vervormingsnelheid klein was in vergelijking met de snelheid van interne herschikking van de gelen.

Hoofdstuk 5. Vervorming van gesimuleerde gelen in rek is alleen onderzocht voor het opleggen van een niet-affiene vervorming. Als het monster de vrijheid werd gegeven te krimpen in richtingen loodrecht op de richting van de trekvervorming, bleef het volume afgezien van een kleine volumetoename in

het begin nagenoeg constant. Experimenten met verschillende inkepingen wat betreft omvang en vorm, geven aan dat het breekgedrag steeds ductiel is. De fractale structuur van de onderzochte gesimuleerde gelen resulteert kennelijk in een groot aantal natuurlijk optredende gaten in het netwerk die zich gedragen als inkepingen. Breuken beginnen daarom in de bulk van het materiaal in plaats van bij de geprepareerde inkeping. Ook simulaties met een lagere viscositeit van de suspensie, waarbij de kleinst onderzochte viscositeit uiteindelijk afhing van de rekensnelheid van onze computers, gaven nog steeds ductiel breekgedrag te zien. Waarschijnlijk treedt brose breuk in deeltjesgelen alleen op bij een zeer lage viscositeit van het suspenderende fluïdum, bijvoorbeeld wanneer dit een gas is en bij een zeer steile interactiepotentiaal.

Acknowledgements

After a little over four years I have reached the end of my PhD project and therefore I would like to take this opportunity to thank the people whose help, support and simple friendliness made it all possible. I have come to Wageningen in the end of 1998, a little by coincidence perhaps, and started to work on my PhD in the Mathematical and Statistical Methods Group. It has turned out to be a truly amazing experience.

First of all I would like to thank my direct supervisor Joost van Opheusden for all his help and encouragement from the very first until the very last day of this project. You have always been able to see the positive aspects of every situation, which gave me the strength to keep on going. Thank you for not only being my mentor in work but also for your understanding of the difficulties I had to face being alone far away from home. Also I would like to thank my second supervisor, Ton van Vliet, for all the discussions we had over the project. Thank you for encouraging me to follow my own ideas and to reach independent conclusions. You have also tried to encourage me to learn Dutch, sorry if this has not turned out entirely successful yet. Johan Grasman I would like to thank for being my promotor. Thank you for your continuous interest in my project and for bringing in your mathematical and modeling point of view in our many discussions.

To all my colleagues from the wiskundevakgroep, thank you for the very friendly and cozy atmosphere. Thank you for all the coffee breaks and the numerous traktaties. I will especially remember our department uitjes in the beginning of summer. Even though we went to places not too far away, each time it was as if we were visiting exotic fairytale places.

Special thanks to the people who were involved in the preparations of the previous promotion parties (and there were four of them before it was my turn), Evert-Jan Bakker, Gerrit Gort, Albert Otten and Eligius Hendrix. Thanks for all the help with computer related problems to our system manager Velu Muniandi and also to Albert Otten. Finally thank you to Ineke Engel, with whom I shared an office in the last few months.

My PhD life wouldn't have been as much fun as it was if it wasn't for my fellow PhD students. As I was the last of the group to arrive, I saw them promote and depart in the following order: Annemarie Pielaat, Eric Boer, Mark Huisjes and João Paulo. I had a great time with you guys! Thank you for welcoming me into your group. For all the fascinating lunches and dinners together. And for countless, unforgettable trips and excursions.

João, thank you for your friendliness and hospitality as my room mate of almost four years! Your cheerful and warm nature made it easier to come to the office every morning. And it felt very homely with all the plants and posters we collected over time. Thank you for our discussions about cooking, living and, what else, the peculiar Dutch! I am also happy that you are going to be my paranimf.

Annemarie, I found you to be a motivated and focused researcher and at the same time a young spirit and truly able to enjoy life. Thank you for the laughs we had together and for trying to explain Mark to me and his Dutch ways, only now I start to see what you meant.

Eric, thanks for being such a good friend over time. Your peacefulness and contentment make people around you comfortable. You have always been great company, able to talk and joke about things you take seriously but at the same time making it clear how you really feel.

Finally Mark, this journey would have been something entirely different if it were not for you. Thank you for your love and support. For always believing in me, which didn't stop you from giving me all your criticism. You have been my greatest luck here! Kocham Cię kochanie moje!

My greatest support and strength has always been from my parents, Teresa and Roman without whom I would never have come so far. Dziękuję kochani! Also my brothers, Andrzej and Tomek made me feel capable of completing my task here. Thanks for lovely holidays at home, summer trips and your visits in Wageningen. Zawsze bądźcie tacy wspaniali!

Finally I thank the Dutch Organization for Scientific Research NWO for financial support of this project.

Anna Rzepiela
Wageningen, 27 February, 2003

Curriculum Vitae

Anna Agnieszka Rzepiela was born on 24 November 1973 in Wrocław, Poland. In 1992 she graduated from high school “Liceum Ogólnokształcące Nr. 1” in Zielona Góra.

Next she studied chemistry at Wrocław University of Technology, where she specialized in computational chemistry at the Institute of Physical and Theoretical Chemistry. The title of her MSc graduation project was ‘The structure, proton affinity, electrostatic properties, and their relation to biological activity of cocaine and its derivatives’.

In 1998 she started her PhD project at the Mathematical and Statistical Methods Group at Wageningen University. This led to a thesis entitled ‘Deformation and fracture behavior of simulated particle gels’.

